DOCTOR OF PHILOSOPHY

Digital Filter Multiplexing-enabled Advanced Networking Devices and PON Architectures for 5G Network Convergence

Dong, Yixian

Award date:
2019

Awarding institution:
Bangor University

Digital Filter Multiplexing-enabled Advanced Networking Devices and PON Architectures for 5G Network Convergence

Yixian Dong

PRIFYSGOL
BANGOR
UNIVERSITY

A thesis submitted for the degree of
Doctor of Philosophy

School of Electronic Engineering
Bangor University

September 2019

Abstract

To meet the stringent 5G network requirements, passive optical networks (PONs) are considered as one of the most promising strategies for seamlessly converging independently developed optical access/metro networks and mobile fronthauls (MFHs)/backhauls (MBHs). To enable PON-based converged 5G networks to offer various on-demand services, apart from the implementation of software defined networking (SDN), it is greatly advantageous if the PONs can provide sufficiently high flexibility, elasticity, reconfigurability and adaptability, as well as transparency to major network design characteristics. In addition, advanced reconfigurable optical add/drop multiplexers (ROADMs) are also envisaged to play a vital role in delivering dynamic and transparent connectivity between an expanded number of individual network nodes over various networks with diversified design/traffic characteristics.

To address all the aforementioned challenges, in this thesis, four advanced techniques targeting the future converged 5G networks are proposed and explored, including: i) multiple channel interference cancellation of digital filter multiple access (DFMA) PONs based on intensity modulation and direct detection (IMDD), ii) hybrid orthogonal frequency division multiplexing (OFDM)-DFMA PONs, iii) hybrid discrete Fourier transform (DFT)-spread OFDM-DFMA PONs, and iv) digital signal processing (DSP)-enabled optical-electrical-optical (O-E-O) conversion-free ROADMs without incorporating optical filters.

The previously reported DFMA PONs utilise SDN controller-managed, DSP-based digital orthogonal filters to perform channel multiplexing/demultiplexing. For the cost-sensitive 5G application scenarios, the degradation of digital filtering-based channel orthogonality introduces significant cross-channel interferences. To effectively reduce the cross-channel interference effect, a DFMA channel interference cancellation (DCIC) technique is proposed and investigated, and a comprehensive DCIC theoretical model is developed. Through extensive numerical fitting with experimental measurements, the developed theoretical model is rigorously verified, and a set of accurate transceiver/system parameters are also identified. Detailed numerical simulations show that the DCIC technique increases the aggregated upstream signal transmission capacity by a factor of >2 and extends the differential optical network unit (ONU) launch power dynamic range by >14 dB. The aforementioned performance improvements are ONU-count independent and just require

one DSP iteration stage. Other salient DCIC advantages include low DSP complexity, negligible latency and excellent transparency to signal modulation format, signal bit rate and initial system operation conditions.

In the IMDD DFMA PONs, the required parallel digital filters implemented in the optical line terminal (OLT) is proportional to ONU count, thus the corresponding DSP complexity increases with ONU count. To further improve the PON performance and simultaneously reduce its hardware/software complexity and installation/operation expenditure, a hybrid OFDM-DFMA PON is proposed and investigated, where multiple independent OFDM channels are multiplexed using ONU-embedded dynamically reconfigurable and adaptive digital filters, and simultaneously recovered in the OLT by a single fast Fourier transform (FFT) operation. The proposed hybrid OFDM-DFMA PONs have all the desired advantages of the DFMA PONs including: i) DSP-enabled dynamic network reconfigurability, flexibility and elasticity, ii) inherent transparency to signal modulation format, signal bit rate and network topologies, and iii) capability of SDN-based network abstraction and virtualization. An analytical theoretical hybrid OFDM-DFMA PON model is developed, based on which extensive numerical simulations of upstream performances are undertaken. It is shown that the proposed PON offers additional unique features including greatly relaxed digital filter DSP complexity and further improved performance flexibility and robustness. Moreover, numerical results also show that the hybrid PONs can increase the differential ONU launch power dynamic range by 16 dB compared to the DFMA PONs.

To overcome high peak-to-average power ratios (PAPRs) of OFDM signals, an advanced variant of hybrid OFDM-DFMA PON, termed hybrid DFT-spread OFDM-DFMA PON, is proposed, which offers all the salient features associated with the hybrid OFDM-DFMA PONs. More importantly, it additionally reduces the upstream signal PAPRs by ≥2 dB. As a direct result, in comparison with the hybrid OFDM-DFMA PON, the hybrid DFT-spread OFDM-DFMA PON can increase the upstream system power budget by ≥3 dB and reduce the minimum required digital-to-analogue converter (DAC)/analogue-to-digital converter (ADC) quantization bits by at least 1 bit.

To cost-effectively provide dynamic and flexible network connectivity with reduced latency, optical filter- and optical-electrical-optical (O-E-O)-free ROADMs with excellent flexibility, adaptability and transparency to physical-layer network characteristics are investigated, which perform DSP-enabled dynamic add/drop operations at wavelength, sub-

wavelength and orthogonal sub-band levels. In IMDD-based network nodes, detailed investigations show that: i) the add/drop operation is digital filtering space location-independent; ii) the add and drop operations introduce around 3 dB power penalties, and iii) for distances of <40 km, the ROADM drop operation is robust to transmission system impairments.

In summary, this PhD dissertation research presents a wide range of major elements required for realising the converged 5G networks. The work paves a solid platform leading to practical implementation of the converged 5G networks in a cost-effective manner.

Acknowledgements

My deep and sincere gratitude firstly goes to my supervisor Prof. Jianming Tang, who expertly guided me through my PhD journey with his support in both constructive insights and detailed suggestions on various aspects of my dissertation research. His wide knowledge and logic way of thinking have been of great values for my research career. I also would like to thank the Sêr Cymru National Research Network which financially supported for my PhD study. In addition, Derek Nesset also deserves my big thanks for his kindness and help when I'm in BT company.

I am also deeply grateful to Dr. Roger Giddings, Dr. Yanhua Hong, Dr. Mingliang Deng, Dr. Wei Jin, Dr. Zhuqiang Zhong and all my colleagues and friends in Bangor University, they not only give me a large amount of research supports but also help me generously in my life in Bangor. Together we spent lots of treasured moments, and I would like to wish them all the best for the future.

I also would like to thank Prof. Kun Qiu for introducing me into the field of optical communications throughout my study for the Master's degree at the University of Electronic Science and Technology of China and his recommendation to study in Bangor University.

Lastly, I would like to sincerely appreciate my parents Fude Dong and Lizhen Yang, for their everlasting love and support. To them I dedicate this dissertation.

Abbreviations

ACI	Adjacent Channel Interference
ADC	Analogue-to-Digital Converter
AM	Amplitude Modulation
APD	Avalanche Photodiode
APON	Asynchronous Transfer Mode-PON
AR	Augmented Reality
ATM	Asynchronous Transfer Mode
AWG	Arrayed Waveguide Grating
BBU	Baseband Unit
BER	Bit Error Rate
BPON	Broadband PON
BS	Base Station
BTB	Back to Back
CapEx	Capital Expenditure
CAP	Carrierless Amplitude Phase
CCIC	Cross-channel interference cancellation
CD	Chromatic Dispersion
CCDF	Complementary Cumulative Density Function
CP	Cyclic Prefix

CPRI	Common Public Radio Interface
C-RAN	Cloud Radio Access Network
CW	Continuous Wave
DAC	Digital-to-Analogue Converter
DBA	Dynamic Bandwidth Allocation
DBPSK	Differential Binary Phase Shift Keying
DCIC	DFMA Channel Interference Cancellation
DFMA	Digital Filter Multiple Access
DFB	Distributed Feedback Laser
DFT	Discrete Fourier Transform
DIC	Direct Interference Cancellation
DML	Directly Modulated DFB Laser
DMT	Discrete Multitone Modulation
DQPSK	Differential Quadrature Phase Shift Keying
DSB	Double Sideband
DSP	Digital Signal Processing
EAM	Electro-Absorption Modulator
eMBB	Enhanced Mobile Broadband
EML	Electro-absorption Modulated Laser
EO	Electrical-to-Optical

EPON	Ethernet Passive Optical Network
EVM	Error Vector Magnitude
FASA	Flexible Access System Architecture
FDM	Frequency Division Multiplexing
FDMA	Frequency Division Multiplexing Access
FEC	Forward Error Correction
FFT	Fast Fourier Transform
FPGA	Field-Programmable Gate Array
FSAN	Full Services Access Network
FWM	Four-Wave Mixing
GEPON	Gigabit-EPON
GPON	Gigabit-Capable Passive Optical Network
GVD	Group-Velocity Dispersion
ICI	Inter-Channel-Interference
IDFT	Inverse Discrete Fourier Transform
IIC	Indirect Interference Cancellation
IFFT	Inverse Fast Fourier Transform
IM	Intensity Modulator
IMDD	Intensity Modulation and Direct Detection
IMT	International Mobile Telecommunications

IoT	Internet of Things
ISI	Inter-Symbol-Interference
ITU	International Telecommunication Union
LPF	Low Pass Filter
LAN	Local Area Network
LSB	Lower Sideband
LTE	Long-Term Evolution
MAC	Media Access Control
MAI	Multiple Access Interference
MBH	Mobile Backhaul
MF	Matching Filter
MFH	Mobile Fronthaul
MIMO	Multiple Input Multiple Output
ML	Maximum Likelihood
MMF	Multi-Mode Fiber
MMSE	Minimum Mean-Square Error
mMTC	Massive Machine Type Communications
MZM	Mach-Zehnder Modulator
NG-PONs	Next Generation Passive Optical Networks
NRZ	Non-Return-To-Zero

OADM	Optical Add Drop Multiplexer
OBI	Optical Beat Interference
OC	Optical Coupler
ODN	Optical Distribution Network
OE	Optical-to-Electrical
O-E-O	Optical-Electrical-Optical
OFDM	Orthogonal Frequency Division Multiplexing
OFDMA	Orthogonal Frequency Division Multiple Access
OLT	Optical Line Terminal
ONU	Optical Network Unit
OOFDM	Optical Orthogonal Frequency Division Multiplexing
OpEx	Operational Expenditure
OSNR	Optical Signal-to-Noise Ratio
OTBPF	Optical Tunable Band-Pass Filters
PAM	Pulse Amplitude Modulation
PAPR	Peak-to-Average Power Ratio
PD	Photodetector
PMD	Polarization Mode Dispersion
PON	Passive Optical Network
P/S	Parallel-to-Serial

PTS	Partial Transmit Sequences
PSK	Phase Shift Keying
QAM	Quadrature Amplitude Modulation
QoS	Quality of Service
RF	Radio Frequency
ROADM	Reconfigurable Optical Add/Drop Multiplexer
ROP	Received Optical Power
RRH	Remote Radio Heads
SBS	Stimulated Brillouin Scattering
SCO	Sampling Clock Offset
SDN	Software Defined Networking
SF	Shaping Filter
SLM	Selective Mapping
SMF	Single-Mode Fiber
SNR	Signal-to-Noise Ratio
S/P	Serial-to-Parallel
SPM	Self-Phase Modulation
SRS	Stimulated Raman Scattering
SSB	Single Sideband
SSMF	Standard Single Mode Fibres

SSS	Spectrum Selective Switches
STO	Symbol Timing Offset/Sample Timing Offset
TDMA	Time Division Multiple Access
TET	Terminal Equipment Transceivers
TRPN	Transponder
TWDM	Time and Wavelength Division Multiplexing
uRLLC	Ultra-reliable and Low Latency Communications
USB	Upper Sideband
VR	Virtual Reality
WDM	Wavelength Division Multiplexing
WDMA	Wavelength Division Multiplexing Access
WSS	Wavelength Selective Switch

Contents

1. Introduction

Contents

1.1 Future Network Challenges

Since the commercialization of 4G wireless networks, 4G end-users have been enjoying a wide diversity of broadband services with their mobile devices. As a direct result of the proliferation of smartphone ownership, vast adoptions of mobile video, augmented reality (AR) and virtual reality (VR), as shown in Fig. 1.1, mobile data traffic has been predicted to increase seven-fold from 2017 to 2022, reaching 77 exabyte per month by 2022 [1]. Unavoidably, such a huge amount of mobile data consumption puts great pressure on current mobile networks in terms of bandwidth, flexibility and latency. Furthermore, a growing number of emerging applications, such as machine to machine (M2M) communication utilized in industrial automation, Internet of things (IoT) in intelligent demand/supply control, cloud services in smart cities are also enriching the network connectivity and usage scenarios [2], which also impose additional stringent new requirements on future wireless networks with regard to cost-effectiveness and connection density [3].

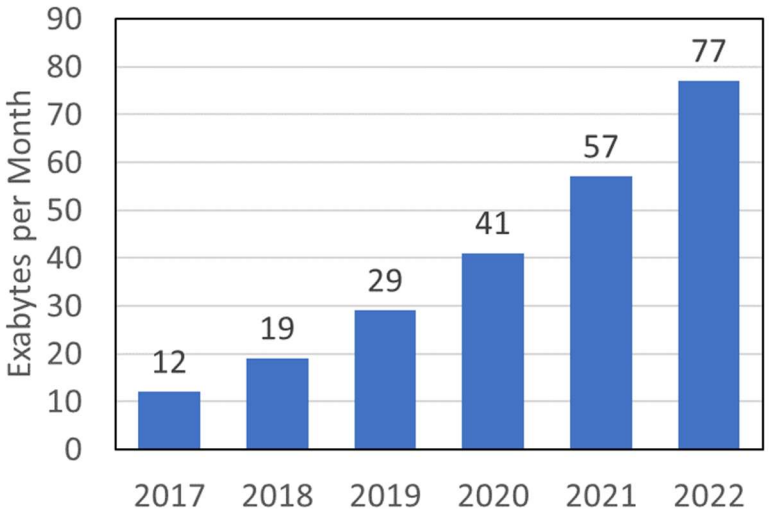

Fig. 1.1 Cisco VNI global mobile data traffic forecast, 2017–2022.[1]

To enable the wireless networks to provide various end-users with high quality of service (QoS) for different usage scenarios, the fifth-generation mobile communication (5G) has been proposed [4]. In early 2012, ITU-R embarked on a programme to define "IMT for 2020 and beyond", and to set a roadmap for 5G research activities that would be emerging worldwide. In IMT-2020, there are three representative usage scenarios [4, 5], including: 1) Enhanced mobile broadband (eMBB), targeting the peak data rate as high as 20 Gb/s for a single mobile station [6]; 2) Ultra-reliable and low latency communications (uRLLC), aiming at decreasing the end-to-end latency below 1 millisecond and increasing the

reliability level above 99.999% [5]. uRLLC is crucial for automatic industrial manufacturing, remote medical surgery and transportation safety; and 3) Massive machine type communications (mMTC), meeting the requirements of increased connection density and scaling up the networks to support billions of connected devices, with a connection density of up to 1000,000 units per square kilometre [6]. In practice, the exact requirements on data rate, latency and connection density may vary from time to time for different applications.

To practically implement 5G networks, a wide range of technologies have been proposed, for example, to offer gigabit transmission data rates to end users, millimetre wave (mmWave) has been proposed to make use of the radio frequency (RF) spectrum approximately between 30 and 300 GHz [7-12]. On the other hand, massive multiple input multiple output (MIMO) has also been widely investigated to enhance the signal transmission capacity by improving the spectral efficiency [7-10]. Apart from the aforementioned two technical strategies, deploying an increased number of small cells including femto/pico/micro cells [13, 14] is also widely considered to be vital solution for not only providing multigigabit bit rates but also significantly enhancing the connection density. Each of the abovementioned individual technologies and/or their combinations can address, to some extent, the stringent requirements associated with specific 5G usage scenarios, however, their implementations also impose unprecedented new technical challenges across all layers of 5G networks. For example, the current interface adopted in MFHs is primarily based on the common public radio interface (CPRI) [15], and the CPRI-associated bandwidth scales linearly with system bandwidth, antenna ports and sampling rate [7]. Unavoidably, the implementation of the newly defined mmWave RF spectrum [14] and/or massive-MIMO in an increased number of small cells greatly increases the involved antenna ports and the required sampling rate, thus leading to the CPRI bit rates well beyond the level that the current MFHs can cope with [7, 16]. Therefore, flexible MFHs capable of transparently supporting various data rates at arbitrary bandwidth granularity is vital for satisfying highly dynamic mobile traffic demands [17]. In addition, the low end-to-end latency required by 5G determines the maximum allowable MFH latency to be in the range of 250 μs [18]. For a 20 km MFH link, its corresponding signal propagation time takes up the majority of the MFH-induced latency, this means that the latency induced by the user equipment, base station signal processing and signal aggregation/deaggregation needs to be just a small fraction of the total MFH latency. To achieve such an objective, the use of

advanced DSP in transceivers, networking devices and network control is greatly advantageous. For example, DSP-based transceivers have been shown to have a round-trip processing latency of several microseconds [16]. On the other hand, the seamless convergence between independently developed/operated mobile networks and optical networks is also an effective way to reduce the end-to-end latency. Apart from the reduced latency, the convergence between MFHs/MBHs with optical access/metro networks further simplifies the overall network architecture, offers dynamic and wide bandwidth connectivity in a cost-effective manner [16, 19, 20], and also further improves the network flexbility [16].

Fig. 1.2 (a) and Fig. 1.2 (b) are the examples of current mobile and fixed network configurations, where MFH/MBH and optical access/metro networks are independently developed [21]. In 4G mobile networks, cloud radio access networks (C-RANs) [18, 22] are widely adopted, where a MFH connects remote radio heads (RRHs) and baseband units (BBUs), while a MBH links BBUs with the core network. To improve the signal processing centralization and traffic/network management efficiency, a BBU pool collocates BBUs by extracting baseband signal processing functions from distributed base stations (BSs) [23] while RRHs encompass the basic radio front-end functions such as MIMO precoding and

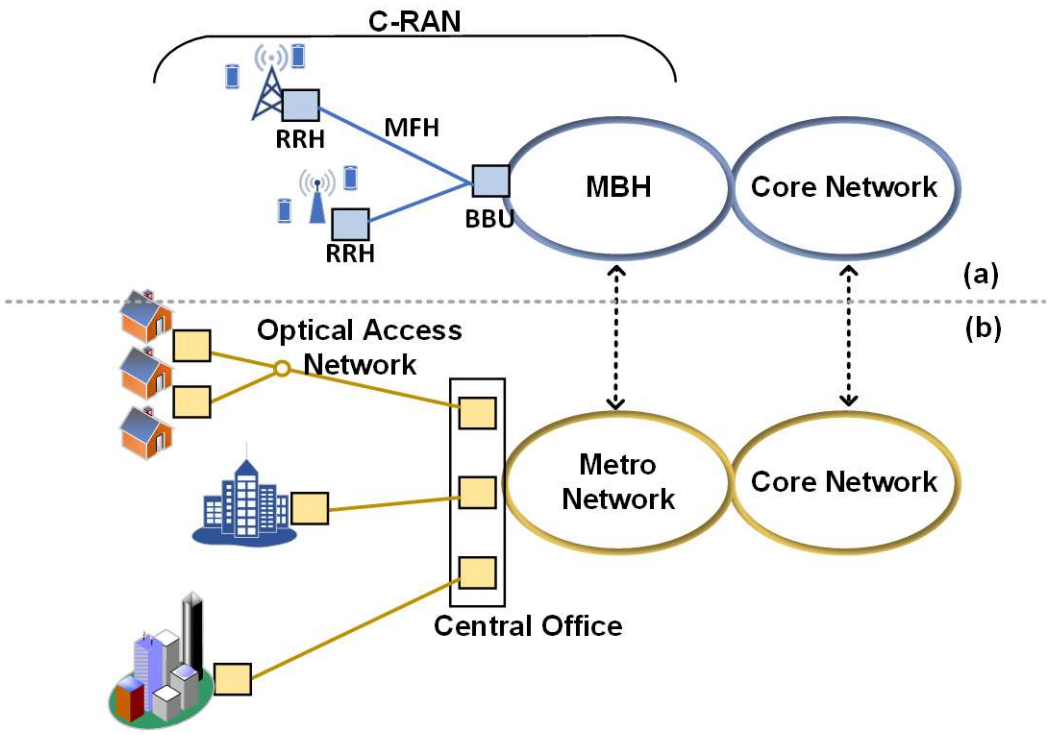

Fig. 1.2 An example of (a) mobile network architecture;(b) fixed network architecture.

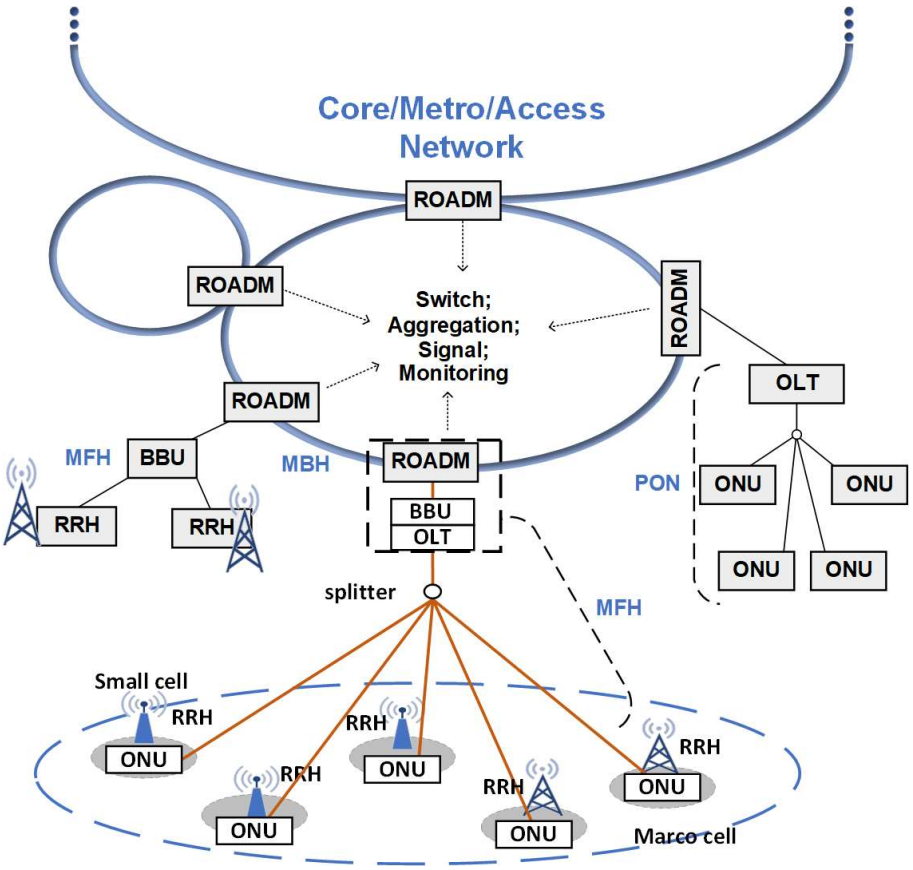

Fig.1.3 An example of the converged fixed-mobile network

resource mapping/demapping [24]. To cost-effectively realise the highly desirable optical access/metro network and MFH/MBH convergence, PONs have been considered as one of the most promising solutions [16, 19-25]. Generally speaking, a PON consists of an OLT at a service provider's central office and a number of ONUs connecting to end-users sharing the same fibre link by an optical splitter/coupler. To illustrate the utilization of the PON architecture to converge fixed-mobile networks, an example of a PON-based MFH [16, 19, 26] is presented in Fig. 1.3, where the OLT and the BBU can be integrated together to realise the joint signal processing procedures from the high layers down to the physical layer, whilst the ONUs connect the RRHs to transmit/receive signals from different end-users. Such a converged network helps to minimize the end-to-end latency by a number of ways, such as through the OLT and BBU collocation, which allows the synchronization of OLT and BBU scheduling mechanisms [19].

To deal with the dynamic traffic pattern associated with a large number of antenna sites in the converged networks, it is highly advantageous if the PON is equipped with sufficient flexibility, elasticity and dynamic reconfigurability. In particular, the PON must have not only strong adaptability to highly dynamic traffic with arbitrary signal bandwidth

granularity, but also excellent transparency to various traffic characteristics including signal modulation format and signal bit rate. To furthermore enhance and effectively deliver the desirable PON features, the implementation of software-defined networking (SDN) in PONs is also critical [27, 28], as SDN makes use of centralized network resource abstraction and network infrastructure virtualization to easily and dynamically reconfigure the networks across all the layers, thus improving network control functionalities and providing connection reconfigurations [29]. In addition, such SDN-based network operations are also capable of providing end-users with on-demand broadband connections/services each tailored to a specific application or service requirement [30]. Furthermore, the PON-based converged networks should also offer good backward compatibility with existing networks, such as OFDM-based 4G networks [30, 31]. Finally, to enhance the signal transmission capacity and compatibility to conventional optical access networks, it is envisaged that the PON-based converged networks may adopt wavelength division multiplexing (WDM) [33-34] in an approach recommended in NG-PON2 [35, 36].

From the practical implementation point of view, to enable the PON-based converged networks to simultaneously process the dynamic data traffic with variable signal bandwidths adopted in the mobile standards, the converged networks should be capable of not only dealing with highly dynamic traffic at wavelength, subwavelength, and sub-band levels, but also simultaneously accommodating a wide diversity of key network design features including, for example, various signal modulation formats, different signal detection schemes, flexible WDM-grids, diversified network topologies, and various multiple access techniques. As such, the dynamic provision of fast on-demand connections/services at wavelength, subwavelength, and sub-band levels is essential. Being one of the most important networking devices offering connectivity between an expanded number of individual optical networks, ROADMs with advanced configurations and flexible functionalities are thus expected to play a vital role in ensuring the achievement of the aforementioned networking features required by the converged networks [19, 32], while still satisfying reduced CapEx and OpEx. As an example shown in Fig. 1.3, multiple ROADMs can be interconnected in a ring network architecture to dynamically distribute the required network resources to various end-points [37].

In terms of the ROADM configurations, today, wavelength selective switch (WSS)-based ROADMs are widely deployed, which include a single WSS for each direction at a node.

This may limit wavelength/direction assignments and cause wavelength-contention conflicts [38]. And the new generation ROADMs have been developed with novel features in terms of colourlessness, directionlessness, contentionlessness and gridlessness [38-41]. However, all of these ROADMs utilise hard-wired switching element [42] operating at the wavelength level only, and they mainly target long-haul optical backbone networks. The above facts significantly limit the ROADM's upgradability, flexibility, cost-effectiveness and adaptability for use in the converged networks. On the other hand, to achieve the end-to-end low latency in a cost-effective manner, O-E-O free ROADM configurations are essential [40, 41]. Since conventional switches always involve O-E-O conversions and sophisticated data processing in the electrical domain, they are bulky, low speed, and high-power consumption, thus well beyond the acceptable level suitable for future converged networks. Therefore, O-E-O free, SDN-controllable ROADM configurations are highly desirable in implementing the converged networks.

Apart from the advanced network architecture and networking devices, as a direct result of the cost-sensitive scenario, the converged fixed-mobile networks also prefer the utilization of low-cost and low-complexity transceivers. One attractive approach is to use advanced modulation enabled by DSP to support high-speed transmissions with low-cost narrow-bandwidth optics [45]. In addition, the utilization of low-cost DACs/ADCs with low resolution are also preferred to reduce the total transceiver cost, but the effect of hardware impairments may result in transmission performance degradation [46]. In addition to that, to reduce the overall cost and transceivers complexity, IMDD is a preferred option compared to other electrical-to-optical/optical-to-electrical (E-O/O-E) conversions such as coherent modulation. However, the IMDD system nonlinearity [47-49] not only considerably degrade the transmission performance but also introduce significant cross channel interferences for multiple channel application scenarios. Thus, either an effective interference cancellation scheme or a new network architecture is required to relax the requirements on the hardware design.

To meet these challenges and fulfil the converged fixed-mobile networks for 5G scenario, this dissertation research proposes, for the first time, a series of novel techniques with potential for implementing the future converged 5G network: i) To improve the PON's reconfigurability, flexibility and elasticity, DFMA PONs have been proposed previously [50], however in practice, IMDD-based DFMA PONs suffer from cross-channel interference

induced by the signal generation, transmission, routing, traffic aggregation/de-aggregation and detection. In this thesis, a multiple channel interference cancellation technique in the IMDD DFMA PONs is thus proposed to improve the transmission performance [51]; ii) A low-cost flexible PON architecture termed hybrid OFDM-DFMA PON is proposed and explored [52], which can maintain highly desirable features associated with the DFMA PONs such as full support of SDN solution, high flexibility and transparency to underlying transmission technologies. More importantly, the proposed hybrid OFDM-DFMA PONs can improve the transmission performance and reduce the digital filter DSP complexity, thus leading a reduction in the transceiver cost; iii) As the hybrid OFDM-DFMA PONs suffer from OFDM-induced high PAPR, hybrid DFT-spread OFDM-DFMA PONs is proposed [53], which compared to hybrid OFDM-DFMA PONs, not only improves the transmission performance, but also relaxes the hardware requirements on DAC/ADC resolution bits; iv) To offer the seamless convergence of the fixed-mobile networks, DSP-enabled O-E-O free ROADMs [54, 55] are proposed and explored to provide dynamic connectivity at wavelength, sub-wavelength and sub-band levels. The proposed ROADMs have excellent transparency to a wide diversity of key network operation features. This dissertation work indicates that the abovementioned four techniques are promising for converged fixed-mobile 5G networks.

1.2 Major Achievements of the Dissertation Research

To address the technical challenges mentioned in subsection 1.1, this dissertation has proposed and explored the following novel techniques: the multiple channel interference cancellation of the IMDD-based DFMA PONs, low-cost flexible PONs termed hybrid OFDM-DFMA PONs and hybrid DFT-spread OFDM-DFMA PONs, as well as O-E-O free and SDN-controllable ROADMs.

- **Multiple Channel Interference Cancellation of Digital Filter Multiple Access PONs** [51]

To realise the seamless convergence of optical access/metro networks with MFHs/MBHs for 5G scenario, and also provide sufficient flexibility, elasticity, reconfigurability, DFMA PONs have been proposed [50], which utilise centralized SDN controller-managed, DSP-based, dynamic software-reconfigurable digital orthogonal filters to perform channel

multiplexing/demultiplexing. For the cost-sensitive IMDD DFMA PON application scenario, the involved digital orthogonal filters are embedded, in the digital domain, in each individual ONU and OLT without requiring any extra electrical and optical components. Thus, DFMA PONs allow multiple independent channels of arbitrary bandwidth granularity to dynamically share a common fibre transmission medium and other relevant network resources. In addition, DFMA PONs also possess the following salient operation features including, for example, i) DSP-enabled dynamic network reconfigurability, flexibility and elasticity, ii) inherent transparency to signal modulation format, signal bit rate, existing PON access techniques and network topologies, and iii) capability of SDN-based network abstraction and virtualization for all the layers including the physical layer. Therefore, the reported DFMA PONs not only offer excellent backward compatibility with existing PONs, but also have great potential for supporting converged networks.

However, the DFMA technique relies on maintaining a relatively high level of orthogonality between digital filters employed by various channels. For the IMDD DFMA PONs, the degradation of digital filtering-based channel orthogonality is unavoidable because of nonlinearities that may be encountered in signal generation, transmission, routing, traffic aggregation/de-aggregation and detection. Thus, the resulting imperfect channel orthogonality results in the IMDD DFMA PONs suffering from cross-channel interference, therefore the maximum achievable DFMA PON transmission performance is degraded. To address this challenge, a DCIC technique is proposed and extensively investigated to significantly improve the downstream and upstream performance of the IMDD DFMA PONs. The proposed DCIC technique utilises DSP-based and transceiver-embedded digital orthogonal filters to simultaneously receive various signals from different ONUs, based on which the interference experienced by each individual ONU is estimated and subsequently subtracted from the initially received signal of the same ONU. Finally, each individual signal with improved quality is demodulated in the receiver. This technique possesses advantages in transparency to modulation formats, signal bit rate and system/network initial conditions, thus giving rise to the improved DFMA PON's reconfigurability, flexibility and elasticity, the DCIC technique also has the unique features of ONU count-independent low DSP complexity and low-latency. As such the DCIC technique offers a promising solution for significantly reducing the DFMA PON interference for its applications in fixed-mobile network convergence.

- **Hybrid OFDM-Digital Filter Multiple Access PONs** [52]

In the IMDD DFMA PONs accommodating a large number of ONUs, the required parallel digital filters implemented in the OLT is proportional to ONU count, as a dedicated pair of a shaping filter (SF) and a matching filter (MF) is needed for each connection. Thus, the corresponding DSP implementation complexity and the network operational expenditure may have to increase with ONU count, this is highly undesirable for cost-sensitive PONs. To solve such a technical challenge, hybrid OFDM-DFMA PONs are proposed and investigated, where DSP-based software-reconfigurable digital filtering is employed for each individual OFDM signal from various ONUs, and a single FFT operation and its following data recovery processes are implemented in a pipelined approach in the OLT. As a direct result of combining both orthogonal frequency division multiple access (OFDMA) and DFMA PON characteristics, the proposed hybrid OFDM-DFMA PONs maintain highly desirable features associated with the DFMA PONs. More importantly, it offers a number of unique advantages including great relaxation of digital filter DSP complexity and considerable reduction in transceiver cost, significantly enhanced upstream PON performance and its robustness and flexibility, as well as excellent backward compatibility with existing OFDM-based 4G networks.

- **Hybrid DFT-spread OFDM-DFMA PONs** [53]

As the hybrid OFDM-DFMA PONs suffer from the OFDM-induced high PAPR. To mitigate this problem and relax the requirements on dynamic variation ranges of low-cost optical/electrical devices, hybrid DFT-spread OFDM-DFMA PONs are proposed, where DSP-based digital filtering is employed for individual DFT-spread OFDM signals from various ONUs, and a single FFT operation and its following data recovery processes are implemented in a pipelined approach in the OLT. As DFT-spread OFDM is utilized in 4G-based Long-Term Evolution (LTE) standards, it gives improved backward compatibility to the existing 4G networks. More importantly, in comparison to hybrid OFDM-DFMA PONs, the proposed PONs not only significantly improve the transmission performance but also reduce the transceiver DSP complexity because of the reduction in minimum required DAC/ADC bit resolution.

- **DSP-Enabled Flexible ROADMs Free from Optical Filters and O-E-O Conversions** [54, 55]

As wavelength-level switching adopted in conventional ROADMs has limitations on ROADM's upgradability and flexibility for providing dynamic connectivity for cost-sensitive converged 5G networks, a DSP-based flexible ROADM free from optical filters and O-E-O conversion with excellent adaptability and transparency to physical-layer network characteristics are proposed and evaluated. By utilizing Hilbert-pair-based digital filtering, the proposed flexible ROADMs not only is capable of dynamically and flexibly performing add/drop operations at wavelength, subwavelength, and spectrally overlapped orthogonal sub-band levels, but also has robustness against variations in modulation formats, transmission system characteristics/impairments.

The above dissertation research work has produced a total of 10 papers, of which as the first author, two papers have been published in Journal of Lightwave Technology, one paper in Journal of Optical Communications and Networking and one conference paper in CLEO/Europe of 2019. The remaining six papers are co-authored, including two in Journal of Lightwave Technology, two in Journal of Optical Communications and Networking, one in Photonics Journal and one conference paper in Optical Fiber Communications Conference and Exhibition of 2015.

1.3 Thesis Structure

This thesis is organized into seven chapters. The fundamental optical communication knowledge and a review of PONs/ROADMs are briefly introduced in chapter 2, and the work performed solely as part of this research is presented in chapters 3-6. These chapters are outlined as follows:

In chapter 2, the optical communications fundamentals including IMDD-based point-to-point transmission systems, various multiple access techniques, the PON architectures and ROADMs are reviewed, together with optical OFDM fundamentals for gaining a better understanding of the research work presented in the thesis.

Chapter 3 describes the multiple channel interference cancellation technique for the IMDD DFMA PONs. As IMDD-based DFMA PONs suffer from imperfect channel orthogonality-induced cross-channel interference, the DCIC technique is extensively investigated. A comprehensive DCIC theoretical model is developed, and through fitting with experimental measurements, the developed theoretical model is rigorously verified, and a set of accurate

transceiver/system parameters is identified. It is shown that DCIC increases the aggregated upstream signal transmission capacity by a factor of >2 and extends the differential ONU launch power dynamic range by approximately 14 dB. Such significant performance improvements are achieved after just one iteration. Other salient DCIC advantages include ONU count-independent low DSP complexity, small latency and transparency to signal modulation format, signal bit rate and initial system operation conditions.

Chapter 4 presents the hybrid OFDM-DFMA PONs, where DSP-based software-reconfigurable digital filtering is employed for each individual OFDM signal from various ONUs, and a single FFT operation and its following data recovery processes are implemented in a pipelined approach in the OLT. In this chapter, an analytical hybrid OFDM-DFMA PON model is developed, and numerical simulations are performed to verify the validity of the proposed technique and also to examine the upstream hybrid OFDM-DFMA PON performance characteristics over representative 25 km standard single mode fibre (SSMF) IMDD PON systems. It is shown that in comparison with the DFMA PONs, the hybrid OFDM-DFMA PON can improve the upstream ONU error vector magnitude (EVM) performance by >10 dB for relatively large received optical powers, and also increases the differential ONU launch power dynamic range by as much as 16 dB.

Chapter 5 introduces the hybrid DFT-spread OFDM-DFMA PONs, where DSP-based digital filtering is employed for individual DFT-spread OFDM signals from various ONUs, and a single FFT operation and its following data recovery processes are implemented in a pipelined approach in the OLT. A full theoretical analysis is undertaken with the differences between this technique and the hybrid OFDM-DFMA PONs being highlighted. The proposed networks maintain all salient features associated with previously reported hybrid OFDM-DFMA PONs, more importantly, they reduce the upstream signal PAPRs by ≥2 dB. As a direct result, in comparison with the hybrid OFDM-DFMA PONs, the proposed PONs increases the upstream system power budget by ≥3 dB and simultaneously reduce the minimum required DAC/ADC quantization bits by at least 1 bit.

In chapter 6, by utilizing Hilbert-pair-based digital filtering, intensity modulation and passive optical coupling, optical filter- and O-E-O conversion-free ROADMs with excellent flexibility, colourlessness, gridlessness, contentionlessness, adaptability, and transparency to physical-layer network characteristics are proposed and evaluated. Extensive numerical simulations are undertaken to explore the operation characteristics of the proposed

ROADMs in IMDD-based optical network nodes. It is shown that the add/drop operation performance is independent of the signal's location in the digital filtering space. In addition, the results also indicate that the drop operation introduces 3 dB optical power penalties, while the optical power penalties induced by the add operation can be 3.5 dB. Furthermore, the results show that the proposed flexible ROADMs not only enable to dynamically and flexibly perform add/drop operations at wavelength, subwavelength, and spectrally overlapped orthogonal sub-band levels, but also have excellent robustness against variations in modulation formats, transmission system characteristics/impairments.

Chapter 7 summarizes the thesis and possible future research topics are also suggested.

References

[1] "Cisco Visual Networking Index: Global Mobile Data Traffic Forecast Update, 2016–2021 White Paper - Cisco." [Online]. Available: https://www.cisco.com/c/en/us/solutions/collateral/service-provider/visual-networking-index-vni/mobile-white-paper-c11-520862.html.

[2] IEEE, "IEEE 5G and Beyond Technology Roadmap White Paper," [Online]. Available: https://futurenetworks.ieee.org/images/files/pdf/ieee-5g-roadmap-white-paper.pdf

[3] E. Dahlman, Mildh. G, and S. Parkvall, et al., "5G Wireless Access: Requirements and Realization," *IEEE Commun. Mag.*, vol. 52, no. 12, pp. 42–47, 2014.

[4] ITU-R, "IMT Vision-Framework and Overall Objectives of the Future Development of IMT for 2020 and Beyond," [Online]. Available: https://www.itu.int/dms_pubrec/itu-r/rec/m/R-REC-M.2083-0-201509-I!!PDF-E.pdf

[5] Next Generation Mobile Networks Alliance, "5G White Paper," [Online]. Available: https://www.ngmn.org/5g-white-paper/5g-white-paper.html

[6] ITU, "Minimum Requirements Related to Technical Performance for IMT-2020 Radio Interface(s)," [Online]. Available: https://www.itu.int/pub/R-REP-M.2410-2017

[7] L. M. Horowitz and S. Strack, "5G: A Tutorial Overview of Standards, Trials, Challenges, Deployment, and Practice," *J. Sel. areas Commun.*, vol. 35, no. 6, pp. 1201–1221, 2017.

[8] O. Semiari, W. Saad, and M. Bennis, et al., "Integrated Millimeter Wave and Sub-6 GHz Wireless Networks : A Roadmap for Joint Mobile Broadband and Ultra-Reliable Low-Latency Communications," *IEEE Wirel. Commun.*, vol. 26, no. 2, pp. 109–115, 2019.

[9] X. Gao, L. Dai, and A. M. Sayeed, "Low RF-Complexity Technologies to Enable Millimeter-Wave MIMO with Large Antenna Array for 5G Wireless Communications," *IEEE Commun. Mag.*, vol. 56, no. 4, pp. 211–217, 2018.

[10] S. A. Busari, K. Huq and S. Mumtaz, et al., "Millimeter-Wave Massive MIMO Communication for Future Wireless Systems : A Survey," *IEEE Commun. Surv. Tutorials*, vol. 20, no. 2, pp. 836–869, 2018.

[11] M. Mezzavilla, M. Zhang, M. Polese, et al., "End-to-End Simulation of 5G mmWave Networks," *IEEE Commun. Surv. Tutorials*, vol. 20, no. 3, pp. 2237–2263, 2018.

[12] "3GPP Specification Series: 38series." [Online]. Available: https://www.3gpp.org/DynaReport/38-series.htm.

[13] V. Jungnickel, K. Manolakis, W. Zirwas, et al., "The Role of Small Cells, Coordinated Multipoint, and Massive MIMO in 5G," *IEEE Commun. Mag.*, vol. 52, no. 5, pp. 44–51, 2014.

[14] D. Muirhead, M. A. L. I. Imran, and K. Arshad, et al., "A Survey of the Challenges , Opportunities and Use of Multiple Antennas in Current and Future 5G Small Cell Base Stations," *IEEE Access*, vol. 4, pp. 2952–2964, 2016.

[15] "Common Public Radio Interface (CPRI); Interface Specification V7.0," [Online]. Available: http://www.cpri.info/downloads/CPRI_v_7_0_2015-10-09.pdf

[16] X. Liu and F. Effenberger, "Emerging Optical Access Network Technologies for 5G Wireless," *J. Opt. Commun. Netw.*, vol. 8, no. 12, pp. B70–B79, 2016.

[17] J. E. Mitchell, "Integrated Wireless Backhaul over Optical Access Networks," *J. Light. Technol.*, vol. 32, no. 20, pp. 3373–3382, 2014.

[18] Next Generation Mobile Networks Alliance, "Further Study on Critical C-RAN Technologes," [Online]. Aavailable: https://www.ngmn.org/publications/all-downloads.html?tx_news_pi1%5Bnews%5D=637&cHash=530691e981def635c13badd861fbf5f7

[19] M. Ruffini, "Multidimensional Convergence in Future 5G Networks," *J. Light. Technol.*, vol. 35, no. 3, pp. 535–549, 2017.

[20] P. T. Dat, A. Kanno, and N. Yamamoto, et al., "Seamless Convergence of Fiber and Wireless Systems for 5G and Beyond Networks," *J. Light. Technol.*, vol. 37, no. 2, pp. 592-605, 2018.

[21] A. Otaka, J. Terada, J. Kani, and K.-I. Suzuki, "Solutions for Future Mobile Fronthaul and Access-Network Convergence," *J. Light. Technol.*, vol. 35, no. 3, pp. 527–534, 2017.

[22] D. H. Hailu, B. G. Gebrehaweria, and S. H. Kebede, et al., "Mobile Fronthaul Transport Options in C-RAN and Emerging Research Directions : A Comprehensive Study," *Opt. Switch. Netw.*, vol. 30, pp. 40–52, 2018.

[23] I. A. Alimi, A. L. Teixeira, and P. P. Monteiro, "Toward an Efficient C-RAN Optical Fronthaul for the Future Networks: A Tutorial on Technologies, Requirements, Challenges, and Solutions," *IEEE Commun. Surv. Tutorials*, vol. 20, no. 1, pp. 708–769, 2018.

[24] C. Ranaweera, E. Wong, and A. Nirmalathas, et al., "5G C-RAN Architecture: A Comparison of Multiple Optical Fronthaul Networks," *Int. Conf. Opt. Netw. Des. Model.*, pp. 1–6, 2017.

[25] N. P. Anthapadmanabhan, A. Walid, and T. Pfeiffer, "Mobile Fronthaul over Latency-optimized Time Division Multiplexed Passive Optical Networks," in *IEEE International Conference on Communication Workshop*, 2015.

[26] T. Pfeiffer, "Next Generation Mobile Fronthaul and Midhaul Architectures [Invited]," *J. Opt. Commun. Netw.*, vol. 7, no. 11, pp. B38–B45, 2015.

[27] P. Chanclou, L. Anet Neto, and K. Grzybowski, et al., "Mobile Fronthaul Architecture and Technologies: A RAN Equipment Assessment [Invited]," *J. Opt. Commun. Netw.*, vol. 10, no. 1, pp. A1–A7, 2018.

[28] I. Chih-Lin, H. Li, and J. Korhonen, et al., "RAN Revolution with NGFI (xhaul) for 5G," *J. Light. Technol.*, vol. 36, no. 2, pp. 541–550, 2018.

[29] N. Cvijetic, "Optical Network Evolution for 5G Mobile Applications and SDN-based Control," in *Proc. 16th Int. Telecommun. Netw. Strateg. Plan. Symp. Networks*, 2014.

[30] N. Cvijetic, "Software-defined Optical Access Networks for Multiple Broadband Access Solutions," in *Proc. OptoElectro. and Commun. Conf. with Inter. Conf. Photonic. in Switch.*, 2013.

[31] K. Habel, M. Koepp, and S. Weide, et al., "100G OFDM-PON for Converged 5G Networks: From Concept to Real-Time Prototype," in *Proc. Opt. Fiber Commun. Conf. Nat. Fiber Optic Eng. Conf.*, 2017.

[32] D. Nesset, "PON Roadmap [Invited]," *J. Opt. Commun. Netw.*, vol. 9, no. 1, pp. A71–A76, 2017.

[33] E. Harstead, D. Van Veen, and V. Houtsma, et al., "Technology Roadmap for Time-division Multiplexed Passive Optical Networks (TDM PONs)," *J. Light. Technol.*, vol. 37, no. 2, pp. 657–664, 2019.

[34] J. Terada, J. Kani, and S.Y. Kim, et al., "Software Implementation of 10G-EPON Upstream Physical-Layer Processing for Flexible Access Systems," *J. Light. Technol.*, vol. 37, no. 6, pp. 1631–1637, 2019.

[35] D. A. Khotimsky, "NG-PON2 Transmission Convergence Layer: A Tutorial," *J. Light. Technol.*, vol. 34, no. 5, pp. 1424–1432, 2016.

[36] S. Gosselin, A. Pizzinat, and X. Grall, et al., "Fixed and Mobile Convergence: Which Role for Optical Networks?," *J. Opt. Commun. Netw.*, vol. 7, no. 11, pp. 1075–1083, 2015.

[37] R. Giddings, X. Duan, and E. Al-Rawachy, et al., "A Review of DSP-based Enabling Technologies for Cloud Access Networks," *Futur. Internet*, vol. 10, no. 11, 2018.

[38] S. Perrin, "Next-Generation ROADM Architectures & Benefits," *Heavy Reading White Paper,* [online] Available: www.fujitsu.com/us/Images/Fujitsu-NG-ROADM.pdf.

[39] W. I. Way, "Optimum Architecture for M × N Multicast Switch-Based Colorless ,and Flexible-Grid ROADM," in *Proc. Opt. Fiber Commun. Conf. Nat. Fiber Optic Eng. Conf.*, 2012.

[40] A. Peters, E. Hugues-Salas, and M. Gunkel, et al., "Key Performance Indicators for Elastic Optical Transponders and ROADMs: the Role of Flexibility," *Opt. Switch. Netw.*, vol. 25, pp. 1–12, 2017.

[41] S. Thiagarajan and S. Asselin, "Nodal Contention in Colorless, Directionless ROADMs using Traffic Growth Models," *in Proc. Opt. Fiber Commun. Conf. Nat. Fiber Optic Eng. Conf.*, 2013.

[42] A. Muhammad, G. Zervas, and G. Saridis, et al., "Flexible and Synthetic SDM Networks with Multi-core-fibers Implemented by Programmable ROADMs," in *Proc.Eur. Conf. Opt. Commun.*, 2014.

[43] S. Zhang, M. Tornatore, and G. Shen, et al., "Evolving Traffic Grooming in Multi-layer Flexible-grid Optical Networks with Software-defined Elasticity," *J. Light. Technol.*, vol. 32, no. 16, pp. 2905–2914, 2014.

[44] Y. Xiong, F. G. de Magalhães, and G. Nicolescu, et al., "Co-design of a Low-latency Centralized Controller for Silicon Photonic Multistage MZI-based Switches," in *Proc. Opt. Fiber Commun. Conf. Nat. Fiber Optic Eng. Conf.*, 2017.

[45] H. Zeng, X. Liu, and S. Megeed, et al., "Digital Signal Processing for High-Speed Fiber-Wireless Convergence [Invited]," *J. Opt. Commun. Netw.*, vol. 11, no. 1, p. A11, 2019.

[46] K. N. Pappi and G. K. Karagiannidis, "Interference Mitigation Techniques for Wireless Networks," *Key Technol. 5G Wirel. Syst.*, pp. 214–235, 2017.

[47] M. Applications and T. Zuo, "IM/DD Transmission Techniques for Emerging 5G," *J. Light. Technol.*, vol. 36, no. 2, pp. 560–567, 2018.

[48] H. Y. Chen, C. C. Wei, and Y. C. Chen, et al., "50-Gbps 100-km EAM-based OFDM-IMDD Transmission Employing Novel SSII Cancellation," in *Proc. Opt. Fiber Commun. Conf. Nat. Fiber Optic Eng. Conf.*, 2014.

[49] F. Boccardi, R. Heath, and A. Lozano, et al., "Five Disruptive Technology Directions for 5G," *IEEE Commun. Mag.*, vol. 52, no. 2, pp. 74–80, 2014.

[50] M. Bolea, R. P. Giddings, and M. Bouich, et al., "Digital Filter Multiple Access PONs With DSP-Enabled Software Reconfigurability," *J. Opt. Commun. Netw.*, vol. 7, no. 4, pp. 215–222, 2015.

[51] Y. Dong, E. Al-Rawachy, and R. P. Giddings, et al., "Multiple Channel Interference Cancellation of Digital Filter Multiple Access PONs," *J. Light. Technol.*, vol. 35, no. 1, pp. 34–44, 2016.

[52] Y. Dong, R. P. Giddings, and J. Tang, "Hybrid OFDM-Digital Filter Multiple Access PONs," *J. Light. Technol.*, vol. 36, no. 23, pp. 5640–5649, 2018.

[53] Y. Dong, W Jin, and R. P. Giddings, et al., "Hybrid DFT-Spread OFDM-Digital Filter Multiple Access PONs for Converged 5G Networks," *J. Opt. Commun. Netw.*, vol. 11, no. 7, p. 347–353, 2019.

[54] W. Jin, X. Duan, and Y. Dong et al., "DSP-Enabled Flexible ROADMs Without Optical Filters and O-E-O Conversions," *J. Light. Technol.*, vol. 33, no. 19, pp. 4124–4131, 2015.

[55] W. Jin, C. Zhang, and X. Duan, et al., "Improved Performance Robustness of DSP-Enabled Flexible ROADMs Free from Optical Filters and O-E-O Conversions," *J. Opt. Commun. Netw.*, vol. 8, no. 8, pp. 521–529, 2016.

2. Converged Network Fundamentals

Contents

This chapter provides the fundamental elements involved in the converged fixed-mobile networks, including IMDD-based point-to-point optical transmission systems, PONs and ROADMs, as well as optical OFDM principles.

2.1 IMDD-based Point-to-Point Transmission Systems

A typical PON transmission system consists of an optical transmitter, an optical receiver, and optical fibres as a communication channel. The role of the optical transmitter is to modulate an electrical signal into an optical signal, and the optical receiver converts the transmitted optical signal into an electrical signal. There are mainly two schemes of optical modulation (detection), i.e. intensity modulation and coherent modulation (direct detection and coherent detection). Since coherent modulation/detection requires expensive and complex optical modulators/detectors, for the cost-effective scenarios of interest of the thesis, IMDD is thus considered throughout this work.

2.1.1 Optical Transmitter

The general principle of optical intensity modulation is that the intensity or the power of a laser light source is modulated by the amplitude of an electrical signal without taking into account the phase information. Considering $A_{ele}(t)$ is the electrical signal biased with the direct current, $A_{ele}(t) > 0$, the optical signal produced by an ideal intensity modulator (IM) can be expressed as:

$$E_{opt}(t) = e^{j2\pi f_0 t} \cdot \sqrt{A_{ele}(t)} \tag{2.1}$$

where f_0 is the optical carrier frequency. Two techniques including direct modulation and external modulation can be used to generate the optical signal, as discussed below.

2.1.1.1 Direct Modulation

Semiconductor lasers are utilized in the direct optical modulation, where the laser driving current originated from an electrical signal changes the intensity of the emitted optical wave. An example of output power of directly modulated distributed feedback laser (DFB) laser (DML) versus the driving current is shown in Fig. 2.1 [1]. In a DML, the optical signal generation and modulation are functionally undertaken within a single device, thus yielding

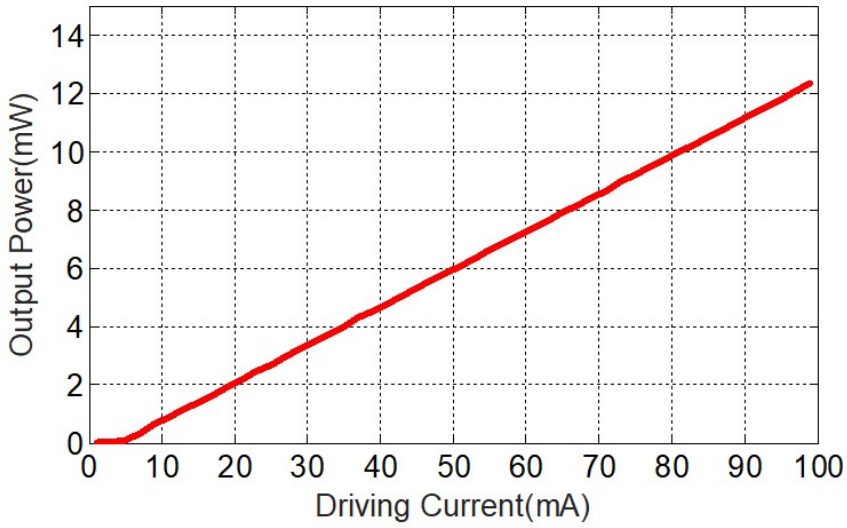

Fig. 2.1 Output power versus the driving current of DML

the simplest and most compact transmitter, as such DMLs are the most commonly used devices in optical transmission systems for the cost-effective scenarios. One of the main operation characteristics of a DML is its 3-dB modulation bandwidth, which is defined as the frequency range over which the power of the transfer function $|H(\omega)|$ is reduced by 3 dB compared with its direct-current (DC) value [2]. Nowadays DMLs with modulation bandwidths of up to 18 GHz are commercially available and modulation bandwidths as high as 59 GHz have also been experimentally demonstrated in research labs [3, 4]. The main drawback of DMLs for high bit rate intensity-modulated transmission over long distances is their inherent frequency chirp, i.e., a residual unwanted data-dependent phase modulation accompanying the desired intensity modulation. Laser chirp broadens the optical signal spectrum, thus leading to increased signal distortions caused by the interaction with fibre chromatic dispersion (CD) and/or fibre nonlinearity [5-7].

2.1.1.2 External Modulation

For high bit rates and long fibre transmission distances, frequency chirps imposed by direct modulation become too large, thus DMLs are not commonly used. For high-speed transmitters, the laser is biased at a constant current to provide the continuous wave (CW) output, and an optical modulator placed next to the laser converts the CW light into a data-coded optical signal [2]. There are two types of external modulator, one is the electroabsorption-modulated laser (EML) formed by an electroabsorption modulator (EAM). Similar to DFBs, EAMs produce some residual and component-specific chirp, which can be used to increases the uncompensated reach of EAM-based transmitters through

counteract with CD [8]. EAMs are attractive because of their small size and integration capabilities with lasers to form EMLs. Another type is the Mach-Zehnder modulator (MZM), using two-branch Mach-Zehnder interferometer to modulate the phase of the optical signal passing through each individual branch [9]. An MZM is able to produce pure amplitude modulation without residual chirp if its two branches are driven with opposite-sign ("differential") driving signals, typically referred to as the "push-pull" operation. The MZMs offer better modulation performance with negligible chirp compared with the DMLs and EMLs, but MZMs have higher device/system complexity and cost, thus it may not be the optimum option for cost-sensitive application scenarios.

2.1.2 Optical Fibre

Optical fibre is a physical media for optical transmission, where the light transmits along its axis due to the total internal reflection between the core and cladding, as the refractive index of the core is greater than that of the cladding. In a single-mode fibre (SMF), which has a small core diameter typically around 8.2-10 μm [10], light can only propagate in one mode, while in a multi-mode fibre (MMF), which has a large core diameter such as 50 μm or 62.5 μm, light can propagate in multiple modes. Since multiple modes will introduce mode delay, resulting in limitations on transmission bandwidth, capacity and distances. Thus SMF is considered throughout the thesis.

2.1.2.1 Fibre Loss

When transmitted through SMFs, the optical signal power is attenuated by fibre loss, which can be described by Eq. (2.2):

$$P_{out} = P_{in} - \alpha L \tag{2.2}$$

where α is the attenuation coefficient and expressed in a unit of dB/km, P_{in} is the fibre input optical power while P_{out} is the fibre output optical power, and L is the fibre length. Rayleigh scattering and material absorption are the main physical mechanisms causing fibre attenuation, and such mechanisms are dependent on the optical wavelength. For the commercially available SMFs, the fibre loss occurs in the C-band (1.53 μm-1.565 μm) with typical value of 0.2 dB/km, an example of wavelength-dependent attenuation coefficient of commercial available SSMF is shown in Fig. 2.2 [10].

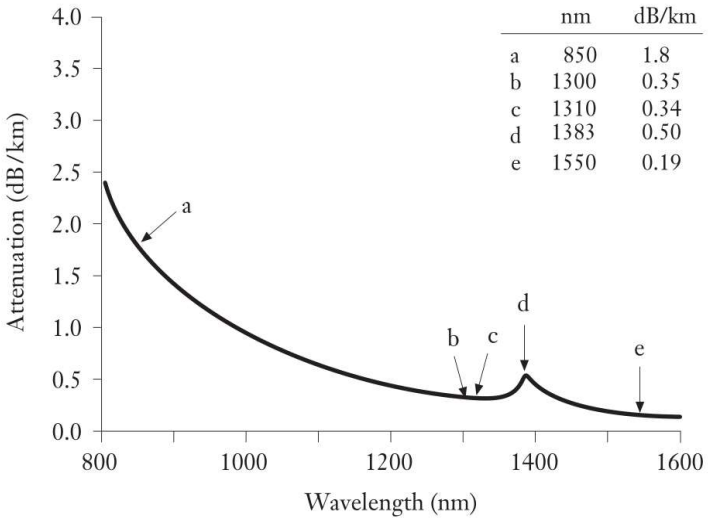

Fig. 2.2 Corning SMF-28 spectral attenuation [10]

2.1.2.2 Chromatic Dispersion

CD is caused by frequency dependence of the refractive index of an optical fibre, and the different frequency components within an optical signal travel at different velocities, resulting in optical signal broadening. When the neighbouring signals cross their allocated time slots, inter-symbol interference (ISI) occurs, therefore limiting the maximum achievable signal transmission bit rates [11]. Assuming $\Delta\lambda$ is the frequency difference of an optical signal, the resulting time delay ΔT for a SMF of length L is given by:

$$\Delta T = DL\Delta\lambda \tag{2.3}$$

where D is the dispersion parameter, defined as $D = d\beta_1/d\lambda$, $\beta_1 = c/n_g$ representing the group velocity, with c being the light speed in vacuum and n_g being the group index [12]. The dispersion parameter D is also used in practise and related to the group-velocity dispersion (GVD) parameter β_2, which satisfies Eq. (2.4)

$$D = \frac{d\beta_1}{d\lambda} = -\frac{2\pi c}{\lambda^2}\beta_2 = -\frac{\lambda}{c}\frac{d^2n}{d\lambda^2} \tag{2.4}$$

Fig. 2.3 shows the dispersion parameter of the commercially available SSMF [10], where the zero-dispersion wavelength is around 1310 nm, and in C-band at 1550 nm the corresponding dispersion parameter is around 17 ps/km/nm, which is located in the

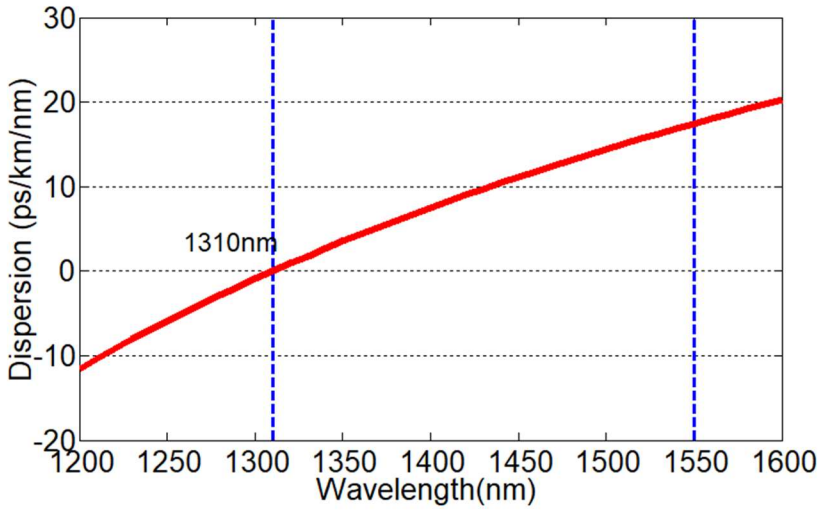

Fig. 2.3 A typical SSMF dispersion parameter

anomalous dispersion regime ($\beta_2 < 0$). Although different types of fibres can have different dispersion parameters, such as dispersion shifted fibre and flat dispersion fibre [13], and they can be used to reduce the dispersion-induced transmission performance degradation, and such fibres are not considered in this thesis. It is noted that in IMDD transmission system, the CD will induce channel fading effect [14]. If only CD effect with the dispersion parameter of 17 ps/km/nm at 1550 nm is considered, for a typical transmission distance of 25 km in optical networks, the first frequency null occurs around 12 GHz [14], and such frequency null may limit the transmission performance of IMDD system.

2.1.2.3 Fibre Nonlinearity

When light propagates through an optical fibre, the electric field of the light can modify the physical properties of the medium. The effect gives rise to fibre nonlinearity, which affects the power and phase of the optical signal when traveling through the SMF. There are two major groups of fibre nonlinearity related either to nonlinear refractive index (Kerr effect) or nonlinear optical scattering.

The category that transfer energy from the optical field to the medium via stimulated inelastic scattering, includes stimulated Brillouin scattering (SBS) and stimulated Raman scattering (SRS). The main difference between these two is that optical phonons participate in SRS while acoustic phonons participate in SBS, both of which result in optical signal power loss and frequency shifts. In SMF transmissions SBS produces back-scattered light downshifted

frequency around 11 GHz, whereas SRS produces both forward and back propagating light as wide as 15 THz [12]. And in SMF transmissions the threshold optical power of SBS is around a few dBm while the threshold value of SRS is around 27 dBm. Therefore, for transmission systems studied in this thesis, SBS may be a detrimental under the condition of a high optical launch power while SRS can be negligible under the typical incident power level.

The Kerr effect occurs due to the dependence of the refractive index on light intensity, and fibre nonlinearities belonging to this category are self-phase modulation (SPM), cross-phase modulation (XPM) and four-wave mixing (FWM). SPM refers to the self-induced phase shift experienced by an optical field during its propagation in an optical fibre, and the nonlinear phase shift imposed on the optical field is proportional to optical intensity, resulting in SPM-induced optical frequency chirp. This increases the spectral width of the pulse [13]. When the normal dispersion of a SMF interacts with the SPM-induced chirp, the optical pulse is broadened as it propagates along the fibre, thus leading to signal distortions. Therefore, SPM is undesirable and needs to be taken into account in the dispersion management of the fibre link. It is also worth mentioning that in IMDD transmission systems, the channel fading effect induced by CD, as mentioned in subsection 2.1.2.2, can be relaxed by SPM when high optical power levels (6 dBm≤ $P_{optical\ power}$ ≤18 dBm) [14] are applied,

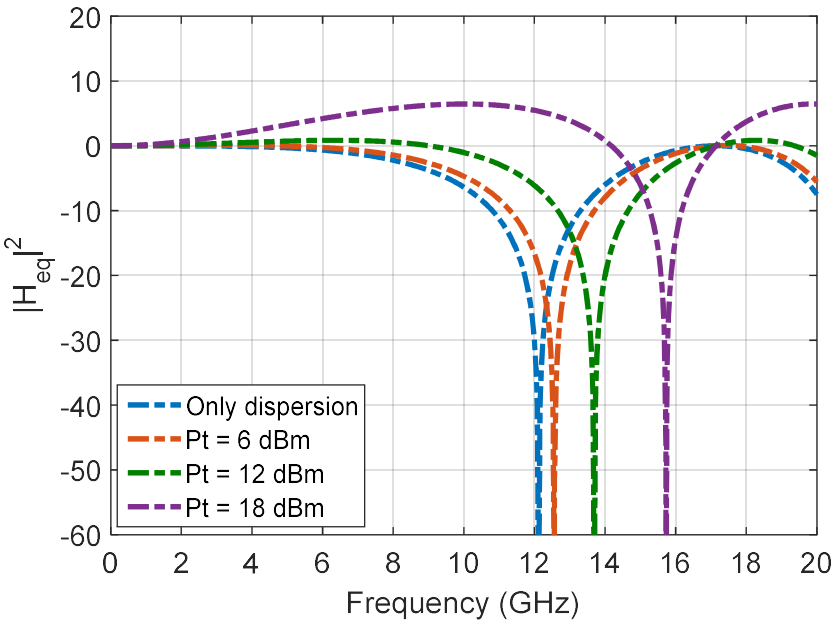

Fig. 2.4 The theory analysis of channel frequency responses of a 25 km SSMF IMDD PON system for various optical launch powers.

this is because SPM shifts the system frequency response null towards the high frequency side (beyond the signal spectral region), as shown in Fig. 2.4.

XPM is generated by the same physical mechanism as SPM, in which the refractive index changes due to variations in power not only in the observed channel but also due to variation in powers of other wavelength channels, thus leading to signal distortions. Similar to SPM, XPM also causes great temporal broadening as the signal propagates along the fibre due to the effect of CD. FWM is another phenomenon caused by Kerr effect, in which multiple signals at different wavelengths interfere and generate refractive index gratings, such gratings interact with the signals and produce new frequencies. This effect occurs only when phase matching between propagating signals is achieved, thus FWM can be reduced either by reducing the power per channel or by preventing the perfect phase matching through increasing the CD or increasing the channel spacing.

For the transmission systems considered in this dissertation research, the XPM and FWM effects are negligible due to relatively small optical launch power levels.

2.1.3 Optical Receiver

In the optical receiver, the transmitted optical signal is detected by a photodetector, which converts the optical signal into the electrical domain. The commercially available photodetectors are PIN photodiode and avalanche photodiode (APD), both of them utilize photodiode to convert the incident optical power P_{in} into the electric current I_p, based on square-law detection as shown in Eq. (2.5)

$$I_p = RP_{in} = R \cdot EE^* \tag{2.5}$$

where $R(A/W)$ refers to the photodiode responsivity, which is related to the quantum efficiency, E is the received optical signal. Such detection is also called direct detection. In practise, two fundamental noise mechanisms including shot noise and thermal noise, cause fluctuations in the generated current I_p even when P_{in} is constant. Thus, the total current I_p can be modified to Eq. (2.6)

$$I = I_p + I_s + I_t \tag{2.6}$$

where I_s and I_t are the are the current fluctuation induced by shot noise and thermal noise respectively, and they are independent random processes with approximately Gaussian statistics.

2.1.3.1 Shot Noise

Shot noise accompanies any generated current within a photodetector and is related to the statistical nature of the carrier transport and the photon detection process. The mean square noise current of shot noise for a photodiode is given by [11]

$$\langle {I_s}^2 \rangle = 2qI_p\Delta f \tag{2.7}$$

where $\langle \cdot \rangle$ refers to mean operator, q is the electron charge, Δf is the signal bandwidth.

2.1.3.2 Thermal Noise

The thermal noise is due to the thermal motion of electrons in conductors and is generated in all resistances of the photodiode. The mean square thermal noise current of a resistor R for a given bandwidth Δf is given by [11]

$$\langle {I_t}^2 \rangle = {4kT\Delta f}/{R} \tag{2.8}$$

where k is Boltzmann's constant and T is the temperature. It is worth noting that $\langle {I_t}^2 \rangle$ does not depend on the photocurrent whereas $\langle {I_s}^2 \rangle$ does. When the injected optical power is small, the thermal noise effect is dominant. The receiver sensitivity $P_{R,PIN}$ for a PIN photodiode can be expressed as [11]:

$$P_{R,PIN} \approx {I_t Q}/{R} = {Q\sqrt{4kT\Delta f}}\Big/{\sqrt{R}} \tag{2.9}$$

where Q is the Q-factor corresponding to bit error rate (BER).

2.2 Passive Optical Networks

Passive Optical Networks (PONs) is a type of point-to-multipoint network standardised by ITU-T and IEEE. From the architecture point of view, a PON consists of three main parts:

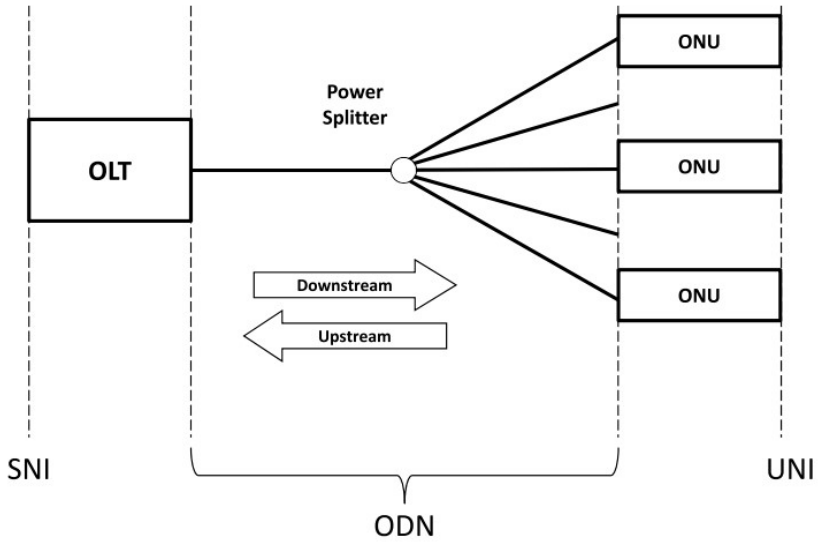

Fig. 2.5 General PON architecture. SNI: service node interface (interface to the metro/core network); UNI: user network interface (interface to the user network) [15]

- Optical Line Terminal (OLT): The OLT is located at the service provider's central office, providing the interface between the access network and the metro/core network. The OLT is also responsible for the enforcement of any media access control (MAC) protocols for upstream bandwidth arbitration.
- Optical Network Unit (ONU): The ONUs are located near end-users, providing the service interface to the end-users through cooperating with the OLT in order to control and monitor all transmissions.
- Optical Distribution Network (ODN): The ODN consists of feeder, distribution fibres and passive optical distribution elements such as splitters/couplers, and the splitting ratio in most cases is between 1:8 and 1:128.

A typical PON architecture is shown in Fig. 2.5 [15], which support bidirectional transmission with downstream and upstream traffic. Since active equipments are eliminated in this architecture, the impact of active equipment failures on the entire network, the total electrical consumption and storage space are reduced, thus the PON provides a cost-effective solution for the optical networks. In addition, the power splitter can be placed anywhere along the fibre link, bringing more topological flexibility. In the downstream direction, the OLT transmits data frames to all connected ONUs over a shared optical fibre network. While in the upstream direction, the OLT schedules ONU transmissions to avoid collisions between ONUs through different access technologies, which include time division multiple access (TDMA), wavelength division multiple access (WDMA), frequency division multiple access

(FDMA). The PON's efficient use of fibre resources and central office equipment, space and power lead to its large-scale deployment worldwide [16]. In the vast majority of deployed PONs, TDMA is widely implemented, which will be introduced in detail in the following subsection.

2.2.1 PON Technology

In this subsection, different access technology-based PON architectures are presented, including TDMA PONs and WDMA PONs, hybrid TDMA/WDMA PONs, and OFDMA PONs, as well as DFMA PONs.

2.2.1.1 TDMA PONs

Fig. 2.6 illustrates a typical TDMA PON, where different time slots are utilized to multiplex/demultiplex signal channels to/from different ONUs. The downstream transmission is point to multipoint, where the traffic is continuously broadcast to all ONUs, and each ONU selects the packets addressed to it and discards the packets addressed to other ONUs. In the upstream link, the bandwidth is shared by various ONUs through TDMA, where each ONU transmits data only during the time slots that are allocated by the OLT. Normally, separate wavelength bands are utilized to carry downstream and upstream traffic, respectively. Such PON architecture has been widely deployed, and the corresponding standards at the gigabit rates are ITU's Gigabit PON (GPON), and the IEEE's Ethernet PON (EPON) or GEPON, which is Gigabit Ethernet over PONs [19-21].

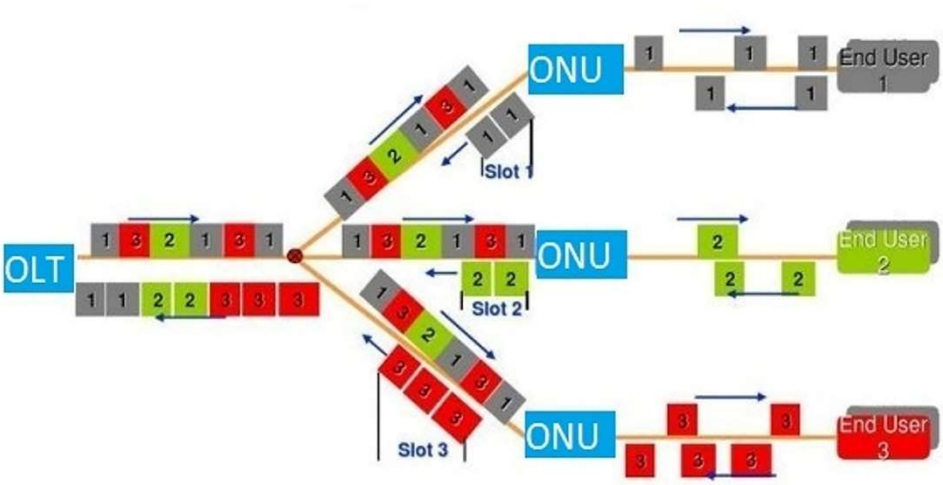

Fig. 2.6 A typical structure of a TDMA PON

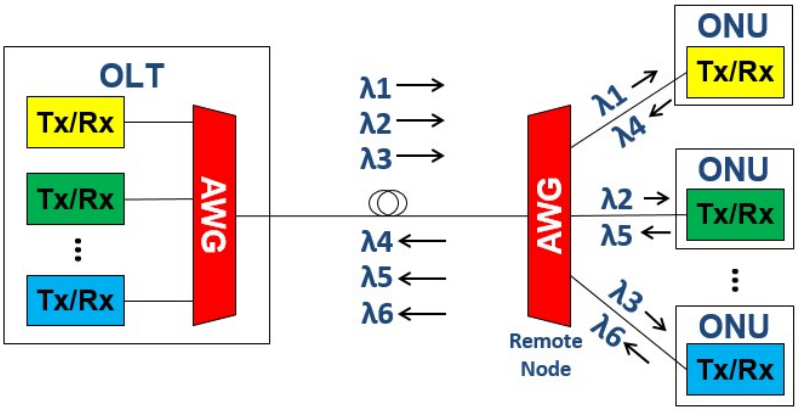

Fig. 2.7 A general WDMA PON architecture

2.2.1.2 WDMA PONs

Fig. 2.7 shows an example of a WDMA PON architecture, where different wavelengths are utilized to multiplex/demultiplex signal channels to/from different ONUs. In the downstream direction, the signals in OLT are individually modulated onto different wavelengths before being multiplexed with an arrayed waveguide grating (AWG) to form a combined WDM signal. And at the remote node another AWG is also employed to separate each individual wavelength, which can be directed to corresponding ONU. In the upstream, each individual ONU generates different wavelength to carry its signal, and these signals from different ONUs are aggregated into WDM signals by the AWG located at the remote node. The receiver in the OLT demultiplexes the received WDM signal using the OLT-embedded AWG and a photodetector array. Due to multiple wavelengths utilized in WDMA PONs, the capacity and flexibility can be increased compared to TDMA PONs. However, their high costs are the major obstacle limiting their practical application in PONs, as either an expensive tuneable laser with a wide detuning range is needed for each ONU, or a broadband optical source array is required at the OLT and/or ONU [22,23].

2.2.1.3 Hybrid TDMA/WDMA PONs

The combination of TDMA and WDMA in a hybrid TDMA/WDMA PON or hybrid TWDM PON could be a cost-effective way of introducing both TDMA and WDMA into an access network. In the hybrid TDMA/WDMA PON shown in Fig. 2.8 [22], one individual wavelength is used in each direction for communications between the OLT and ONU, and each wavelength can also be shared among several ONUs by using TDMA, thus the ONU

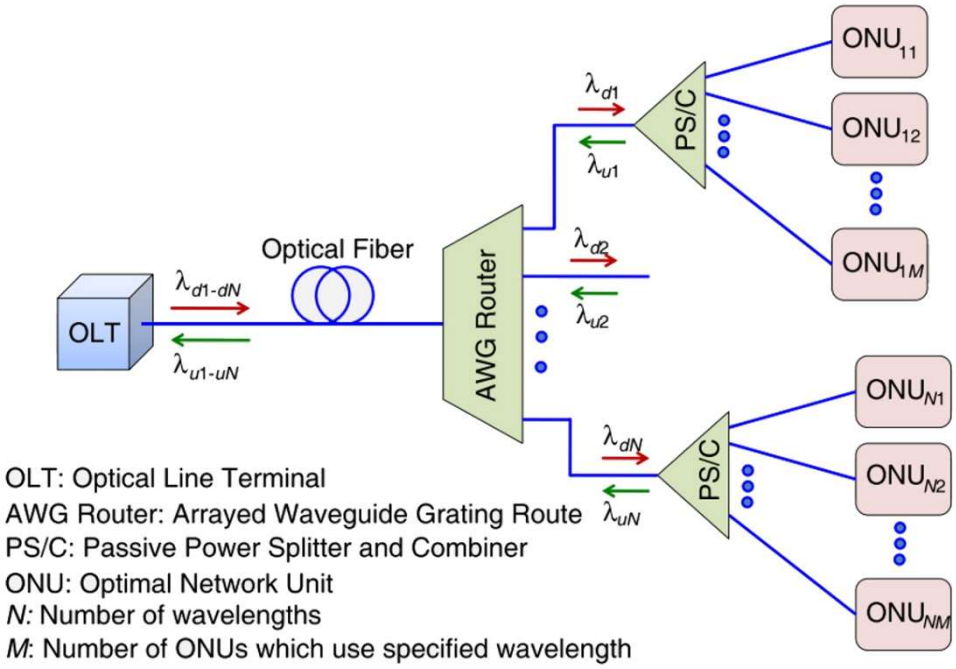

Fig. 2.8 Architecture of the hybrid TDMA/WDMA PON [22]

count can be increased. Since hybrid TDMA/WDMA PONs make use of the bandwidth of each wavelength efficiently and provide services to more subscribers, it has been selected as the base technology for NG-PON2 by the Full Services Access Network (FSAN) group [23, 24].

2.2.1.4 OFDMA PONs

OFDM is widely used in both wired and wireless access technologies [11], not only because OFDM provides high spectral efficiency, but also due to its high flexibility on both multiple services provisioning and dynamic bandwidth allocation (DBA). Fig. 2.9 shows an example of an OFDMA PON architecture [25], where different subcarriers and time slots are

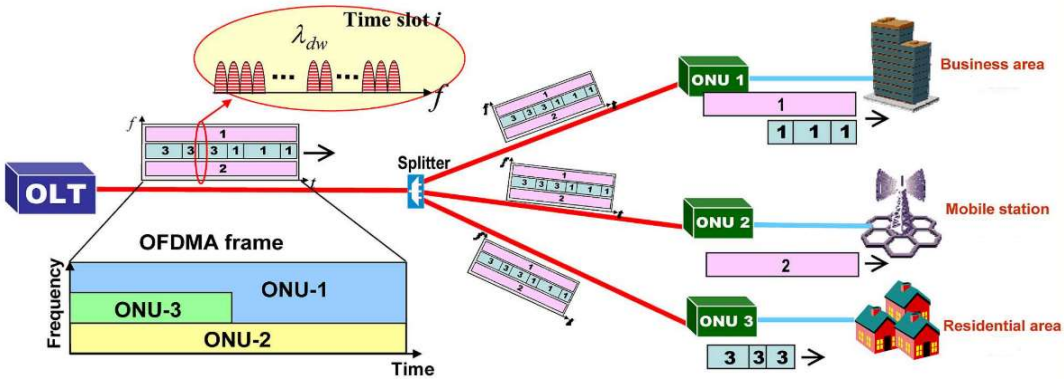

Fig. 2.9 OFDMA PON architecture [25]

allocated to different ONUs for various application scenarios. Taking the cost-effective IMDD OFDMA PON as an example, in the upstream transmission, each ONU maps its signal onto the allocated subcarrier(s) and/or time slot(s) and sets all other subcarriers to zeros and completes the OFDM modulation to generate an electrical OFDM frame. Afterwards, the generated OFDM frame is converted into optical OFDM (OOFDM) signal by an optical intensity modulator, and after coupling at the optical coupler from different ONUs, the coupled OOFDM signal is produced for the fibre transmission. After transmission through the ODN, the OOFDM signal is detected by a single photodetector at the OLT receiver. For the downstream transmission, when the OOFDM signal reach the ONUs, each ONU selects its own data from the pre-allocated subcarrier(s) and/or timeslot(s).

OFDMA PONs have enormous advantages including high spectral efficiency, adaptive signal modulation according to channel characteristics, DBA with fine bandwidth granularity, trivial equalization through simple complex multiplication per subcarrier, as well as excellent tolerance to CD. In terms of implementation of the OFDMA PON, DSP can be utilized to realise highly cost-effective and flexible OFDM transceivers. Furthermore, OFDMA PONs can coexisted with legacy optical networks [25]. For example, 1510nm-1540nm downstream and 1340nm-1360nm upstream OFDMA PON operations can enable its coexistence with GPON, XG/10 G-EPON, and legacy RF video overlays [25]. The OFDMA PON also has good compatibility with OFDM-based 4G networks and future 5G networks. As such, the OFDMA PON is promising for converged fixed-mobile networks.

2.2.1.5 DFMA PONs

Recently, a novel DFMA PON [26] has been proposed, where DSP-enabled, software reconfigurable, digital orthogonal filtering is employed in each individual ONU and the OLT to enable all ONUs to dynamically share the transmission medium under the control of the centralized software-defined controller and the transceiver-embedded DSP controllers. As the digital filtering in the proposed DFMA PONs is DSP controlled, enabling the DFMA PONs to fully support the SDN solution with the network control further extended to the physical layer, this greatly eases the transparent abstraction and virtualization processes because of inherent rich DSP-enabled network intelligence. The diagram of the DSP-enabled

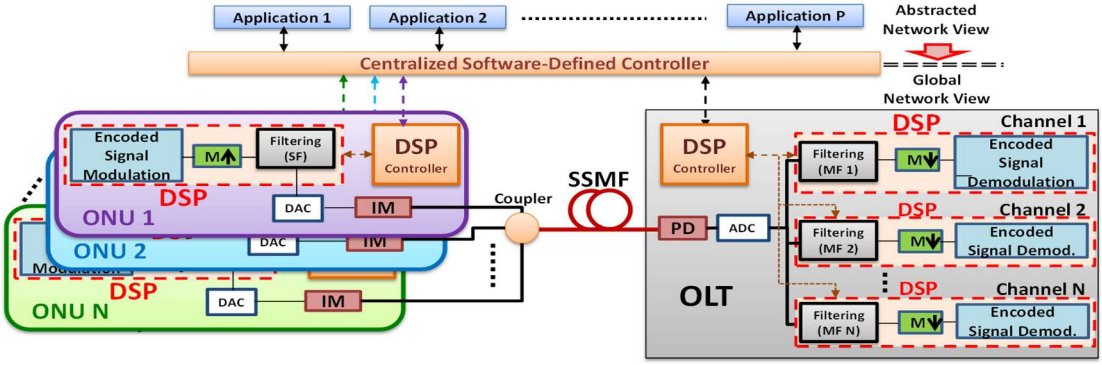

Fig. 2.10 DFMA PON architecture [26]

software reconfigurable DFMA PONs based on IMDD is illustrated in Fig. 2.10, where digital orthogonal filters are employed for multiplexing/demultiplexing various downstream/upstream encoded signals in the digital domain.

Taking the upstream operation for example, the *i*-th ONU data digitally encoded by an arbitrary signal modulation format is up-sampled ($M\uparrow$) by a factor of M via inserting M-1 zeroes between two consecutive original data samples. The up-sampled data sequence is subsequently passed through a digital SF. According to the prevailing services and dynamic network characteristics including total number of ONUs accommodated, by working together with both the centralised SDN controller and the OLT DSP controller, the ONU-embedded DSP controller computes a set of shaping filter coefficients to perform the filtering process required by the ONU. This leads to the on-line establishment of software reconfigurable connections in the physical layer. Having been digitally filtered, the resulting data sequence is passed through a DAC. The generated analogue electrical signal is then fed to an optical intensity modulator to perform the electrical-to-optical (E-O) conversion. Different optical signals from various ONUs attached to the DFMA PON are finally passively combined by a coupler in the remote node and propagated through the fibre transmission link to the OLT.

In the OLT, the optical signal is electrically converted by a photodetector and digitalized by an ADC. After that, the data stream corresponding to the *i*-th ONU is demultiplexed by the corresponding MF, whose coefficients are computed by the OLT-embedded DSP controller following a procedure similar to its' ONU counterpart. In addition, via periodically communicating with each ONU DSP controller, the OLT-embedded DSP controller also takes full responsibility of maintaining the orthogonality among all the filters employed in

the DFMA PON. After digital filtering, the demultiplexed signal is then down-sampled ($M\downarrow$) by selecting every M-th sample, and finally the i-th ONU data is recovered after decoding. Thus, a DSP-enabled dedicated physical connection between the i-th ONU and the OLT is established, which is on-line software reconfigurable. Of course, such a connection can be further extended to link any users inside and/or outside the network if these users are served by the same centralized software-defined controller.

In the DFMA PONs, use can be made of the Hilbert-pair approach [27] to construct required digital orthogonal filters. The impulse responses of the i-th Hilbert-pair, $h_i(t)$, can be written as:

$$\begin{aligned} h_i^I(t) &= p(t)\cos(2\pi f_{ci}t) \\ h_i^Q(t) &= p(t)\sin(2\pi f_{ci}t) \end{aligned} \tag{2.10}$$

where f_{ci} corresponds to the central frequency of the i-th Hilbert-pair and $p(t)$ is the baseband pulse having a square-root raised-cosine form expressed as:

$$p(t) = \frac{sin[\pi(1-\alpha)t'] + 4\alpha t' cos[\pi(1+\alpha)t']}{\pi t'[1-(4\alpha t')^2]}$$

$$t' = {}^{t}/_{T} \tag{2.11}$$

where T is the sampling period prior to oversampling and the α parameter controls the excess of bandwidth of the square-root raised-cosine function. The superscripts "I" and "Q" indicate the in-phase and quadrature-phase filter components of the Hilbert-pair, respectively. Each of these components can be independently utilised to convey an individual signal channel. The impulse responses of the OLT filters are written as a matched version of the corresponding ONU Hilbert-pair, $g_i(t)$,

$$\begin{aligned} g_i^I(t) &= h_i^I(-t) \\ g_i^Q(t) &= h_i^Q(-t) \end{aligned} \tag{2.12}$$

with

$$g_i^A(t) \otimes h_j^B(t) = \begin{cases} \delta(t-t_0) & A = B \text{ and } i = j \\ 0 & A \neq B \text{ or } i \neq j \end{cases} \tag{2.13}$$

where the subscripts A and B each denote I or Q, respectively. t_0 corresponds to the time delay induced by the filtering process. For supporting N independent ONU channels, the minimum oversampling factor, M, satisfies $M = N$. In addition, the central frequencies, f_{ci}, of the i-th Hilbert-pair is given by:

$$f_{ci} = (2i - 1)\frac{f_{DAC/ADC}}{2N} \quad i = 1,2,3 \cdots \tag{2.14}$$

where $f_{DAC/ADC}$ is the DAC/ADC sampling speed. Here the central frequency of the Hilbert-pair is chosen to uniformly distribute the filter frequency responses within the available spectral region determined by the DAC/ADC.

An example of how different orthogonal filters are dynamically assigned to individual ONUs is illustrated in Fig. 2.11 [26], where the frequency responses of both the in-phase and quadrature-phase components of these Hilbert-pairs at different central frequencies are plotted. In Fig. 2.11, each ONU can be assigned independently to a filter component, for instance, ONU 1, ONU 3 and ONU 5 employ filter 1 (the I component of the first Hilbert-pair), filter 6 (the Q component of the third Hilbert-pair) and filter 5 (the I component of the third Hilbert-pair), respectively. Different filters can also be assigned to the same ONU when the ONU requires higher transmission bandwidth, as illustrated in Fig. 2.11 for ONU 2.

From the above description it can be seen that: 1) both digital filtering and adaptive signal encoding/decoding are undertaken using DSPs in hardware; 2) via the DSP controllers embedded in both the ONUs and OLTs, digital filter parameters can be adjusted dynamically and adaptively according to traffic and transmission characteristics, 3) one or more signal

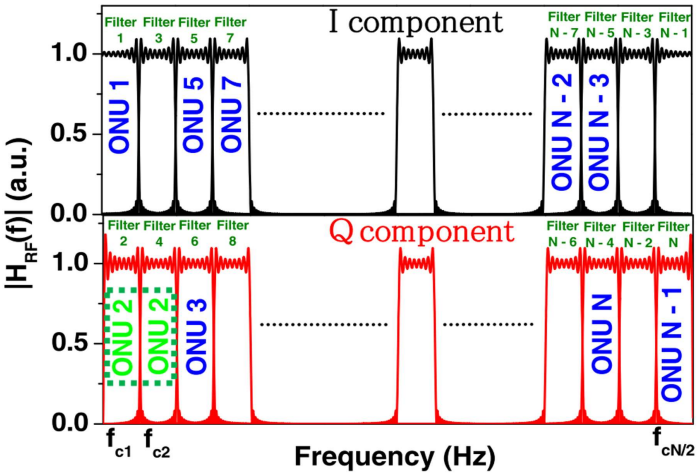

Fig. 2.11 Frequency responses of the shaping filters and corresponding ONU channel allocations. [26]

channels can be assigned to a single high-speed ONU, and a single channel can also be shared among different low-speed ONUs via TDMA, and 4) standard synchronization [17, 21] is still applicable in the DFMA PONs. In summary, the DFMA PON's advantages are: 1) offering a useful framework for developing universal optical transceivers for cost-sensitive ONUs, 2) providing good backward compatibility with all existing PONs, 3) transparent to both underlying transmission technologies and network topologies, such as modulation formats and signal bit rates, 4) enhanced data security in the physical layer as received data cannot be decoded without the full perception of filter design parameters, 5) compatibility with the preferred "pay as you grow" network operation model.

2.2.2 Evolution of PON Standards

Table 2.1 PON International Standards

Technology	Standard	Year	Downstream Bitrate [Gb/s]	Upstream Bitrate [Gb/s]
APON/BPON	ITU-T G.983.1 ÷ G.983.5	2001	⩽1.25	⩽0.625
EPON	IEEE 802.3ah	2004	1.25	1.25
10G-EPON	IEEE 802.3av	2009	10	1
GPON	ITU-T G.984	2004	2.5	1.25
XGPON	ITU-T G.987	2010	⩽10	10
NG-PON2	ITU-T G.989.1 (specifications)	2013	40	10

There are two standardisation bodies that have created PON standards, as shown in Table 2.1, the ITU-T develops standards for the GPON family, while the IEEE develops standards for the EPON family, both of them have enjoyed widespread implementation and deployment.

2.2.2.1 APON/BPON

APON is an abbreviation for Asynchronous Transfer Mode (ATM)-PON, while BPON refers to Broadband PON, and both of them utilise TDM technology. The standardization of APON was finished by ITU-T G.983.1 in 1998 [30], whilst BPON is a higher speed version of APON and was specified in G.983.3 in 2001 [31], and we usually use BPON to refer to this class of PONs subject to G.983 series. APON can provide signal bit rates of 155 Mb/s in both upstream and downstream over 20 km, with the bandwidth shared by 32~64 ONUs, and ONU can only obtain 5 to 20 Mb/s [30]. BPON can support signal bit rates of 155 Mb/s upstream and 622 Mb/s downstream over 20 km [31]. As specified in the standards, BPON use 1260-1360 nm for upstream and 1480-1500 nm for downstream, with 1550-1560 nm

used for video overlay services [31]. As the limited performance, BPON has already been replaced by EPON/GPON worldwide.

2.2.2.2 EPON/GPON

Gigabit-capable PON (GPON) is an evolution of BPON with a high data rate, its standard is G.984 series [32], inherited many ideas covered in the G.983 standards, such as utilizing ATM cells [33]. While EPON uses Ethernet packets and has been developed by the IEEE 802.3ah study group at the same time of GPON around 2004 [34]. Both of them support gigabits level data rate, with GPON supporting 1244.16 Mbps/ 2488.32 Mbps for downstream and 155.52 Mbps/ 622.08 Mbps/ 1244.16 Mbps/ 2488.32 Mbps for upstream, while EPON offering symmetrical 1.25 Gb/s transmission speed for both uplink and downlink. At the physical layer both standards adopted the same wavelength plan at 1310/1490 nm wavelength for upstream/downstream direction, respectively. In GPON, the split ratio can be up to 1:128, supporting transmission reach of at least 20 km, which is the same reach supported by EPON, but the corresponding split ratio of EPON is normally from 1:16 to 1:64, this is because GPON adopted an additional ODN class (ODN class C) resulting in 5 dB higher maximum signal losses, with the maximum power loss at 25dB [35]. There is no denying that EPON and GPON are the most popular versions of PONs used today. In comparison, there are many aspects to be compared between EPON and GPON including data rates, QoS and costs, and it would be fair to conclude that GPON performs better than EPON overall, however EPON would be preferable in terms of cost and time saving [36]. GPON is the most popular in the U.S., such as Verizon's Foist system, while EPON are more prevalent in Asia and Europe [37].

2.2.2.3 10 Gigabit Capable PON

IEEE and ITU-T along with the FSAN group have defined 10 Gbit/s solutions, in an effort to support the ever-increasing bandwidth demand, and the solutions are XG-PON standardized by ITU-T (G.987) in 2010 [38] and 10G-EPON defined by IEEE 802.3av in 2009 [39], respectively. And both of them use TDMA.

XG-PON is generally known as NG-PON1, and it is a smooth evolution of ITU-T G.984 GPON as XG-PON inherits all the requirements of GPON with a few new additions such as higher bit rate for downlink transmission. To achieve the backward compatibility and co-

existence of GPON, the optical wavelengths that have been selected for XG-PON are the "O-band" (for the upstream ranging from 1260 to 1280 nm) and the "1577 nm" (for the downstream ranging from 1575 to 1580 nm) [40]. And a total power budget of approximately 28.5 dB to 31 dB is also defined in XG-PON, supporting a minimum power split ratio of 1:64 and a minimum physical reach of 20 km. And the asymmetrical bit rates of 10 Gb/s for downstream and 2.5 Gb/s for upstream are defined in XG-PON.

For 10G-EPON, in the downlink, the 1 Gbit/s and 10 Gbit/s channels are divided based on their wavelengths, with the 1 Gbit/s transmission using the 1480 to 1500 nm band and 10 Gbit/s spreads from 1575 to 1580 nm. In the uplink, there is an overlap between them, i.e., 1 Gbit/s uses the 1260 to 1360 nm band, whereas 10 Gbit/s spread from 1260 to 1280 nm. The deployment of 10 Gb/s class PONs is currently ramping up.

2.2.2.4 Next-Generation PON Stage 2 (NG-PON2)

Based on the current application demands and technological maturity, FSAN divides NG-PONs into two phases shown in Fig. 2.12 [41], including NG-PON1 and NG-PON2. NG-PON1 is a mid-term upgrade, which is compatible with legacy GPON, as mentioned above, and NG-PON2 is a long-term solution in PON evolution that can be deployed independent of GPON standards. In 2010, FSAN started deliberations on the 40-Gigabit capacity PON called NG-PON2 which was standardized in the framework of ITU-T G.989 series [42] in 2015. NG-PON2 exploits both the time and wavelength domains, it contains wavelength channel pairs of two types known as TWDM channels and Point-to-Point WDM channels.

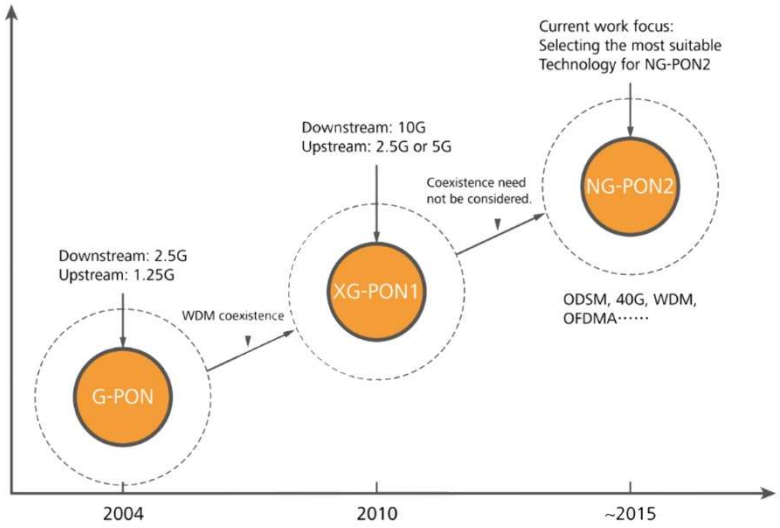

Fig. 2.12 NG-PON roadmap by FSAN [41]

The former provides point-to-multipoint connectivity using conventional TDMA technology. The latter provides point-to-point connectivity using some externally specified synchronous or asynchronous mechanisms, such as Gigabit or 10 Gigabit Ethernet [43]. For uplink transmissions, wavelengths between 1524-1544 nm are selected to provide maximum 40 Gb/s with four wavelengths.

With the up-coming 5G, some of the key features of 5G are expected to be up to 10 Gb/s capacity on the air interface, including massive MIMO, dense small cells, and a new functional split for fronthaul. With such features in scope, future fronthaul may be expected to be transported over a hybrid TWDM PON as defined in NG-PON2 [15, 33].

2.2.2.5 100G-EPON

To meet the increasing bandwidth demands induced by IoT, IP video and mobile broadband, the IEEE 100G-EPON Task Force [45] is targeting a 100 Gb/s capacity PON (4 × 25 Gb/s). And very recently, the joint ITU-T and IEEE 802 Study Group 15 workshop met as part of the processes to finalize IEEE 802.3ca [46]. The working group proposed three level of target rates such as 25 Gb/s, 50 Gb/s and even 100 Gb/s, targeting using single-wavelength 25Gb/s PON as the mainstream technology, and providing 4x25 Gb/s (100 Gb/s) to users through wavelength multiplexing. To boost the single-wavelength rate from 10 Gbit/s to 25 Gbit/s while achieving the coexistence with the incumbent network technologies, a number of technological challenges in single-wavelength 25 Gb/s transmissions need to be overcome, such as dispersion penalties and nonlinear effects [47]. OFDM is a promising technology for 100 Gb/s while still using low bandwidth optical components in cost-effective IMDD scenario [48].

2.3 ROADM Fundaments

Today's optical networks have developed from simple point-to-point connections, to multi-node rings, to all-optical interconnected mesh topologies, and it connects the long-haul backbone through regional, metro networks and the access networks. To allow wavelengths to added/dropped in the nodes, ROADMs are utilized in the WDM optical networks to multiplex and route different wavelength into or out of the optical networks. The traditional ROADM used the fixed lasers/filters for fixed wavelengths, but now it cannot meet the

increasing use of bandwidth, thus driving the improvement from the classic ROADMs to new generation of ROADMs.

2.3.1 Classical ROADMs

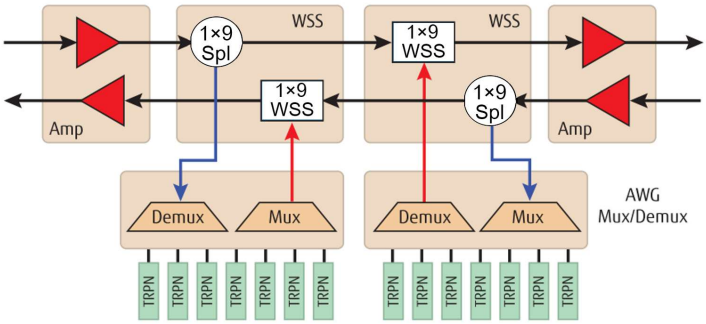

Fig. 2.13 A classic ROADM architecture [50]

A classic ROADM [49] consists of optical amplifiers, optical switching, multiplexer/demultiplexer, transponder, and muxponder cards, thus enabling a complete optical transport node. Such ROADMs can add or drop a certain set of wavelengths dedicated to specific WDM channels. Through the add and drop operations, ROADMs not only provide flexibility to the WDM networks, but also alleviate data traffic disruptions in the WDM channels, thus ROADMs can reduce OpEx. A typical ROADM is shown in Fig. 2.13 [50], where the multiplexer/demultiplexer is a passive device implemented with AWG, which separates each wavelength into individual input and output ports, but only pre-defined fixed wavelengths can be added/dropped. As the bandwidth utilization efficiency and dynamic traffic demand are increasing, new ROADM generations are thus required.

2.3.2 CDC/G ROADMs

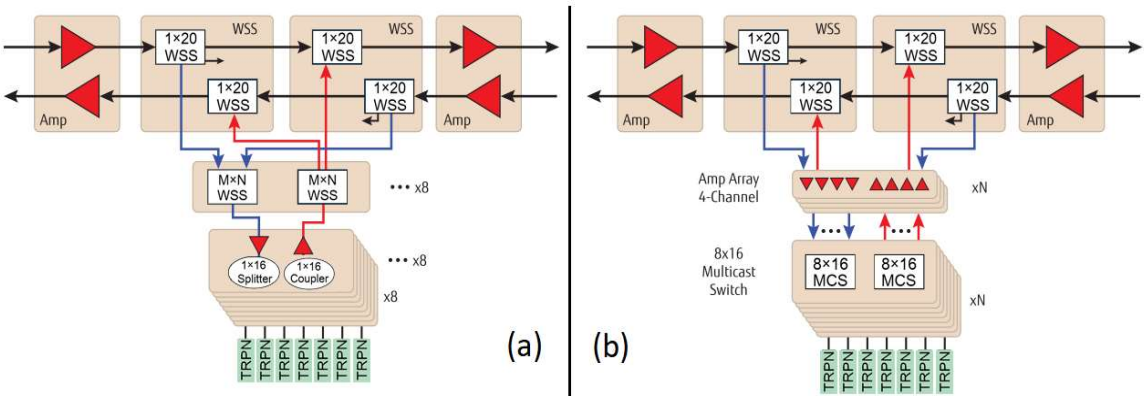

Fig. 2.14 CDG versus CDC/G ROADM [50]

The new generation ROADMs have been developed with novel features in terms of colourlessness, directionlessness, contentionlessness and gridlessness (CDC/G). Colourless ROADMs [55-57] can remotely assign any wavelength to a particular multiplex port by involving additional WSSs in place of different multiplexers and demultiplexers. And broadcasting and selecting function of spectrum selective switches (SSSs) and multicast switches (MCSs) are utilized to realise directionless ROADMs [55-58], allowing any wavelength to be routed to any direction. And SSSs can also be used to provide finer spectrum switching granularity to realise the gridlessness function [59-63]. In addition, to implement contentionless ROADMs, redundant components are pre-installed to enable different coloured wavelengths to be associated with different structures [62,63].

An example of CDC ROADMs is shown in Fig. 2.14 (a) [50], where the broadcast and select architecture used on classic ROADM is replaced with a route-and-select architecture based WSS modules. In addition, the fixed port AWG multiplexer/demultiplexer are replaced with flexible drop-side architectures that allow any transponder or muxponder to be assigned to any wavelength and sent to any WDM degree. Another example of a CDC/G ROADM is shown in Fig. 2.14 (b) [50], and the drop side is implemented using multicast switch modules, enabling any wavelength from any degree to be dropped to any client port.

All the proposed ROADM technologies only work at the wavelength level, and they are also expensive and bulky due to the utilisation of hard-wired switching elements, which significantly limits the ROADM's flexibility, upgradability, as well as its adaptability and cost-effectiveness in converged 5G networks. To satisfy the stringent requirements of optical access/metro network converging with mobile fronthaul/backhaul, new features should be added to the ROADMs, including high flexibility and add/drop operations at wavelength, subwavelength and sub-band levels, as well as low-cost and low energy consumption characteristics.

2.4 OFDM Fundamentals

OFDM has been studied for a couple of decades, and now it is widely used in 4G LTE standards, and it is also widely envisaged that the initial stage of 5G should also have sufficient transparency to OFDM-based 4G networks [60]. As OFDM can offer a number of well-documented salient advantages as mentioned in subsection 2.2.1.4, it is expected to play a crucial role for converged 5G networks.

2.4.1 OFDM Basics

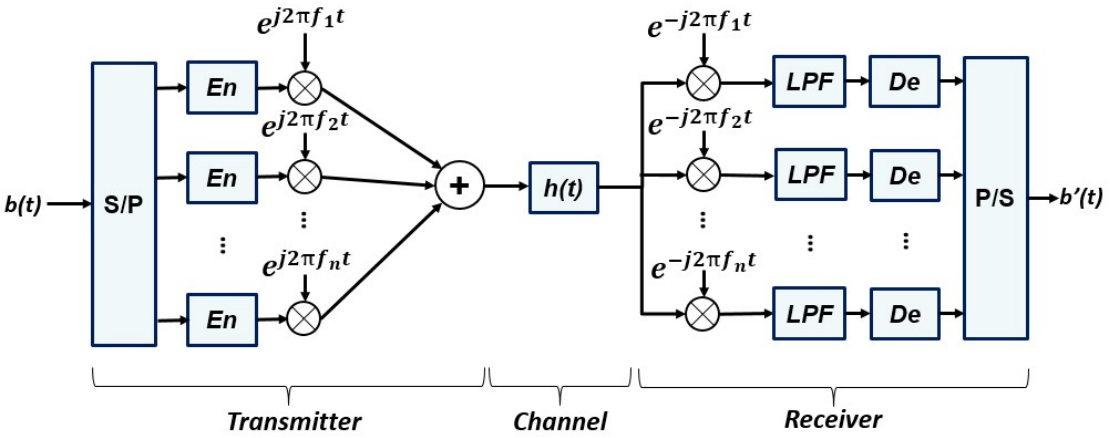

Fig. 2.15 Block diagram of a typical FDM. S/P: Serial-to-Parallel, P/S: Parallel-to-Serial, LPF: Low-pass Filter, En: Encoder, De: Decoder.

OFDM is a special class of FDM in which the data information is carried over many lower rate subcarriers, and a typical FDM diagram is shown in Fig. 2.15. In the transmitter, a serial of bit stream is converted into parallel bit streams, which are encoded by classical modulation formats such as M-ary quadrature amplitude modulation (QAM). And each of these encoded data stream is simultaneously modulated onto different subcarriers operating at different RF, and the frequency guardband between two adjacent subcarrier frequencies is sufficiently wide as illustrated in Fig. 2.16 (a). Before transmission in the channel the different modulated subcarriers are multiplexed together. In the receiver, the parallel data streams are recovered by demodulating each subcarriers with an identical RF frequency of the transmitter, followed by the low pass filtering and decoding process. Compared with FDM, OFDM precisely chooses the inter-subcarrier RF spacing such that all RF frequencies are harmonically related and thus ensure orthogonality between subcarriers. The

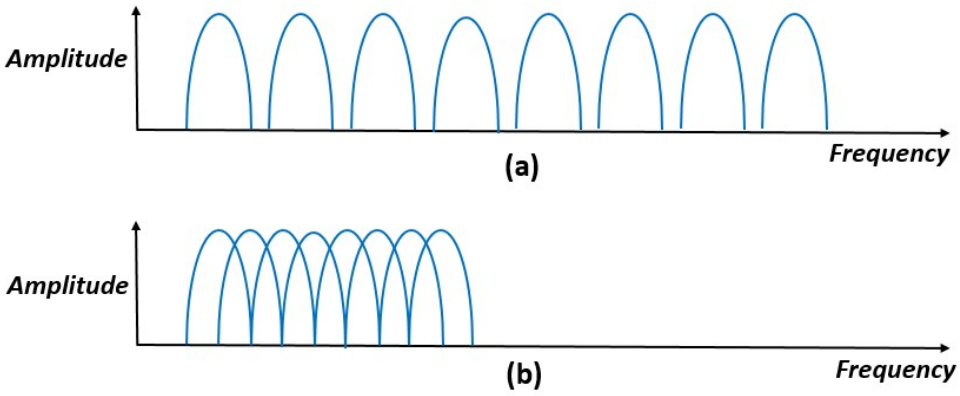

Fig. 2.16 Spectra of (a) FDM, (b) OFDM.

orthogonality allows spectral overlap between subcarriers without interference and this results in significant enhancement in spectral efficiency, as shown in Fig. 2.16 (b).

In the time domain, the *n*-th OFDM symbol with N subcarriers has a form of

$$x_n(t) = \sum_{k=1}^{N} d_{k,n} e^{j2\pi f_k t} \tag{2.15}$$

where $d_{n,k}$ is *k*-th subcarrier in the *n*-th OFDM symbol in a form of

$$d_{n,k} = \left[R_k e^{j\theta_k}\right] h(t) \tag{2.16}$$

where $h(t)$ is a rectangular pulse of unity amplitude and duration of one symbol period. R_k is the *k*-th subcarrier's amplitude and θ_k is its phase. And the central frequency f_k of each OFDM subcarrier satisfies:

$$f_k = f_c + \frac{k}{T_s}, k = 1,2, \ldots, N \tag{2.17}$$

where f_c is a frequency offset common to all subcarriers, generally set to zero. T_s is the symbol period, and in this case each subcarrier has exactly an integer number of oscillating cycles in the time interval T_s, and the number of oscillating cycles between adjacent subcarriers differs exactly by one. This property accounts for the orthogonality between different subcarriers [61].

A fundamental challenge with OFDM is that, if a large number of subcarriers are needed, an extremely complex architecture is required, which involves many oscillators and filters at both the transmit and receive ends. Weinsten and Ebert first revealed that OFDM modulation/demodulation can be implemented by using the inverse discrete Fourier transform (IDFT)/DFT [11]. Assuming $x_n(t)$ is sampled at an interval of T_s/N, then the m-th sampled $x_n(m)$ can be written, in a discrete form, as:

$$x_n(m) = \sum_{k=1}^{N} d_{n,k} e^{j2\pi f_k \frac{T_s m}{N}} = \sum_{k=1}^{N} d_{n,k} e^{j2\pi \frac{km}{N}} \tag{2.18}$$

where $m = 1, \ldots, N$. Since Eq. (2.18) is identical to IDFT, thus the OFDM signal can be directly produced by the IDFT operation. Similarly, the *k*-th subcarrier $d_{n,k}$ can be recovered by the DFT:

$$d_{n,k} = \sum_{m=1}^{N} x_n(m) e^{-j2\pi \frac{km}{N}} \quad (2.19)$$

To implement the IDFT and DFT efficiently with hardware-based DSP algorithms, the inverse fast Fourier transform (IFFT) and FFT are used as they considerably reduce the number of complex computations required.

2.4.2 Cyclic Prefix of OFDM

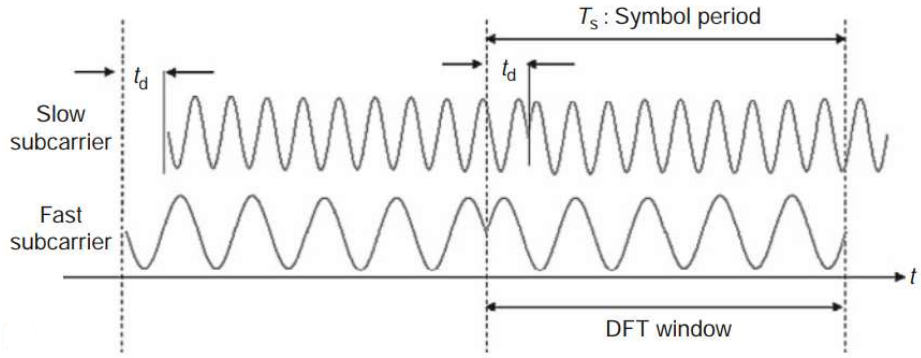

Fig.2.17 ISI and ICI caused by a dispersive channel. [11]

For a practical transmission channel with CD, different subcarriers locating at different RFs in an OFDM signal will have different delays. If the maximum differential delay between the slow subcarrier and fast subcarrier is t_d, and the DFT window containing a complete OFDM symbol is assumed for the fast subcarrier, as shown in Fig. 2.17. It is apparent that the slow subcarrier has crossed the symbol boundary, thus leading to ISI between the neighbouring OFDM symbols. Furthermore, because the OFDM waveform in the DFT window for the slow subcarrier is incomplete, the critical orthogonality condition for the subcarriers is imperfect, resulting in an inter-carrier interference (ICI) penalty. Cyclic prefix (CP) was proposed to resolve the channel dispersion-induced ISI and ICI [11]. CP is a copy of the last fraction of each OFDM symbol and inserted at the beginning of each OFDM

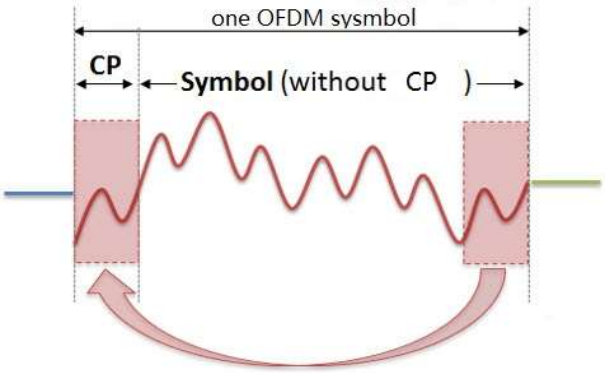

Fig. 2.18. OFDM symbol with CP

symbol, as shown in Fig. 2.18. If the time duration of the CP is T_p, the real information occupies a time period of $T_s - T_p$ in each OFDM symbol, thus CP will reduce the overall data rate as it does not carry any useful information. Throughout the thesis, the CP parameter is defined as

$$\eta = \frac{T_p}{T_s - T_p} \tag{2.20}$$

To maintain the ISI-free OFDM transmission, the CP time duration should be longer than the maximum delay spread of the transmission link [11].

2.4.3 ADC/DAC, Quantization and Clipping

The generated digital OFDM signal in the transmitter must be converted into an analogue form for transmission, and must be converted back to the digital domain for data recovery in the receiver. The digital-to-analogue conversion in the transmitter and analogue-to-digital conversion in the receiver are performed by a DAC and ADC respectively. As the DAC/ADC has limited bit resolution of b, the OFDM signal samples can only by represented by $2^b - 1$ discreet levels, thus quantization noise is present. In addition, when generating the OFDM signal, the independently modulated subcarriers are added coherently, resulting in the signal's envelope exhibiting high peaks, which leads to high PAPR of OFDM signal [62]. Considering an OFDM symbol $x(m)$ from Eq. (2.18), where N subcarriers are added together, the PAPR is defined as the ratio of the maximum instantaneous power to the average power, which can be expressed as:

$$\mathrm{PAPR}(x[m]) = \max_{1 \le n \le N=1} \frac{|x[m]|^2}{E[|x[m]|^2]} \tag{2.21}$$

Where $E[\cdot]$ is the expectation operator. High PAPR not only produces signal excursions into nonlinear operation region of electrical/optical devices, thereby leading to nonlinear distortions and spectral spreading [62], but also produces high quantization noise for fixed quantization bits induced by the resolution-limited ADC/DAC. Therefore, as one of the simplest way to reduce the PAPR, clipping is applied to the OFDM signal. For a given clipping level of $\pm\Lambda$, and assuming $A(t)$ is real, the clipped signal is given by:

$$A_{clip}(t) = \begin{cases} A(t), & -\Lambda \le A(t) \le \Lambda \\ \Lambda, & A(t) > \Lambda \\ -\Lambda, & A(t) < -\Lambda \end{cases} \tag{2.22}$$

The clipping ratio (peak power / average power) ξ (in dB) is defined as

$$\xi = \frac{\Lambda^2}{P_m} \tag{2.23}$$

with P_m being the normalised average signal power. Fig. 2.19 clearly shows the OFDM signals before and after clipping, where the PAPR is reduced. An optimum clipping ratio exists as excessive clipping will cause the signal distortion, while insufficient clipping will leave the signal with high PAPR which may result in an increased quantization noise effect.

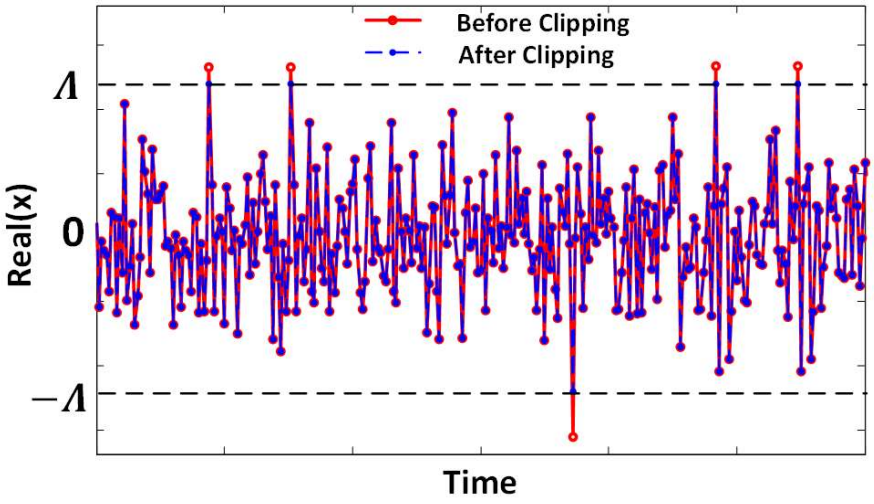

Fig. 2.19 OFDM signal before and after clipping.

After clipping, $A_{clip}(t)$ is linearly quantized into a set of equally distributed quantization levels within a range of [-Λ, Λ]. The quantization process can be described as follows:

$$A_Q = \sum_{i=-\frac{L}{2}+1}^{\frac{L}{2}} \frac{A_i + A_{i-1}}{2} g(A_s, A_i, A_{i-1}) \tag{2.24}$$

where A_Q is the quantized value, A_s is the sampled OFDM values, A_i, $A_{i-1}$are the i-th and (i-1)-th the quantization levels, L is the number of quantization levels given by $L = 2^b$ with b being the quantization bits, g is the rectangular function defined as:

$$g(x, x_1, x_2) = \begin{cases} 1, x_1 \le x \le x_2 \\ 0, otherwise \end{cases} \tag{2.25}$$

Based on the above analyses, it can be seen that quantization noise is introduced by the quantization process, as the continuous amplitude waveform of A_s is mapped onto a set of discrete values within the dynamic range of $[-\Lambda, \Lambda]$. Therefore, the quantization bit is required to be sufficiently high for reducing the quantization noise. However, the higher quantization bit can increase the DAC/ADC complexity and cost for specific sampling speeds, thus, it is vital to identify the optimum quantization bit by exploring the trade-off between the transmission performance and DAC/ADC characteristics.

2.4.4 Channel Estimation and Equalization for OFDM

When OFDM signals transmit over an optical channel, the channel frequency response will introduce rotations and size-variations of the received OFDM constellation, and such an issue can be compensated by channel estimation and equalization in the receiver. Channel estimation and equalization can be realised by pilot-assisted approach [11], and it is utilized throughout the thesis.

In the time domain, assuming the k-th subcarrier channel impulse response is $h_k(t)$, the corresponding noise is $w_k(t)$, and the transmitted OFDM signal for the k-th subcarrier is $x_k(t)$, after transmission the received k-th subcarrier $y_k(t)$ is:

$$y_k(t) = x_k(t) \otimes h_k(t) + w_k(t) \tag{2.26}$$

The time domain convolution between the transmitted OFDM signal and the channel response is equivalent to the multiplication of the OFDM signal spectrum X_k with the channel frequency response H_k. Thus the k-th subcarrier $y_k(t)$ in the frequency domain is:

$$Y_k = X_k H_k + W_k \tag{2.27}$$

To perform channel estimation, a number of pilots that are known are interspersed with the user data and transmitted. From Eq. (2.27), the channel response of k-th subcarrier based on the pilots can be obtained by:

$$H_k = Y_{p,k} / X_{p,k} \tag{2.28}$$

where noise is ignored, $X_{p,k}$ and $Y_{p,k}$ are transmitted and received pilots of the k-th subcarrier before IFFT in the transmitter and after FFT in the receiver, respectively. To

realise the channel equalization, the OFDM receiver restores the transmitted signal by multiplying the received signal with the inverse of the estimated subcarrier channel response H_k^{-1}, which is given by

$$X_k' = Y_k H_k^{-1} = X_k + \frac{W_k}{H_k} \tag{2.29}$$

where X_k' is the recovered complex data and W_k is the complex channel noise for the k-th subcarrier. Eq. (2.29) represents a simple "one-tap" OFDM equalizer, and it can be seen that the channel noise cannot be removed, which distorts the signal significantly when the received OFDM signal has a low power. For AWGN-limited channels, such an issue can be efficiently solved by averaging the estimated subcarrier channel frequency response over a long time duration.

2.4.5 IMDD Optical OFDM Transceiver

As an OFDM signal can be generated and recovered by IFFT/FFT, the OFDM modulation/demodulation can be easily implemented through DSP, and the DSP-based OFDM modem is inserted in Fig. 2.20. For a cost-effective IMDD transmission system of interest of the thesis, the optical modulator is low-complexity and low-cost intensity modulator, and the detection is carried out with square-law photodetector.

In the IMDD OOFDM transmission system shown in Fig. 2.20, an incoming binary data sequence is encoded to a serial of complex numbers by using various modulation formats. A serial-to-parallel converter truncates the encoded complex data sequence into a set of subcarriers. Meanwhile, to generate real-valued OFDM signal to directly drive an intensity modulator, the truncated original complex parallel subcarriers and corresponding complex conjugated subcarriers are arranged to satisfy Hermitian symmetry, which is expressed as,

$$X_k = \begin{cases} 0 & k = 0 \\ X_k & k = 1,2, \ldots \frac{N}{2} - 1 \\ 0 & k = \frac{N}{2} \\ X_{N-k}^* & k = \frac{N}{2} + 1, \ldots, N - 1 \end{cases} \tag{2.30}$$

All the subcarriers X_k are input to the transmitter IFFT, thus the parallel real-valued OFDM signals can be generated [61]. According to the selected CP length, CP samples can be

inserted in the way as mentioned in subsection 2.4.2. Afterwards, the parallel-to-serial conversion is performed to generate the data sequence, which is fed into a DAC to produce analog electrical signal at a given sampling speed of the DAC. After the E-O conversion in the optical modulator, the OOFDM signal is injected into the fibre link. In the receiver, after the square-law photodetection, the OFDM signal demodulation are following the reverse procedures as in the transmitter, which include serial-to-parallel conversion, CP samples removal, FFT, and the one-tap equalization before de-mapping to recover a desired data bit stream.

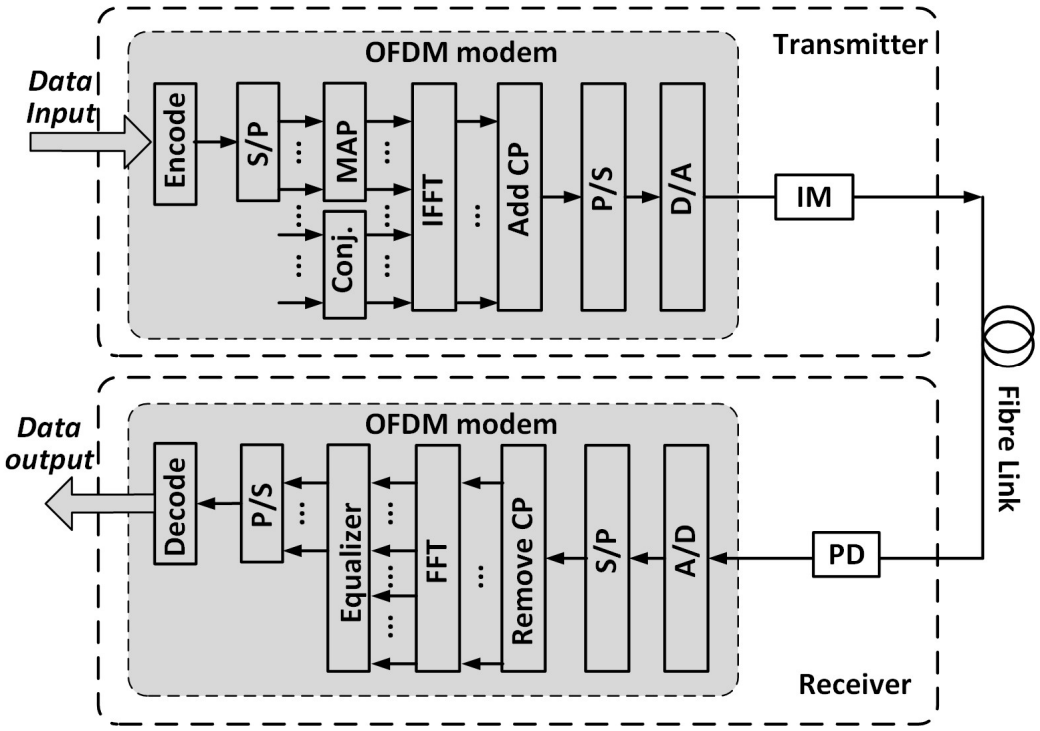

Fig. 2.20 System diagram of IMDD Optical OFDM. Conj.: conjugated subcarriers; IM: intensity modulator; PD: photodetector.

References

[1] J. L. Wei, C. Sánchez, and R. P. Giddings, et al., "Significant Improvements in Optical Oower Budgets of Real-time Optical OFDM PON Systems," *Opt. Express*, vol. 18, no. 20, pp. 20732–20745, 2010.

[2] M. S. Alencar and V. C. Da Rocha, *Fiber-Optic Communication Systems*. 2005.

[3] S. Mieda, N. Yokota, and W. Kobayashi, et al., "Ultra-Wide-Bandwidth Optically Controlled DFB Laser With External Cavity," *IEEE J. Quantum Electron.*, vol. 52, no. 6, pp. 1–7, 2016.

[4] Y. Matsui, R. Schatz, T.Pham, et al., "55 GHz Bandwidth Distributed Reflector Laser," *J. Light. Technol.*, vol. 35, no. 3, pp. 397–403, 2017.

[5] X. Zheng, X. Jin, R. Giddings, and J. Wei, "Negative Power Penalties of Optical OFDM Signal Transmissions in Directly Modulated DFB Laser-Based IMDD Systems Incorporating Negative Dispersion Fibers," *IEEE Photonics*, vol. 2, no. 4, pp. 532–542, 2010.

[6] M. R. Phillips, T. E. Darcie, and D. Marcuse, et al., "Nonlinear Distortion Generated by Dispersive Transmission of Chirped Intensity-Modulated Signals," *IEEE Photonics Technol. Lett.*, vol. 3, no. 5, pp. 481–483, 1991.

[7] K. Sato, S. Kuwahara and Y. Miyamoto, "Chirp Characteristics of 40-Gb/s Directly Modulated Distributed-Feedback Laser Diodes," *J. Light. Technol.*, vol. 23, no. 11, pp. 3790-3797, 2005.

[8] E. B. Gary and C. C. John, "Overview of Optical Modulators and the Properties That Affect Transmission System Performance," in *Broadband Optical Modulators*, CRC Press, pp. 93–126, 2011.

[9] A. Chen and E. J. Murphy, *Broadband Optical Modulators*. 2012.

[10] Corning, "Corning SMF-28 Optical Fiber Product Information," [Online]. Availalbel:https://www.corning.com/media/worldwide/coc/documents/Fib

er/SMF-28%20Ultra .pdf

[11] W. Shien and I. Djordjevic, *OFDM for Optical Communications*. 2010.

[12] G. P. Agrawal, *Nonlinear Fiber Optics*. 2013.

[13] H. Venghaus and N. Grote, "Fibre Optic Communication Key Devices," *Proc. Natl. Acad. Sci.*, vol. 161, no. 25, pp. 10335–10339, 2012.

[14] X. Gong, L. Guo, and Y. X. Dong, et al., "SPM-Improved Transmission Performance of Software Reconfigurable IMDD PONs based on Digital Orthogonal Filtering," *J. Light. Technol.*, vol. 35, no. 20, pp. 4488-4496, 2017.

[15] D. Nesset, "NG-PON2 Technology and Standards," *J. Light. Technol.*, vol. 33, no. 5, pp. 1136–1143, 2015.

[16] F. J. Effenberger, "The Future of Higher Speed PONs," in *Proc.Asia Communications and Photonics Conference*, 2018.

[17] C. F. Lam, "PON Architectures Review," *Passive Optical Networks*, pp. 19–86, 2007.

[18] E. Harstead, D. Van Veen, and V. Houtsma, et al., "Technology Roadmap for Time-Division Multiplexed Passive Optical Networks (TDM PONs)," *J. Light. Technol.*, vol. 37, no. 2, pp. 657–664, 2019.

[19] Z. Zhang, Q. Guo, and C. Ju, et al., "Optical- and Electrical-Domain Compensation Techniques for Next-Generation Passive Optical Networks," *IEEE Commun. Mag.*, vol. 57, no. April, pp. 144–150, 2019.

[20] D. Nesset, "Network Operator Perspective on WDM-PON Systems and Applications," in *Proc. Eur. Conf. Exhib. Opt. Commun.*, 2013.

[21] P. Vetter, "Tutorial Next Generation Optical Access Technologies," in *Proc. Eur. Conf. Exhib. Opt. Commun.*, 2012.

[22] R. Shaddad, A. Mohammad, and S. Idrus, "Emerging optical broadband access networks from TDM PON to OFDM PON," *PIERS Proceedings*, pp. 102–106, 2015.

[23] D. Nesset, "PON Roadmap [Invited]," *J. Opt. Commun. Netw.*, vol. 9, no. 1, pp. A71–A76, 2017.

[24] I. A. Alimi, A. Tavares, and C. Pinho, et al., "Enabling Optical Wired and Wireless Technologies for 5G and Beyond Networks," *Telecommun. Syst.*, 2019. [Online]. Available: https://www.intechopen.com/online-first/enabling-optical-wired-and-wireless-technologies-for-5g-and-beyond-networks.

[25] N. Cvijetic, "OFDM for Next Generation Optical Access Networks," *J. Light. Technol.*, vol. 30, no. 4, pp. 384–398, 2012.

[26] M. Bolea, R. P. Giddings, and M. Bouich, et al., "Digital Filter Multiple Access PONs With DSP-Enabled Software Reconfigurability," *J. Opt. Commun. Netw.*, vol. 7, no. 4, pp. 215–222, 2015.

[27] R. P. Giddings, M. Bolea and J. M. Tang, "Digital Orthogonal Filter-Enabled Optical OFDM Channel Multiplexing for Software-Reconfigurable Elastic PONs," *J. Light. Technol.*, vol. 32, no. 6, pp. 1200–1206, 2014.

[28] X. Q. J. and J. M. Tang, "Experimental Investigations of Wavelength Spacing and Colorlessness of RSOA-Based ONUs in Real-Time Optical OFDMA PONs," *J. Light. Technol.*, vol. 30, no. 16, pp. 2603–2609, 2012.

[29] X. Duan, R.P. Giddings, and M. Bolea, et al., "Real-time Experimental Demonstrations of Software Reconfigurable Optical OFDM Transceivers Utilizing DSP-based Digital Orthogonal Filters for SDN PONs," *Opt. Express*, vol. 22, no. 16, pp. 19674–19685, 2014.

[30] "G.983.1 : Broadband Optical Access Systems Based on Passive Optical Networks (PON)." [Online]. Available: https://www.itu.int/rec/T-REC-G.983.1-200501-I/.

[31] "G.983.3 : A broadband Optical Access System with Increased Service Capability by Wavelength Allocation." [Online]. Available: https://www.itu.int/rec/T-REC-G.983.3/_page.print.

[32] "G.984.1 : Gigabit-capable Passive Optical Networks (GPON): General

Characteristics," [Online]. Available: https://www.itu.int/rec/T-REC-G.984.1.

[33] "G.984.5:Gigabit-capable Passive Optical Networks (GPON): Enhancement Band," [Online]. Available: https://www.itu.int/rec/T-REC-G.984.5/en.

[34] L. GW Technologies CO., "EPON Technology White Paper." [Online]. Available: http://www.argo-contar.com/solutions/EPON%20Technology%20White%20Paper.pdf.

[35] O. León, J. Hernández-Serrano, and M. Soriano, "Performance Evaluation of GPON vs EPON for Multi-service Access," *Int. J. Commun. Syst.*, vol. 23, no. 5, pp. 633–652, 2010.

[36] COMMSCOPE, "EPON vs. GPON A Comparative Study," [Online]. Available: http://www.commscope.com/Docs/GPON_EPON_Comparison_WP-107286.pdf.

[37] "What's The Difference Between EPON And GPON Optical Fiber Networks?" [Online]. Available: https://www.electronicdesign.com/what-s-difference-between/what-s-difference-between-epon-and-gpon-optical-fiber-networks.

[38] ITU-T, "(XG-PON) systems: Definitions, Abbreviations and Acronyms," [Online]. Available: https://www.itu.int/rec/T-REC-G.987/en.

[39] "Introduction to IEEE 802.3av 10Gbit/s Ethernet Passive Optical Networks (10G EPON) White Paper," [Online]. Available: https://pdfs.semanticscholar.org/a647/5dd4822aa079d7b1fb37699ecbd949b27877.pdf.

[40] C. Konstadinidis, P. Sarigiannidis, and P. Chatzimisios, "A Multilayer Comparative Study of XG-PON and 10G-EPON Standards." [Online]. Available: https://arxiv.org/abs/1804.08007.

[41] HUAWEI, "Next-Generation PON Evolution," [Online]. Available: https://www.huawei.com/ilink/en/download/HW_077443.

[42] ITU-T, "(NG-PON2): Physical Media Dependent (PMD) Layer Specification," G.989.2 Amendment 2, [Online]. Available: https://www.itu.int/rec/T-REC-G.989.2.

[43] D. A. Khotimsky, "NG-PON2 Transmission Convergence Layer: A Tutorial," *J. Light. Technol.*, vol. 34, no. 5, pp. 1424–1432, 2016.

[44] A. Otaka, J. Terada, J. Kani, and K.-I. Suzuki, "Solutions for Future Mobile Fronthaul and Access-Network Convergence," *J. Light. Technol.*, vol. 35, no. 3, pp. 527–534, 2017.

[45] "IEEE P802.3ca 100G-EPON Task Force." [Online]. Available: http://www.ieee802.org/3/ca/index.shtml.

[46] "Next Generation PON 100G-EPON (IEEE 802.3ca)," [Online]. Available: https://www.itu.int/en/ITU-T/Workshops-and-Seminars/20180127/Documents/2.%20Curtis%20Knittle.pdf.

[47] F. Obite, E. T. Jaja, and G. Ijeomah, et al., "The Evolution of Ethernet Passive Optical Network (EPON) and Future Trends," *Optik (Stuttg).*, vol. 167, pp. 103–120, 2018.

[48] T. Takahara, T. Tanaka, and M. Nishihara, et al., "Discrete Multi-Tone for 100 Gb/s optical access networks," *Conf. Opt. Fiber Commun. Tech. Dig. Ser.*, pp. 3–5, 2014.

[49] N. Antoniades, G. Ellinas, and J. Homa, et al., "ROADM Architectures and WSS Implementation Technologies," *Convergence of Mobile and Stationary Next-Generation Networks*, Hoboken, NJ, USA: John Wiley & Sons, Inc., pp. 643–674, 2010.

[50] Fujitsu Network Communications Inc., "CDC ROADM Applications and Cost Comparison," [Online]. Available: https://www.ofcconference.org/getattachment/188d14da-88ba-4a63-91d6-1cc14b335d8b/CDC-ROADM-Applications-and-Cost-Comparison.aspx.

[51] T. Watanabe, K. Suzuki, and T. Goh, et al., "Compact PLC-based Transponder Aggregator for Colorless and Directionless ROADM," *in Proc. Opt. Fiber Commun. Conf. Nat. Fiber Optic Eng. Conf.*, 2011.

[52] F. Roadm and W. I. Way, "Optimum Architecture for M × N Multicast Switch-Based Colorless ,and Flexible-Grid ROADM," *in Proc. Opt. Fiber Commun. Conf. Nat.*

Fiber Optic Eng. Conf., 2012.

[53] R. Jensen, "Optical Switch Architectures for Emerging Colorless/Directionless/ Contentionless ROADM Networks," *in Proc. Opt. Fiber Commun. Conf. Nat. Fiber Optic Eng. Conf.*, 2011.

[54] W. I. Way, "Next Generation ROADM Architectures," in *Asia Commun. and Photon. Conf.*, 2012.

[55] S. L. Woodward and M. D. Feuer, "Benefits and Requirements of Flexible-Grid ROADMs and Networks [Invited]," *J. Opt. Commun. Netw.*, vol. 5, no. 10, pp. A19–A27, 2013.

[56] A. Hirano, T. Tanaka, and K.-I. Sato, et al., "A Novel Semi-flexible Grid Optical Path Network That Utilizes Aligned Frequency Slot Arrangement," *in Proc. Eur. Conf. Opt. Commun.*, vol. 1, no. 1, pp. 459–461. 2013.

[57] S. Thiagarajan and S. Asselin, "Nodal Contention in Colorless, Directionless ROADMs using Traffic Growth Models," *in Proc. Opt. Fiber Commun. Conf. Nat. Fiber Optic Eng. Conf.*, 2013.

[58] M. D. Feuer, S. L. Woodward, and P. Palacharla, et al. , "Intra-node contention in dynamic photonic networks," *J. Light. Technol.*, vol. 29, no. 4, pp. 529–535, 2011.

[59] W. I. Way, P. N. Ji, and A. N. Patel, "Wavelength Contention-Free via Optical Bypass Within a Colorless and Directionless ROADM [Invited]," *J. Opt. Commun. Netw.*, vol. 5, no. 10, pp. A220–A229, 2013.

[60] "Release 15." [Online]. Available: https://www.3gpp.org/release-15.

[61] J. M. Tang, P. M. Lane, and K. A. Shore, "High-speed Transmission of Adaptively Modulated Optical OFDM Signals Over Multimode Fibers Using Directly Modulated DFBs," *J. Light. Technol.*, vol. 24, no. 1, pp. 429–441, 2006.

[62] Y. Rahmatallah and S. Mohan, "Peak-to-average Power Ratio Reduction in OFDM Systems: A survey and Taxonomy," *IEEE Commun. Surv. Tutorials*, vol. 15, no. 4, pp. 1567–1592, 2013.

3. Multiple Channel Interference Cancellation of Digital Filter Multiple Access PONs

Contents

3.1 Introduction

Driven by the increasing bandwidth requirements, PONs have become a technical necessity for providing end-users with unprecedented emerging bandwidth-hungry Internet applications and services [1-4]. As such, recent years have seen PON architectures quickly evolving from traditional TDMA PONs [5], to WDMA PONs [6], to hybrid TDMA/WDMA PONs [6], to FDMA PONs [7], and to optical OFDMA PONs [8]. On the other hand, to accommodate highly dynamic traffic patterns, significant improvements should also be made in PON reconfigurability, flexibility and elasticity. In practically realising these desired PON networking functionalities in a cost-effective manner, SDN has to be implemented, which makes use of centralized network resource abstraction and network infrastructure virtualization to easily and dynamically reconfigure the networks across all the layers down to the physical layer. Such network operations are capable of providing end-users with on-demand broadband connection/services each tailored to a specific application or service requirement. Furthermore, from the PON backward compatibility point of view, it is also greatly advantageous if a universal PON access technique is developed to ensure that various existing PON access techniques can operate simultaneously over already installed PON architectures.

To address the aforementioned challenging objectives, DFMA [9] has been proposed recently, which utilises centralized SDN controller-managed, DSP-based, dynamic software-reconfigurable digital orthogonal filters to perform channel multiplexing/ demultiplexing. DFMA allows multiple independent channels of arbitrary bandwidth granularity to dynamically share a common fibre transmission medium and other relevant network resources. For the cost-sensitive IMDD DFMA PON application scenario of interest of the thesis, the involved digital orthogonal filters can be embedded, in the digital domain, in each individual ONU and OLT without requiring any extra electrical and optical components. It has been shown [9] that DFMA PONs possess the following salient operation features including, for example, i) DSP-enabled dynamic network reconfigurability, flexibility and elasticity, ii) inherent transparency to signal modulation format, signal bit rate, existing PON access techniques and network topologies, and iii) capability of SDN-based network abstraction and virtualization for all the layers including the physical layer. Therefore, DFMA PONs not only offers excellent backward compatibility, but also have great potential for supporting future C-RANs, which are capable of seamlessly integrating

traditional optical access networks, metropolitan optical networks and MFH/MBH networks when combined with DFMA compatible ROADMs [10, 11].

It has been shown [9] that the DFMA technique relies on maintaining a relatively high level of orthogonality between digital filters employed by various channels. However, for practical transmission systems, the degradation of digital filtering-based channel orthogonality is unavoidable because of nonlinearities that may be encountered in signal generation, transmission, routing, traffic aggregation/de-aggregation and detection. Thus, the resulting imperfect channel orthogonality results in the DFMA PONs suffering from cross-channel interference, therefore the maximum achievable DFMA PON transmission performance is degraded.

Generally speaking, to alleviate cross-channel interference in various modern communications systems, over the past few decades, various DSP-based techniques have been proposed, which can be broadly classified into two main categories: indirect interference cancellation (IIC) and direct interference cancellation (DIC) [12]. The representative examples of the IIC category techniques are minimum mean-square error (MMSE) detection [13, 14] and maximum likelihood (ML) detection [15]. As the DSP complexity of the IIC category techniques increases exponentially with increasing user count [16], thus this category is not practically feasible for use in a DFMA PON accommodating a large number of ONUs.

On the other hand, the DIC category can be further divided into two subcategories, i.e., serial interference cancellation and parallel interference cancellation [16]. The serial scheme [17, 18] is multi-user detection-based, in which various signals from different users are firstly detected, and subsequently the interferences among them are cancelled serially in the order of perceived reliability. Whilst the parallel scheme [19, 20] collectively cancels the interferences induced by all other users from the received signal of a targeted user. Clearly, the serial scheme is simple and relatively accurate, but it yields significantly high DSP-induced latency. Whilst the parallel scheme has relatively low latency, but it suffers high overall DSP complexity because the interferences from all users have to be estimated in parallel within each individual iteration stage, and the total number of iteration stages required for achieving an acceptable performance accuracy is relatively large [16, 21]. Apart from the abovementioned drawbacks, the performances of all techniques in the IIC and DIC categories are also very sensitive to initial operation conditions, and also dependent upon

signal modulation format. Obviously, all these disadvantages associated with the available techniques in both categories considerably restrict their applicability in the DFMA PONs.

More recently, by making use of DSPs similar to the parallel scheme of the DIC category, a very simple but effective cross-channel interference cancellation (CCIC) technique has been proposed and experimentally demonstrated for point-to-point IMDD DFMA PON systems [22]. The CCIC's unique features include the independence of both initial condition setting and signal modulation format, as well as extremely fast convergence. In addition, the CCIC technique also has the potential not only to drastically improve the transmission performance of point-to-point DFMA PON systems, but also to significantly reduce the latency and DSP implementation complexity.

In this chapter, by significantly extending the previously reported CCIC technique from point-to-point DFMA PON systems to multipoint-to-point DFMA PON architectures, a more general and comprehensive multi-channel interference cancellation technique, termed DCIC, is proposed and extensively investigated, for the first time, for applications in IMDD DFMA PON architectures. As a variant of the parallel scheme in the DIC category, the proposed DCIC technique utilises DSP-based and transceiver-embedded digital orthogonal filters to simultaneously receive various signals from different ONUs, based on which the interference experienced by each individual ONU is estimated and subsequently subtracted from the initially received signal of the same ONU. Finally, each individual signal with improved quality is demodulated in the receiver. Our investigations show that, for multipoint-to-point upstream IMDD DFMA PONs conveying OOFDM signals, with one iteration only the DCIC technique can achieve a reduction in individual OOFDM subcarrier BER of more than 1000 times, an increase in signal transmission capacity by as much as 2 times and an increase in differential ONU launch power dynamic range by as much as 14 dB. In addition to the aforementioned excellent operation performance, other major advantages associated with the proposed DCIC technique are summarized below:

- Transparency to both signal modulation format and signal bit rate, and independence to initial system operation condition setting. These features ensure the DCIC's compatibility to DFMA PONs, equally important, further improve DFMA PON's reconfigurability, flexibility and elasticity.

- Low latency, as for the vast majority cases, only one iteration is sufficient for improving the DFMA PON performance to acceptable BER levels. From the practical implementation point of view, as the DCIC technique is application specific integrated circuit (ASIC)-based, one iteration is estimated to take a few microseconds only. Thus the DCIC-induced latency is at least several times faster than the aforementioned techniques of the DIC category. For future 5G networks, low latency communications are crucial for applications such as automotive, medical and other types of tactile internet applications requiring real-time user feedback mechanisms. On the other hand, for PON application scenarios, low latency communications are also vital for maintaining the performances of active ONUs when new ONUs are introduced.
- Low DSP complexity. Compared to existing techniques of the DIC category, the DCIC DSP complexity is extremely low, especially for DFMA PONs accommodating a large number of ONUs. This arises due to ONU count-independent operation performance, as discussed in detail in subsection 3.4.2.

As already stated above, the DFMA PONs are inherently transparent to various signal modulation formats including, for example, non-return-to-zero (NRZ) and four-level pulse-amplitude modulation (PAM-4). In this chapter, special attention is focused on OOFDM, as OOFDM is regarded as a promising candidate for 5G networks because of its high spectral efficiency and DSP richness.

This chapter is organised as following: In subsection 3.2, a theoretical DCIC model is established to offer an in-depth understanding of the operating principles of the proposed DCIC technique. In subsection 3.3, the validity of the theoretical model is rigorously examined via numerical fitting with experimental measurements for various DFMA PON systems. For upstream IMDD DFMA PONs, subsection 3.4.1 extensively explores the DCIC-induced performance improvements in terms of aggregated upstream transmission capacity and differential ONU launch power dynamic range. In addition, the impact of ONU count on the DCIC performance is also investigated in subsection 3.4.2. Finally, the chapter is concluded in subsection 3.5.

3.2 Theoretical Model

Fig. 3.1 (a) illustrates a diagram of the considered DSP-enabled software reconfigurable upstream DFMA PON based on IMDD. As the downstream operating principle of the DFMA PON is very similar to point-to-point DFMA PON transmission systems [22], here special attention is, therefore, given to the multipoint-to-point upstream operation and the operating principle of the proposed DCIC technique. For the upstream DFMA PON, the DCIC technique is just applied before signal demodulation in the OLT, as shown in Fig. 3.1(a).

3.2.1 Upstream DFMA PONs

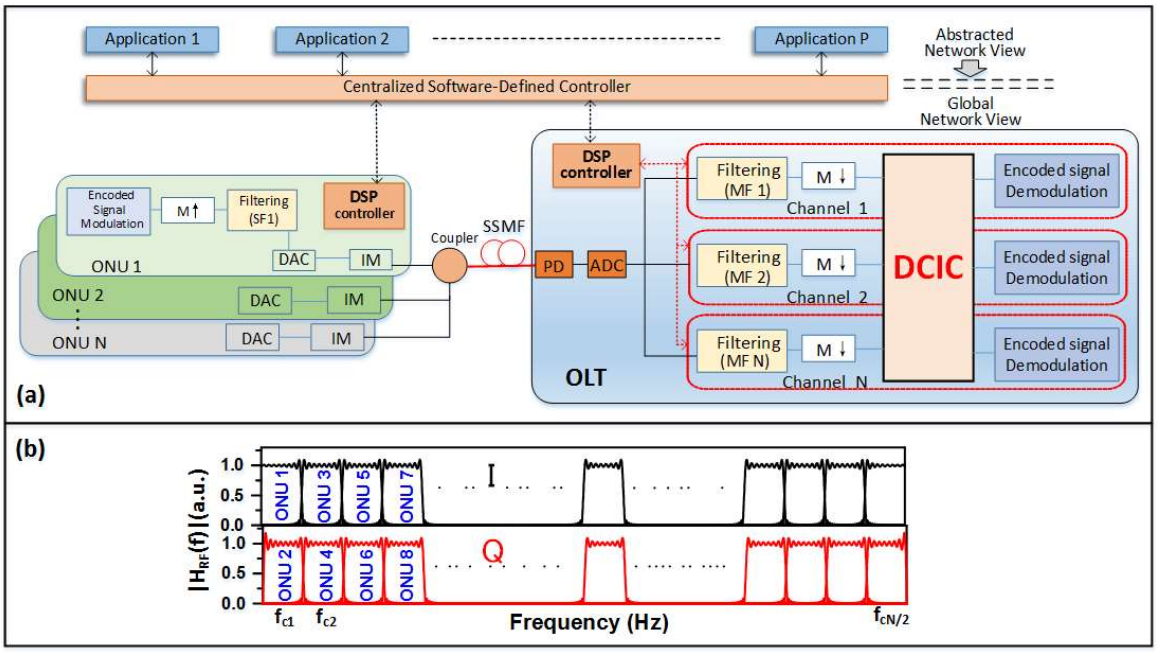

Fig. 3.1 (a) DFMA PON diagram. For upstream, DCIC is applied in the OLT. (b) Example of channel allocation of multiple ONUs involved in the DFMA PON.

Considering an upstream DFMA PON conveying *N* different ONU channels, the *i*-th ONU channel digitally encoded by an arbitrary signal modulation format is first up-sampled by a factor of *M*, and then passed through a digital orthogonal SF [9]. The digitally filtered data sequence is fed to a DAC to generate an analogue electrical signal, which is utilized to drive an optical IM, as seen in Fig. 3.1 (a). Finally, different optical signals from various ONUs are passively combined by an optical coupler, and the generated optical signal can be expressed as

$$S_{opt}(t) = \sum_{i=1}^{N}\left[\sigma_i(t)e^{j\beta_i(t)} \cdot \sqrt{y_i(t)}\right] \cdot e^{j2\pi f_0 t} \tag{3.1}$$

with

$$y_i(t) = a_i(t) \otimes s_i(t) \tag{3.2}$$

where f_0 is the optical carrier frequency, $\sigma_i(t)e^{j\beta_i(t)}$ takes into account the optical intensity modulation impacts on the amplitude $\sigma_i(t)$ and phase $\beta_i(t)$ of the i-th optical signal, $y_i(t) > 0$ is the optimum DC current biased, real-valued i-th ONU electrical signal fed to the optical IM, $a_i(t)$ is the up-sampled digital data sequence and $s_i(t)$ is the impulse response of the SF occupied by the i-th ONU. The generated optical signals propagate through the fibre transmission link to the OLT.

In the OLT, the received optical signal is firstly converted to the electrical domain via square-law photo detection and subsequently digitised by an ADC. After that, the digital data stream corresponding to the i-th ONU is demultiplexed by applying a corresponding digital orthogonal MF. After digital filtering, the demultiplexed signal is down-sampled by selecting every M-th sample from the synchronised data sequence, and then the DCIC technique is applied and the i-th ONU data is finally decoded.

The construction of various digital orthogonal SF and MF filters employed in the ONUs and OLT is undertaken using the Hilbert-pair approach [9], as described in subsection 2.2.1.5 from Eq. (2.10) to Eq. (2.14). An example of how different orthogonal filters are assigned to individual ONUs is illustrated in Fig. 3.1 (b), where the gapless frequency responses of both I and Q components of these Hilbert-pairs at different central frequencies are plotted. The allocation of individual ONUs to available orthogonal filters is completely flexible and dynamic as this is achieved by simply reconfiguring the digital filter parameters in the digital domain. In addition to the case discussed above, several DFMA channels can also be assigned simultaneously to a single ONU, and a single DFMA channel can also be shared by two or more ONUs using a multiple access method such as TDMA. Here it is also worth emphasizing that the digital filtering is undertaken using DSP controllers embedded in both the ONUs and the OLT. As shown in Fig. 3.1(a), to establish a connection, by working together with the centralized SDN controller, the digital filter parameters can be adjusted dynamically and adaptively according to transmission system spectral characteristics and network traffic status, once a SF filter and the corresponding MF filter are chosen, a DSP-enabled dedicated physical connection between an ONU and the OLT is thus established, which is online software-reconfigurable.

3.2.2 DCIC Operating Principle

In the OLT, the transmitted optical signal is directly detected by a square-law photo detector. Let $r(t)$ denote the detected signal, which is given by

$$r(t) = \sum_{i=1}^{N} \rho_i(t) \cdot y_i(t) \otimes h_i(t) + v(t) \tag{3.3}$$

where $h_i(t)$ is the electrical-domain *i*-th channel impulse response taking into account all the electrical/optical effects related to DAC/ADC and fibre transmission, and $v(t)$ represents all optical and electrical noise associated with the entire channel. $\rho_i(t)$ represents the E-O/O-E conversion-induced impacts on the *i*-th channel signal. Before down-sampling, the corresponding MF ($m_i(t)$) de-multiplexed *i*-th ONU signal is given by

$$a_i'(t) = \sum_{n=1}^{N} \rho_n(t) \cdot y_n(t) \otimes h_n(t) \otimes m_i(t) + v_i(t) \otimes m_i(t) \tag{3.4}$$

where $v_i(t)$ is the noise associated with the *i*-th channel,$h_n(t)$ leads to the generation of interference from the *n*-th ONU to the *i*-th ONU, which cannot be removed by the selective MF in the OLT. By further expanding Eq. (3.4), we have

$$\begin{aligned} a_i'(t) = \ & \rho_i(t) \cdot a_i(t) \otimes h_i(t) \otimes \delta(t - t_i) + \sum_{n=1, n\neq i}^{N} \rho_n(t) \cdot \\ & a_n(t) \otimes s_n(t) \otimes h_n(t) \otimes m_i(t) + v'(t) \end{aligned} \tag{3.5}$$

where t_i is the signal propagation time delay. The first term of the right side of Eq. (3.5) contains the desired *i*-th ONU signal, which is affected only by the corresponding channel impulse response; the second term represents the sum of all interference components from all the other ONUs, and the last term is the received noise component. By making use of Eq.(3.5), a conventional interference cancellation-free receiver is not capable of recovering the first term. As the practical channel impulse response is non-ideal, the interference term may seriously degrade the system performance.

When the most significant first-order interference components are considered only, these interference components are linearly combined with the wanted signal received, thus the received signal quality can be improved by subtracting the corresponding interference components using the formula below

$$a_i^{<1>}(t) = a_i'(t) - \sum_{n=1, n\neq i}^{N} L_{n\to i}^{<1>}(t) \tag{3.6}$$

where $a_i^{<1>}(t)$ is the interference-subtracted i-th ONU signal after the first iteration. $\sum_{n=1,n\neq i}^{N} L_{n\to i}^{<1>}(t)$ is the sum of the interference components induced by all the other N-1 ONUs. From Eq. (3.5), $L_{n\to i}^{<1>}(t)$ can be expressed as

$$L_{n\to i}^{<1>}(t) = \rho_n(t) \cdot a_n(t) \otimes s_n(t) \otimes h_n(t) \otimes m_i(t) \tag{3.7}$$

From the discussions in subsection 3.2.1, it is easy to understand that the SF and MF impulse responses, $s_n(t)$ and $m_i(t)$, are made known to the DSP controller, and the channel frequency response representing the entire transmission system of the n-th channel from the DAC input in the transmitter to the ADC output in the receiver, can also be measured easily by a training sequence-based channel estimation function. As the exact n-th signal is not available at the receiver, the signal, $a_n'(t)$, received before signal demodulation, is thus used as the best estimation of the n-th ONU signal. In addition, to take into account the effect arising from $\rho_n(t)$, each individual interference component should be scaled appropriately. Thus Eq.(3.6) can be rewritten as

$$a_i^{<1>}(t) = a_i'(t) - \sum_{n=1,n\neq i}^{N} C_{in}^{<1>}(t) \cdot L_{n\to i}^{<1>}(t) \tag{3.8}$$

with

$$L_{n\to i}^{<1>}(t) = a_n'(t) \otimes s_n(t) \otimes h_n(t) \otimes m_i(t) \tag{3.9}$$

and

$$C_{in}^{<1>}(t) = A_{in}^{<1>}(t) \cdot e^{-j\varphi_{in}^{<1>}(t)} \tag{3.10}$$

where $C_{in}^{<1>}(t)$ is the scaling factor representing the interference from the n-th ONU to the i-th ONU in the first iteration stage. To further improve the accuracy of the received signal, more iteration stages can be applied successively as follows

$$a_i^{<2>}(t) = a_i^{<1>}(t) - \sum_{n=1,n\neq i}^{N} C_{in}^{<2>}(t) L_{n\to i}^{<2>}(t) \tag{3.11}$$

where $L_{n\to i}^{<2>}(t)$ is generated by using the corrected signal after the first iteration. It should be noted that multiple DCIC iteration stages not only prolong the latency but also increase the

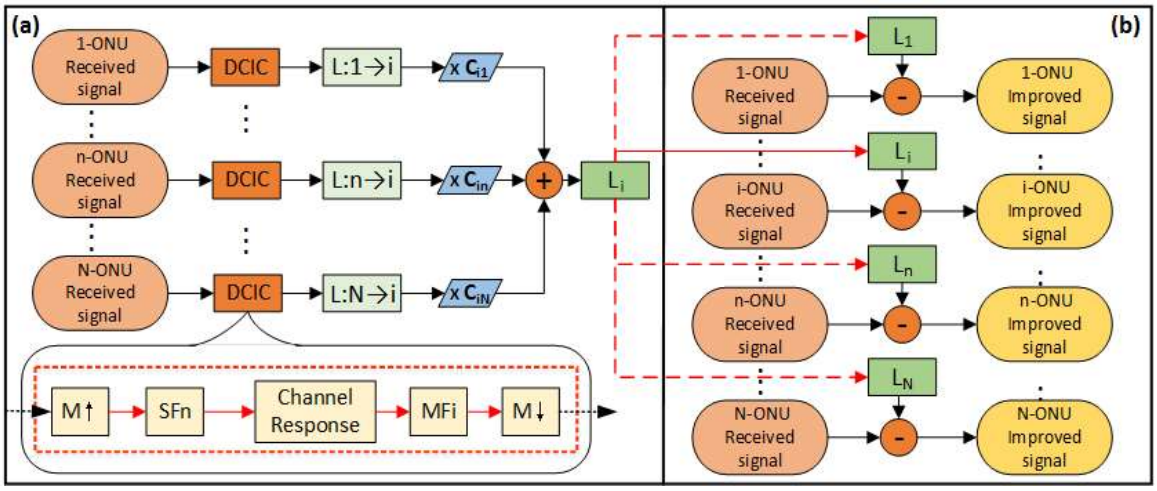

Fig. 3.2 DCIC operating principle. (a) Scaling and summing interference from all other channels; (b) Subtracting the interference. 'L' refers to interference.

DSP implementation complexity.

To improve the DCIC operation accuracy and simultaneously reduce the iteration stages required, full use can be made of the essential scaling process. In practice, for each individual ONU, the frequency-dependent scaling is undertaken in the frequency domain by utilising a training sequence inserted in the corresponding data sequence. The interference between different training sequences from different ONUs can be calculated in the same way as described above. For a specific ONU, with an initially selected scaling factor applied, the interference-subtracted training sequence is then compared with the known training sequence to obtain a corresponding BER of the training sequence for the ONU. Based on the BER, a fine adjustment of the scaling factor can be made. As a result, an optimum frequency dependent scaling factor for the ONU is obtained when the corresponding BER is minimised. Such an optimum scaling factor identification process results in that only one iteration stage is sufficient for achieving acceptable BERs for different ONUs. This greatly reduces not only the latency and DCIC DSP complexity but also the error propagation effect, thus the effectiveness of the DCIC technique is improved enormously. It is also important to note that, except Fig. 3.11, all results presented in this chapter are obtained with one iteration only.

The above-mentioned DCIC operating principle is illustrated in Fig.3.2, where the '*i*-ONU received signal' is referred to as $a_i'(t)$. Firstly, the interferences from all other ONUs to the *i*-th ONU ($L_{n\to i}^{<1>}(t)$) are estimated, such a procedure is repeated by *N-1* times. Then the scaling factor is applied, and finally the combined interference estimate is subtracted from

$a_i'(t)$. For the upstream DFMA PONs, the received signals from different ONUs are made known to the OLT, thus all the interference estimations from different ONUs can be produced in parallel.

3.3 Model Evaluation and Parameter Identification

In order to numerically explore the feasibility of utilizing the proposed DCIC technique to improve the upstream performance of the multipoint-to-point DFMA PONs, it is vital to rigorously evaluate the validity of the digital orthogonal filtering process, as such process is the heart of both point-to-point and multipoint-to-point DFMA PON architectures. In addition, to ensure that the theoretical predictions are practically achievable, it is also important to identify a set of accurate system parameters representing the E-O/O-E impacts and DAC/ADC-induced frequency response roll-off. To achieve these two objectives, in this subsection, extensive comparisons are made between numerical simulations and experimental measurements.

3.3.1 Simulation Models and Numerical Fitting Procedure

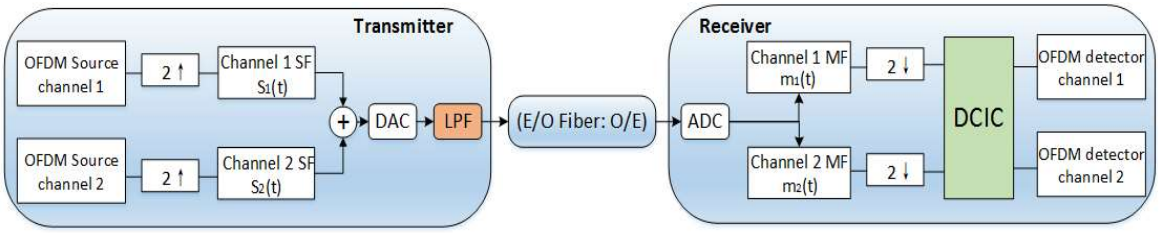

Fig. 3.3 Two-channel DFMA PON system diagram adopted in both experiments and numerical fitting.

The two-channel point-to-point IMDD DFMA PON system adopted in the numerical fitting is illustrated in Fig. 3.3, which is identical to that employed in our experimental measurements [22], except that an electrical low pass filter (LPF) is introduced in the transmitter in this chapter to collectively take into account the effects that are not directly measurable in the experiments. These effects include, for example, i) nonlinear effects associated with the EML adopted in the experiments [22]; ii) the EML-induced frequency chirp effect, and iii) the overall frequency response associated with all electrical/optical components. The introduction of such an LPF in the transmitter also allows the utilisation of

an ideal optical intensity modulator in the numerical simulations instead of a complicated EML model. This speeds up the simulation process.

In numerical fitting, the digital orthogonal filters, SF and MF, are constructed following the procedures previously described in subsection 3.2. An OOFDM signal is considered for each channel to be consistent with the experimental measurements [22]. In addition, a number of other theoretical models developed and verified in [23] are also adopted in the numerical simulations, which include: i) an electrical OFDM transceiver with adaptive subcarrier bit loading; ii) a standard SSMF transmission model incorporating the effects of loss, chromatic dispersion, and various Kerr effect-induced fibre nonlinearities, and iii) a square-law photo detection model with both shot and thermal noise being present.

All the transceiver and transmission system parameters reported in [22] are adopted here and kept as constants in the numerical simulations. A summary of those parameters are listed in Table 3.1, where typical SSMF parameters are also presented. In particular, the adopted key SF and MF filter parameters are: the total number of filter taps of 32 and an excess of bandwidth of $\alpha=0$, which are also identical to those adopted in the experiments [22]. Theoretically speaking, the impulse response function of a baseband digital filter constructed using the Hilbert-pair approach is the *sinc* function when $\alpha = 0$, with its side lobes decreasing rapidly over time. From the implementation point of view, a practical digital filter always has a limited number of taps, and the corresponding impulse response function can be considered to be a truncated version of the *sinc* function. As such the practical digital filter can result in signal distortions, which, however, decrease with increasing tap count (DSP complexity). Therefore, it is vital to identify an optimum trade-off between the digital filter DSP complexity and its corresponding system transmission performance for a specific application scenario. Our FPGA-based real-time experimental results [24] have shown that, for the DFMA PONs, when the digital filter tap count is ≥ 32, the system BER performance becomes stable, this indicates tap counts as small as 32 can be a practical choice for constructing practically acceptable digital filters with $\alpha = 0$.

By expanding Eq.(3.10), the frequency dependent scaling factors corresponding to individual OFDM subcarriers can be written in a form of

$$C_{in}^{<1>} = \begin{bmatrix} A_{in,1}^{<1>} \cdot e^{-j\varphi_{in,1}^{<1>}} \\ \vdots \\ A_{in,k}^{<1>} \cdot e^{-j\varphi_{in,k}^{<1>}} \end{bmatrix} \tag{3.12}$$

where $A_{in,k}^{<1>} \cdot e^{-j\varphi_{in,k}^{<1>}}$ is the scaling factor for the *k*-th subcarrier in the first iteration, *k* is the subcarrier index. In numerical simulations, the scaling factor for each subcarrier is finely adjusted according to the method mentioned previously.

In the process of numerical fitting with the experimental results, the magnitude and phase response of the introduced LPF are finely adjusted to provide the best fit with all the experimental results in terms of both individual subcarrier BER performances and system transmission BER performances. The resulting optimum LPF frequency response are plotted in Fig. 3.4. The observed frequency response roll-off of 5 dB within a 0~1 GHz spectral range is mainly contributed by the inherent sin(x)/x response of the DAC/ADC, the effects of various low pass filters employed in the experimental setup, and also the EML nonlinearities. Due to the abovementioned effects, Fig. 3.4 also shows almost linear frequency dependent phase variations of 0.97 ns (1.10 ns) at 200 MHz (900 MHz).

Table 3.1 List of Parameters

PARAMETER	VALUE	PARAMETER	VALUE
DAC sample rate	2 GS/s	DAC resolution	8 bits
Clipping ratio	13 dB	Cyclic Prefix	25%
Modulation formats	16 QAM	Total number of IFFT/FFT points	32
Transmitted optical power	2 dBm	Received optical power	-14 dBm
SSMF length	26 km	Up sampling factor *M*	2
Digital filter taps	32	Excess of the bandwidth α	0
PIN detector bandwidth	12.5 GHz	PIN detector sensitivity/bandwidth	-19 dBm/ 12.5 GHz
Fiber dispersion	17 ps/nm/km	Fiber dispersion slope	0.07 ps/nm/km
Fibre Kerr coefficient	2.35e-20 m^2/W	Fiber loss	0.2 dB/km

3.3.2 Experimental and Theoretical Results Comparison

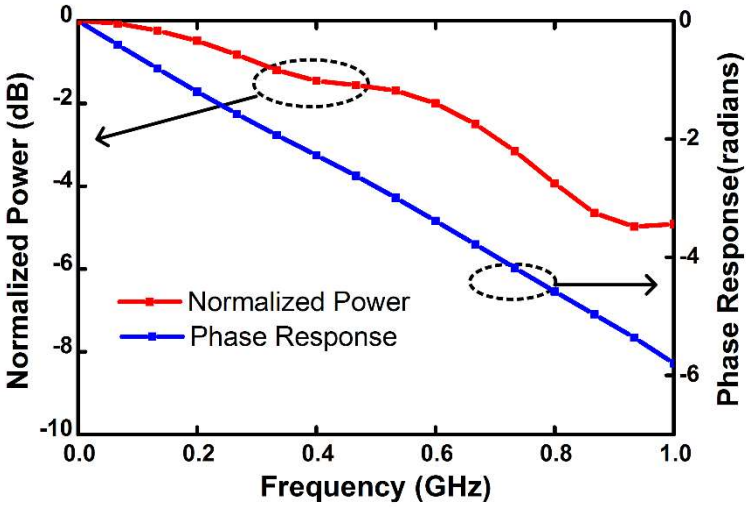

Fig. 3.4 Frequency response of the low pass filter introduced in the transmitter.

By making use of the obtained LPF frequency response presented in Fig. 3.4, as well as the transceiver and transmission system parameters summarised in Table 3.1, in this subsection, for two cases of including and excluding the proposed DCIC technique, detailed comparisons between numerical simulations and corresponding experimental measurements are made for different experimental system configurations.

After 26 km SSMF transmissions of an optical signal consisting of two spectrally overlapped I and Q channels, here referred to as Channel 1 and Channel 2, respectively, numerically simulated BER performances of 15 data-bearing subcarriers of each channel are plotted in Fig. 3.5, where their corresponding experimentally measured BER performances are also given. It can be seen in Fig. 3.5 that, for both cases where the DCIC technique is included and excluded, the simulated BER performances nearly perfectly overlap with the corresponding experimental results across all the subcarriers for both channels.

It should be noted that relatively low DCIC performances for the low frequency subcarriers are seen in Fig. 3.5. This is because the signal spectrum after up-sampling in the transmitter consists of two mirrored spectral images, and each subcarrier imagine is mapped to both the upper sideband and the lower sideband. Thus the lower frequency subcarriers have greater frequency separation than the higher frequency subcarriers, as a direct result, they suffer greater amplitude variations at the receiver due to the system frequency response roll-off effect. As the interference cancellation relies on $a_n'(t)$, which includes the frequency

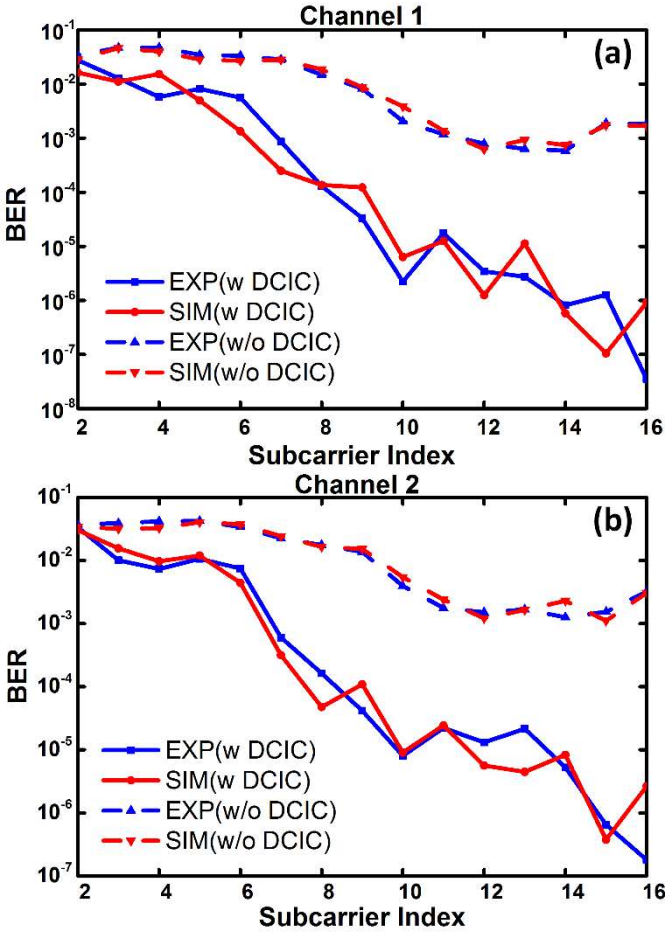

Fig. 3.5 Comparison of the BER distribution across all the subcarriers between numerical simulations and experimental measurements. (a) I channel referred to as Channel 1, (b) Q channel referred to as Channel 2. 'w DCIC' refers to as system with DCIC, 'w/o DCIC' refers to as system without DCIC

components from each sideband, the larger the amplitude variation between the two sidebands, the more the error in $a_n'(t)$, thus the weaker the DCIC operation effectiveness.

To further examine the validity of the theoretical model and the accuracy of the identified parameters, for both Channel 1 and Channel 2, total channel BER versus received optical power (ROP) performance comparisons between numerical simulations and experimental measurements are also made in Fig. 3.6, where the transmission system configuration and its relevant parameters are identical to those adopted in Fig. 3.5. For the case excluding DCIC, the curves obtained in simulations and experiments show an almost identical performance for both channels, the similar behaviours also hold for the case including DCIC, especially in the vicinity of a BER = 1.0×10^{-3}.

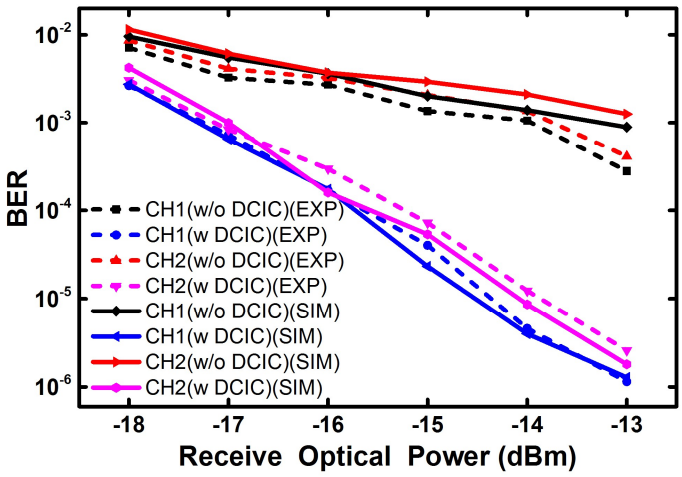

Fig. 3.6 Comparison of the BER versus receive optical power between numerical simulations and experimental measurements. 'CH1' refers to the I channel while 'CH2' refers to the Q channel.

The excellent agreements between numerical simulations and experimental measurements in Fig. 3.5 and Fig. 3.6 in terms of subcarrier BER performance and total channel BER versus ROP system performance strongly confirm not only the validity of the developed DCIC theoretical model, but also the accuracy of the transceiver/transmission system parameters. As such, unless stated explicitly in relevant texts, both the LPF frequency response and the parameters listed in Table 3.1 are adopted as default throughout this chapter.

3.4 DCIC-enabled Improvement of DFMA PON Performance

Based on the verified theoretical model and by making use of the parameters identified in subsection 3.3, DCIC-enabled maximum achievable performances of multipoint-to-point upstream DFMA PONs are extensively explored numerically in this subsection. To highlight the DCIC effectiveness for various DFMA PON architectures, performance comparisons are also made between the cases of including and excluding DCIC.

3.4.1 DCIC-enabled Performance Improvement of Two ONU DFMA PONs

Here a multipoint-to-point upstream DFMA PON accommodating only two ONUs is considered, in which ONU1 and ONU2 utilise the '*I*' and '*Q*' components of a single Hilbert-pair at the same central RF frequency, respectively, thus these two ONUs occupy the same spectral region, as shown in Fig. 3.1 (b). To explore the impact of DCIC on the upstream

performance of the DFMA PONs operating at widely adopted DAC/ADC sampling rates of $f_{DAC/ADC}$=12.5 GS/s, the frequency response of the LPF introduced in the transmitter in Fig. 3.3 is linearly scaled to ensure that the previously identified amplitude roll-off and phase profiles are still maintained over the extended signal spectral region. Such linear frequency scaling process is conducted using the formula below:

$$f \rightarrow (\frac{f_c'}{f_c})f \tag{3.13}$$

where f_c'=1 GHz and f_c=6.25 GHz are the previous and new signal bandwidths, respectively. All other simulation parameters that are adopted in the simulations but not explicitly mentioned above are identical to those listed in Table 3.1.

For a specific transmission distance, to explore the maximum achievable aggregated upstream signal transmission capacity, adaptive bit loading is employed on each individual subcarrier conveyed by each channel, a signal modulation format is selected from 256-QAM, 128-QAM, 64-QAM, 32-QAM, 16-QAM, DQPSK and DBPSK. In implementing adaptive bit loading, a highest possible signal modulation format is always chosen to ensure the achievement of a maximum transmission capacity under the condition that the total BER of a targeted channel is still below the forward error correction (FEC) limit of 1.0×10^{-3}. A subcarrier is dropped completely if excessive errors occur when the lowest signal modulation format is taken. The signal transmission capacity, R_b, of each channel is calculated by

$$R_b = \frac{f_{DAC}\sum_k^{N_S} n_{kb}}{2(N_s+1)(1+C_p)M} \tag{3.14}$$

Where n_{kb} is the number of binary information bits conveyed by the k-th subcarrier within one OFDM symbol period, N_s is the total number of data-bearing subcarriers and $C_p$is the overhead parameter associated with the cyclic prefix and training sequence, and M is the up-sampling factor.

The simulated performance of maximum achievable aggregated upstream transmission capacity versus reach is shown in Fig. 3.7, where the total optical launch power is kept at 2 dBm. It is shown in Fig. 3.7 that, for a transmission distance of 5 km, DCIC gives rise to an aggregated maximum transmission capacity as large as 32.5 Gb/s, which is >2.5 times higher than that obtained without DCIC. In addition, the DCIC-induced transmission capacity improvement is also feasible cross a wide transmission distance range varying from 5 km to

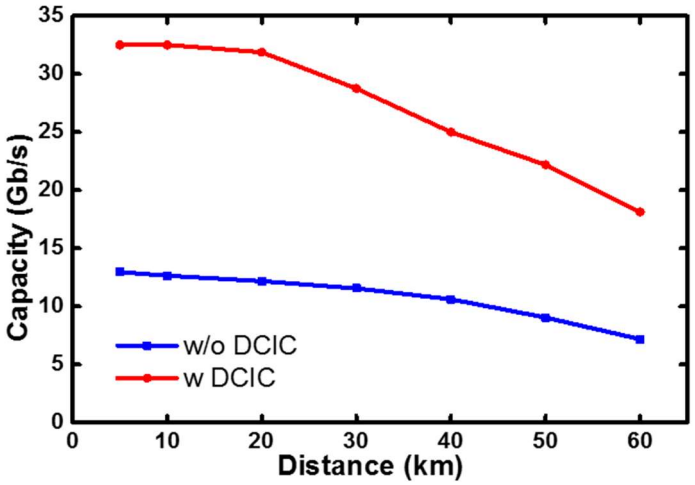

Fig. 3.7 Aggregated upstream transmission capacity versus transmission distance for the IMDD DFMA PONs with two ONUs.

60 km. Furthermore, it is also seen in Fig. 3.7 that the effectiveness of DCIC increases with decreasing transmission distance. This is because for relatively short transmission distances, the effective optical signal-to-noise ratio (OSNR) is relatively high, thus the channel interference plays a dominant role in determining the maximum achievable transmission performance. As the transmission distance increases, the effective OSNR decreases, thus both the reduced OSNR and long transmission distance-enhanced channel interference become important. As a direct result, the DCIC-induced improvement in signal transmission capacity for long transmission distances is not as pronounced as those for shorter transmission distances. Here it is also worth mentioning that when the number of ONUs increases, the above-discussed DCIC-enabled improvement in aggregated upstream transmission capacity still holds, because the aggregated upstream transmission capacity is ONU-count independent [9].

Given the fact that a practical PON may have >15 dB differential losses on the fibre plant and also requires >3 dB launch power tolerances, to explore the DFMA PON's capability of satisfying such requirements, the performance robustness of the two ONU DFMA PON to differential ONU launch power is examined in Fig. 3.8, where the total channel BER performance of a power-varying ONU is plotted as a function of its optical launch power, whilst the other power-fixed ONU launch power is set at -1 dBm. The ROP in the OLT is always fixed at -3 dBm. All other system parameters are identical to those employed in Fig. 3.7, except that a 26 km SSMF is chosen here to be consistent with the previously discussed experimental case. Moreover, as shown in Fig. 3.7, as the DCIC-free 26 km PON system

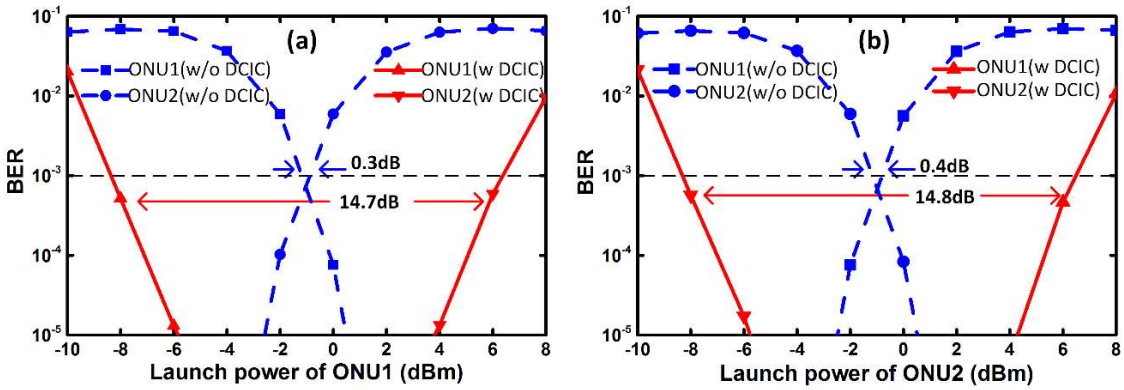

Fig. 3.8 BER performance versus ONU optical launch power. (a) power-varying ONU1 employing the "I" component, (b) power-varying ONU2 employing the "Q" component. Dashed blue curves refer to the cases without DCIC, solid red curves refer to the cases with DCIC.

corresponds to a maximum aggregated signal transmission capacity of 11.9 Gb/s, the corresponding signal modulation format profile is thus employed in Fig. 3.8 for fair comparison. As expected, it can be seen in Fig. 3.8 that an increase in optical launch power from one ONU improves its own BER performance, but simultaneously degrades the BER performance of the other ONU. This mainly results from the opposite changes in effective OSNR experienced by different ONUs.

In this context, the differential ONU launch power dynamic range is defined, for a fixed ROP in the OLT, as the maximum allowable variation range of the optical launch power from a specific ONU, over which the total BERs of all individual ONU signals simultaneously transmitted over the system are still less than the adopted FEC limit. As the signal transmission capacity is the maximum value for the DCIC-free 26 km DFMA PON system, a very narrow differential launch power dynamic range is thus observed for both ONU1 and ONU2 in Fig. 3.8 (a) and (b). However, after applying DCIC, the differential launch power dynamic range of ONU1 (ONU2) significantly increases from 0.3 dB (0.4 dB) to 14.7 dB (14.8 dB), indicating that the effectiveness of DCIC in enhancing the differential ONU launch power dynamic range. As a representative PON can be largely regarded as a linear system, the aforementioned differential ONU launch power dynamic range can also be considered as the ROP dynamic variation range of an ONU. The above discussions imply that DCIC can considerably enhance the robustness of the DFMA PONs.

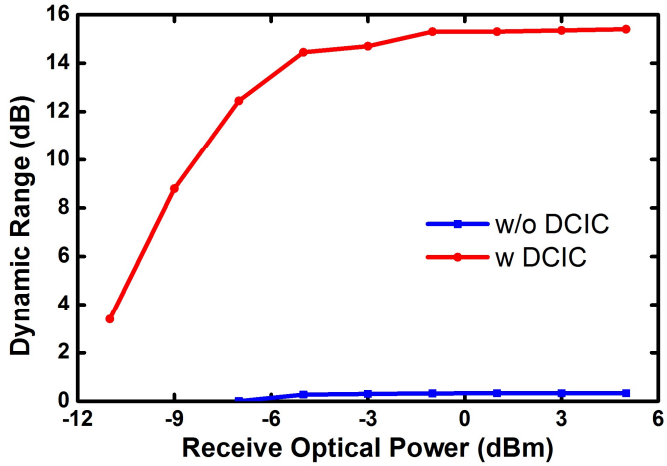

Fig. 3.9 Optical launch power dynamic range of ONU1 as a function of received optical power.

The ROP-dependent differential launch power dynamic range characteristics are explored in Fig. 3.9, where ONU1 is power-varying with all other parameters kept identical to those adopted in Fig. 3.8 (a). It is shown in Fig. 3.9 that for the case of excluding DCIC, the differential launch power dynamic range of around 0.3 dB is almost ROP-independent, whilst when DCIC is included, the dynamic range increases almost linearly from 4 dB to 15 dB with increasing the ROP from -11 dBm to -3 dBm, beyond which the differential launch power dynamic range is flatten at around 15 dB. The flatten maximum differential launch power dynamic range is mainly attributed to nonlinearities and noise associated with the transmission channel. As expected from Fig. 3.8, the same ROP-dependent differential launch power dynamic range characteristics also hold when ONU2 power varies.

3.4.2 DCIC-enabled DSP Complexity Reduction in Multiple ONU DFMA PONs

Having studied the effectiveness of DCIC in remarkably improving both the aggregated upstream signal transmission capacity and the differential launch power dynamic range in two ONU DFMA PONs, this subsection further extends the DCIC's application scenario to multiple ONU DFMA PONs. Apart from the DCIC-enabled performance improvement, here special attention is given to DCIC's another unique feature, i.e., significant reductions in both DSP complexity and latency. As the ONU count grows, the number of interference components increases very rapidly, this may lead to expansions in DCIC DSP complexity and latency.

In order to identify how the DCIC DSP complexity and relevant latency can be reduced without affecting the DCIC effectiveness in enhancing the upstream DFMA PON performance, the interferences from different ONUs to a specific ONU are estimated separately for comparison. For simplicity but without losing generality, 8 ONUs are considered here, and the corresponding up-sampling factor M is chosen to be equal to the total number of ONUs simultaneously accommodated, i.e., M=8 [25]. The channel allocation is as labelled in Fig. 3.1 (b). To make the following comparisons fair, 16-QAM is applied in each individual subcarrier for all these ONUs, and the total optical launch power is still fixed at 2 dBm. All other parameters including the digital orthogonal filters, the LPF and the transmission distance are kept consistent with those employed in Fig. 3.8.

The BER performances of ONU1 and ONU2 versus subcarrier index are plotted in Fig. 3.10 (a) and Fig. 3.10 (b), respectively. In each figure, eight different cases are presented, which include one DCIC-free case, and seven DCIC-related cases each just removing the interference from one ONU only. The inserted legend of 'ONU2'-'ONU8' refers to which ONU the removed interference comes from. Fig. 3.10 (a) shows that the ONU1's subcarrier BER performance in the case of just removing the interference from ONU2 agrees very well with those observed in Fig. 3.5, and, more importantly, is approximately 10000 times lower than other six cases that remove the interferences from ONU3-ONU8. The subcarrier BERs of these six other cases overlap with that corresponding to the DCIC-free case. Very similar subcarrier BER performances are also observed in Fig. 3.10 (b). Furthermore, the subcarrier BER performances of the other 6 ONUs are also numerically examined in the aforementioned eight different cases, as their performances are virtually identical to those in Fig. 3.10 (a) and Fig. 3.10 (b), the results are not displayed.

As seen in Fig. 3.1 (b), ONU1 and ONU2 occupy two digital orthogonal filters forming a single Hilbert-pair, thus they share an identical signal spectral region. This indicates that, for any targeted ONU, the cancellation of the interference caused by the spectrum-sharing ONU is sufficient, and the interferences contributed from all the remaining ONUs are negligible. This contrasts sharply to the conventional multi-channel transmission cases, where the combined interference contributed by all the channels are typically Gaussian noise-like, as a direct result, such Gaussian noise-like channel interferences invalidates available channel interference cancellation techniques when the number of channels are large [12, 16, 20].

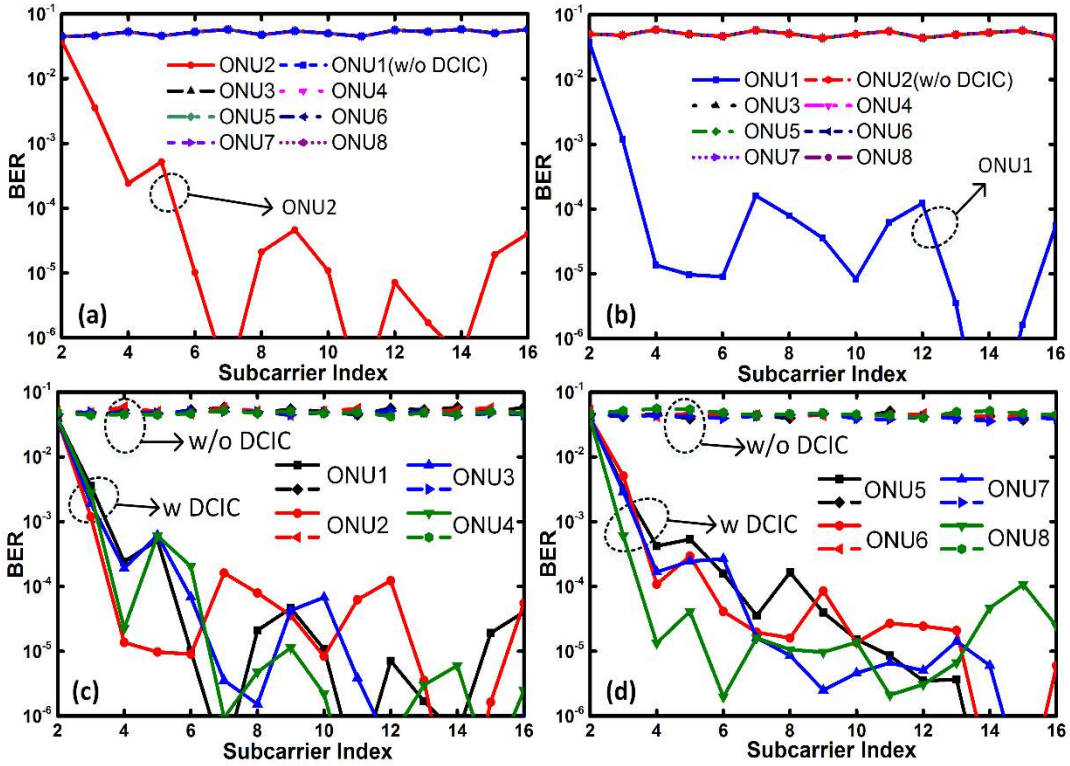

Fig.3.10 (a) BER performance of ONU1 versus subcarrier index in an 8-ONU DFMA PONs; (b) BER performance of ONU2 versus subcarrier index in an 8-ONU DFMA PON; In (a) the inserted legend of 'ONU2'- 'ONU8' refers to which ONU the removed interference comes from, in (b) the inserted legend of 'ONU1'- 'ONU8' refers to which ONU the removed interference comes from. (c) (d) BER comparison between including DCIC and excluding DCIC of all eight-involved ONUs with the cancellation of the interference caused by the spectrum-sharing ONU only. ONU1-4 and ONU5-8 are plotted in (c) and (d) respectively.

To further validate the simplified interference cancellation approach, all ONU subcarrier BER performances involved in the eight ONU DFMA PONs are investigated in Fig. 3.10 (c) and Fig. 3.10 (d), where only one interference from the spectrum-sharing ONU is removed. The comparisons of BER performance versus subcarrier index between the cases of excluding and including DCIC are presented, of which ONU1-4 and ONU5-8 are plotted in Fig. 3.10 (c) and Fig. 3.10 (d), respectively. It is clear that without DCIC, all eight ONUs' initially received signals are destroyed, but after applying DCIC, the BERs of the vast majority of subcarriers are reduced far below the adopted FEC limit of 1.0×10^{-3}.

Based on the above discussions, it is concluded that for any targeted ONU, the cancellation of the interference caused by the spectrum-sharing ONU only is sufficient to significantly

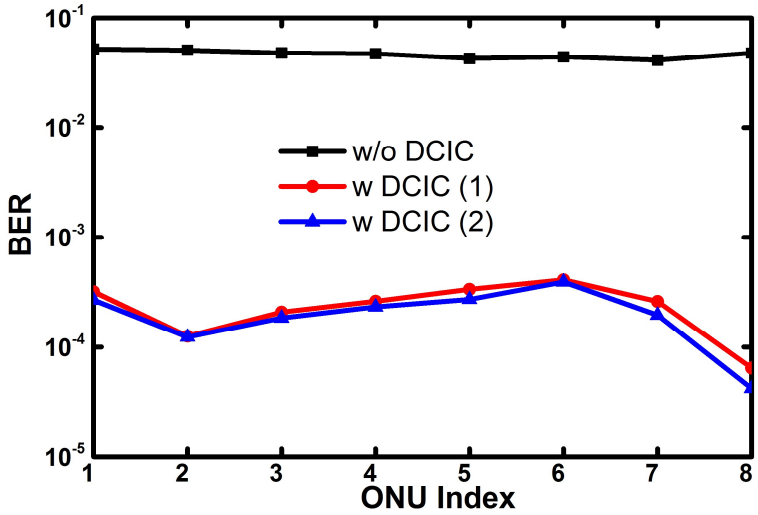

Fig. 3 11 Total BER performance of 8 ONUs, 'w/o DCIC' refer to case without DCIC, "w DCIC(1)" refer to the case with DCIC after one iteration, "w DCIC(2)" refer to the case with DCIC after two iterations.

enhance the multiple ONU DFMA PON performance to a level similar to two ONU DFMA PONs. Clearly, such an ONU count-independent interference cancellation feature considerably reduce its DSP implementation complexity and operation latency without affecting the maximum achievable DFMA PON performance.

A reduction in the minimum required number of iteration stages can further lower the DCIC DSP implementation complexity and corresponding latency, thus reducing its cost and power consumption. The iteration stage-dependent DCIC performance is explored in Fig. 3.11, where the total channel BER comparisons are made between one iteration and two iterations for the eight ONU DFMA PONs. In obtaining Fig. 3.11, only the interference caused by the spectrum-sharing ONU is cancelled, and the second subcarrier used by each ONU is dropped as this subcarrier fails to work in all cases. Fig. 3.11 shows that only one iteration is sufficient for greatly improving the DFMA PON performance, and that a second iteration offers little improvement. This suggests that, regardless the ONU count, sufficiently accurate signal estimations are obtainable after just one iteration stage.

3.5 Conclusions

The DCIC technique has been proposed and investigated, for the first time, to effectively cancel the imperfect channel orthogonality-induced cross-channel interference in both

downstream and upstream DFMA PONs based on IMDD. A comprehensive DCIC theoretical model has been developed, and through extensive numerical fitting with experimental measurements, the developed theoretical model has been rigorously verified and a set of accurate transceiver/system parameters has also been identified. Detailed numerical simulations have shown that the proposed DCIC technique can increase the aggregated upstream signal transmission capacity by a factor of >2 and extends the differential ONU launch power dynamic range by >14 dB. The aforementioned performance improvements are ONU-count independent and just requires one iteration stage. Other salient DCIC advantages include low DSP complexity, small latency and transparency to signal modulation format, signal bit rate and initial operation conditions.

References

[1] "IMT Vision-Framework and Overall Objectives of the Future Development of IMT for 2020 and Beyond," [Online]. Available: https://www.itu.int/ dms_pubrec/itu-r/rec/m/R-REC-M.2083-0-201509-I!!PDF-E.pdf.

[2] Cisco, "Cisco Visual Networking Index : Forecast and Trends, 2017–2022," [Online]. Available: https://www.cisco.com/c/en/us/solutions/collateral/service-provider/visual-networking-index-vni/white-paper-c11-741490.html.

[3] A. Otaka, J. Terada, J. Kani, and K.-I. Suzuki, "Solutions for Future Mobile Fronthaul and Access-Network Convergence," *J. Light. Technol.* vol. 35, no. 3, pp. 527–534, 2017.

[4] X. Liu and F. Effenberger, "Emerging Optical Access Network Technologies for 5G Wireless," *J. Opt. Commun. Netw.*, vol. 8, no. 12, pp. B70, 2016.

[5] N. Kim, H. S. Park, and H. S. Lim, "Adaptive Packet Transmission Scheduling Using Multicast Service Efficiency in TDM-PON," *J. Light. Technol.*, vol. 32, no. 9, pp. 1759–1769, 2014.

[6] J. Kani, "Enabling Technologies for Future Scalable and Flexible WDM-PON and WDM/TDM-PON Systems," *J. Sel. Top. Quant. Electron.*, vol. 16, no. 5, pp. 1290–1297, 2010.

[7] P. C. Schindler, R. Schmogrow, and M. Dreschmann, et al., "Colorless FDMA-PON With Flexible Bandwidth Allocation and Colorless, Low-Speed ONUs [Invited]," *J. Opt. Commun. Netw.*, vol. 5, no. 10, pp. A204, 2013.

[8] K. Habel, M. Koepp, and S. Weide, et al., "100G OFDM-PON for Converged 5G Networks: From Concept to Real-Time Prototype," *in Proc. Opt. Fiber Commun. Conf. Nat. Fiber Optic Eng. Conf.*, 2017.

[9] M. Bolea, R. P. Giddings, and M. Bouich, et al., "Digital Filter Multiple Access PONs With DSP-Enabled Software Reconfigurability," *J. Opt. Commun. Netw.*, vol. 7, no. 4, pp. 215, 2015.

[10] W. Jin, X. Duan, Y. Dong, et al., "DSP-Enabled Flexible ROADMs Without Optical Filters and O-E-O Conversions," *J. Light. Technol.*, vol. 33, no. 19, pp. 4124–4131, 2015.

[11] W. Jin, C. Zhang, X. Duan, et al., "Improved Performance Robustness of DSP-Enabled Flexible ROADMs Free from Optical Filters and O-E-O Conversions," *J. Opt. Commun. Netw.*, vol. 8, no. 8, pp. 521–529, 2016.

[12] H. V. Poor, "Multiple-Access Interference," in *Classical, Semi-classical and Quantum Noise*, 2012.

[13] F. Lin and L. B. Milstein, "Successive Interference Cancellation in Multicarrier DS/CDMA," *IEEE Trans. Commun.*, vol. 48, no. 9, pp. 1530–1540, 2000.

[14] C. Youngkwon and L. Jae Hong, "Analysis of An Adaptive SIC for Near-far Resistant DS-CDMA," *IEEE Trans. Commun.*, vol. 46, no. 11, pp. 1429–1432, 1998.

[15] S. Verdu, "Optimum Multiuser Signal Detection (Ph.D. Abstr.)," *IEEE Trans. Inf. Theory*, vol. 31, no. 4, pp. 557–557, 1985.

[16] J. G. Andrews, "Interference Cancellation for Cellular Systems: A Contemporary Overview," *IEEE Wirel. Commun.*, vol. 12, no. 2, pp. 19–29, 2005.

[17] A. J. Viterbi, "Very Low Rate Convolution Codes for Maximum Theoretical Performance of Spread-spectrum Multiple-access Channels," *IEEE J. Sel. Areas Commun.*, vol. 8, no. 4, pp. 641–649, 1990.

[18] A. Duel-Hallen, "Decorrelating Decision-feedback Multiuser Detector for Synchronous Code-division Multiple-access Channel," *IEEE Trans. Commun.*, vol. 41, no. 2, pp. 285–290, 1993.

[19] Y. C. Yoon, R. Kohno, and H. Imai, "A Spread-spectrum Multiaccess System with Cochannel Interference Cancellation for Multipath Fading Channels," *IEEE J. Sel. Areas Commun.*, vol. 11, no. 7, pp. 1067–1075, 1993.

[20] M. Latva-aho and J. Lilleberg, "Parallel Interference Cancellation in Multiuser Detection," in *Proceedings of International Symposium on Spread Spectrum*

Techniques and Applications, vol. 3, pp. 1151–1155, 1996.

[21] P. Patel and J. Holtzman, "Performance Comparison of a DS/CDMA System Using a Successive Interference Cancellation (IC) Scheme and A parallel IC Scheme under Fading," in *Proc. ICC/SUPERCOMM'94 - Int. Conf. Commun.*, 1994.

[22] R. P. Giddings, X. Duan, and J. M. Tang, "Experimental Demonstration of Cross-Channel Interference Cancellation for Digital Filter Multiple Access PONs," in *Proc. Opt. Fiber Commun. Conf. Nat. Fiber Optic Eng. Conf.*, 2016.

[23] J. L. Wei, A. Hamié, R. P. Gidding, et al., "Adaptively Modulated Optical OFDM Modems Utilizing RSOAs as Intensity Modulators in IMDD SMF Transmission Systems," *Opt. Express*, vol. 18, no. 8, pp. 8556–8573, 2010.

[24] E. Al-Rawachy, R. P. Giddings, and J. Tang, "Experimental Demonstration of a Real-Time Digital Filter Multiple Access PON with Low Complexity DSP-Based Interference Cancellation," *J. Light. Technol.*, vol. 37, no. 17, pp. 1–1, 2019.

[25] M. Bolea, R. P. Giddings, and J. M. Tang, "Digital Orthogonal Filter-enabled Optical OFDM Channel Multiplexing for Software-reconfigurable Elastic PONs," *J. Light. Technol.*, vol. 32, no. 6, pp. 1200–1206, 2014.

4. Hybrid OFDM-Digital Filter Multiple Access PONs

Contents

4.1 Introduction

The exponential growth in Internet traffic has significantly increased the demand for high bandwidth connectivity in both business and residential premises. The current global overwhelming 5G network development not only further intensifies such a tendency but also brings a number of other formidable technical challenges including dynamic reconfigurability, flexible and elastic functionality, significantly reduced system/network simplicity, as well as improved installation/operation cost-effectiveness [1]. To provide a dynamically reconfigurable, flexible, reliable, secure, transparent, smart and high-performance environment to meet these stringent requirements [1-4], it is essential to seamlessly converge traditional optical access networks, metropolitan area networks and mobile fronthaul/backhaul networks, which have been separately developed and independently operated over the past a couple of decades [5,6]. PONs are considered worldwide as one of the most promising candidates for realizing the highly desired network convergence [2,7]. On the other hand, it is also widely envisaged that the initial stage of 5G should also have sufficient transparency to OFDM-based 4G [8,9]. As such, optical OFDMA PONs are expected to play a crucial role in future converged networks, as they can offer a number of well-documented salient advantages including high spectral efficiency, adaptive signal modulation according to channel characteristics, DBA with fine bandwidth granularity, trivial equalization through simple complex multiplication per subcarrier, as well as excellent tolerance to chromatic dispersion. For the network convergence, studies have shown that OFDMA PONs can provide high-capacity and long-reach operation [10-14]. Moreover, their performances can be further improved by non-optical carrier single-sideband modulation [15], and their physical-layer security enhancement is also achievable when use is made of chaotic constellation transformation and pilot-aided secure key agreement [16] or three-dimension Brownian motion and chaos in cell [17].

However, OFDMA PONs have the following three major drawbacks: a) a typical OFDM signal has relatively large side lobes that result in the leakage of signal powers among different channels; b) FFTs and IFFTs implemented in very cost-sensitive ONUs are required to support the full subcarrier count even though individual ONUs would only be assigned a sub-set of the available subcarriers; and c) additional DSP is necessary to minimise the ICI effect between different upstream signals from various ONUs sharing

different subcarrier subsets of an OFDM channel. Unavoidably these drawbacks considerably add the DSP complexity to ONU transceivers.

To address these technical challenges, DFMA PONs [18] have recently been proposed for applications in cost-effective, SDN scenarios, which make use of DSP-based dynamic software-reconfigurable digital orthogonal filters to perform channel multiplexing/demultiplexing. Recent numerical simulations and experimental demonstrations [18, 19] have shown the feasibility of utilising the technique in cost-sensitive IMDD DFMA PON application scenarios. In addition, the physical-layer security improvement of the DFMA PONs can also be achieved by phase masking and hybrid time-frequency domain chaotic scrambling [20].

However, for an IMDD DFMA PON consisting of a larger number of ONUs, the unavoidable problem is that the number of required parallel digital filters implemented in the OLT is proportional to ONU count, as a dedicated pair of SF and MF are needed for each connection. This suggests that the corresponding DSP implementation complexity and operational expenditure may have to increase with ONU count, which is highly undesirable for cost-sensitive PONs. Moreover, in practical transmission systems, digital filtering-associated signal distortions are unavoidable due to non-perfect digital filter implementation and transmission system nonlinearity-induced imperfect digital filter orthogonality. In addition, the finite out-of-band attenuation of the digital filters also results in DFMA PONs suffering from adjacent channel interference (ACI). All the abovementioned unwanted effects constrict the practically achievable DFMA PON transmission performance.

To effectively address the abovementioned challenges associated with the IMDD DFMA PONs, in this chapter, a novel technique termed hybrid OFDM-DFMA is proposed and extensively investigated, for the first time, for IMDD PONs. In an upstream hybrid OFDM-DFMA PON, regardless of the number of ONUs each having an embedded dynamic digital filter, in the OLT a single FFT operation and its following data recovery DSP processes are implemented in a pipelined way, instead of repeating these DSP functions in a parallel way for each ONU. Apart from the above unique aspects, the proposed hybrid OFDM-DFMA PONs still follow the same operating principle of the previously reported DFMA PONs in the ONU transmitter, in which the generated OFDM signals are firstly filtered by individual SFs in the digital domain, after DAC and electrical-to-optical (EO) conversion, the passively coupled optical signal then propagates through the fibre transmission link to the OLT. In the

OLT, without utilising parallel MFs, the signals from various ONUs are demultiplexed and recovered simultaneously in the digital domain by a sequence of pipelined DSP procedures described in subsection 4.2. As a direct result of combining both OFDMA and DFMA characteristics, the proposed hybrid OFDM-DFMA technique still maintains the capability of dynamic and transparent channel reconfiguration and control via the centralised SDN controller in association with the OLT/ONU-embedded DSP controllers.

More importantly, our investigations show that in comparison with the IMDD DFMA PON, the IMDD hybrid OFDM-DFMA PON can considerably improve the upstream transmission performance and differential ONU launch power dynamic range. In addition, the hybrid OFDM-DFMA PON still offers a number of salient advantages associated with the DFMA PON in terms of: a) full support of the SDN solution with network control further extended to the physical layer; b) great ease in transparent abstraction and virtualization; c) high flexibility via centralized control to dynamically realise network reconfiguration and management, and d) inherent transparency to both underlying transmission technologies and network topologies. In particular, the hybrid OFDM-DFMA PON has the unique advantages summarised below:

- Great relaxation of ONU-embedded SF DSP complexity requirement. For achieving a targeted upstream performance, the proposed technique is insensitive to SF-induced signal distortions, as discussed in subsection 4.3. This allows low complexity SFs to be implemented, thus significantly reducing the ONU cost.
- Significant simplification of the OLT DSP complexity and considerable reductions in the OLT cost. As discussed in subsection 4.2, in the upstream operation, various independent signals from different ONUs are simultaneously demultiplexed and recovered with a pipelined approach. This eliminates the implementation of numerous parallel MFs and their corresponding data recovery DSP functions in the OLT. The complexity reduction is evident from the fact that, the required MF taps (multiplier count) is proportional to channel count, thus total MF complexity increases in proportion to the square of channel count, whereas in the L-point FFT-based hybrid OFDM-DFMA case, multiplier count is $L/2(log_2 L)$ with L proportional to channel count. Thus for increasing channel count the DFMA complexity will rapidly exceed the complexity in the hybrid OFDM-DFMA case.

- Significantly enhanced upstream PON performance and its robustness and flexibility because of the proposed technique's unique feature of excellent tolerance to signal distortions and the ACI effect.
- Excellent backward compatibility with existing OFDM-based 4G networks.

In this chapter, an analytical model of the hybrid OFDM-DFMA PON is developed in subsection 4.2, which offers an in-depth understanding of the operating principles of the proposed technique. In subsection 4.3, upstream transmission performances of the proposed OFDM-DFMA PON over a representative 25km SSMF IMDD PON are numerically explored for different application scenarios subject to various levels of signal distortion and interference. Subsection 4.4 further explores other performance characteristics of the hybrid OFDM-DFMA PON in terms of differential optical launch power dynamic range and ONU count-dependent upstream performance. Finally, the chapter is concluded in subsection 4.5.

4.2 Hybrid OFDM-DFMA Operating Principle and Theoretical Model Development

The system diagram of the proposed hybrid OFDM-DFMA PON is depicted in Fig. 4.1, here special attention is given to the multipoint-to-point upstream operation principle only. As shown in Fig. 4.1, the hybrid OFDM-DFMA PON conveys B channels each occupied by a single ONU, labelled as the 0th, 1st, 2nd… b-th… (B-1)-th ONU, and each ONU signal is OFDM modulated. The k-th subcarrier of the m-th OFDM symbol of each channel is given by:

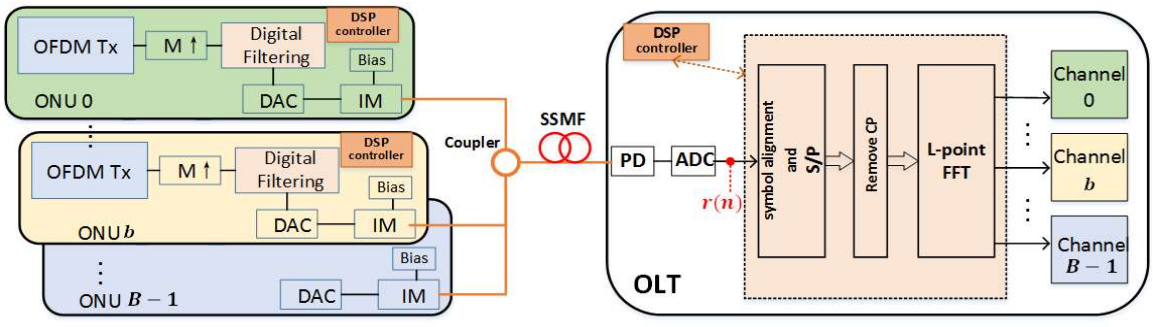

Fig. 4.1 Schematic diagram of the proposed hybrid OFDM-DFMA PONs simultaneously transmitting B ONUs over IMDD SSMFs. DAC: digital-to-analog conversion; ADC: analog-to-digital conversion; IM: intensity modulation; PD: photodetector; S/P: serial-to-parallel conversion; CP: cyclic prefix.

$$d_{k,m} = \left[R_{k,m} e^{j\theta_{k,m}}\right] h(t) \tag{4.1}$$

where $h(t)$ is a rectangular pulse of unity amplitude and duration of one symbol period. $R_{k,m}$ is the *k*-th subcarrier's amplitude and $\theta_{k,m}$ is its phase. The *m*-th OFDM symbol is generated by the *N*-point IFFT of the set of *N* subcarriers, given by:

$$x_m(n) = \sum_{k=-\frac{N}{2}}^{\frac{N}{2}-1} d_{k,m} e^{j\frac{2\pi k(n-mN)}{L}}, k = -\frac{N}{2}, \dots, \left(\frac{N}{2}\right) - 1, m = 0,1,2, \dots \tag{4.2}$$

where *L* is the symbol length in samples. For conventional OFDM we have *L*=*N*. To generate real-valued OFDM signals, the following conditions have to be satisfied:

$$d_{-k,m} = d_{k,m}^{*}\ ,\ d_{0,m} = d_{-\frac{N}{2},m} = 0 \tag{4.3}$$

Thus there are $\frac{N}{2} - 1$ data-carrying subcarriers for each ONU channel. As illustrated in Fig. 4.1, for each ONU channel, prior to digital filtering, the process of up-sampling by a factor of *M* needs to be applied, which can be considered as *M*× over-sampling followed by multiplication by a sequence of impulses. Firstly, over-sampling by a factor of *M* increases the OFDM symbol length to $L = MN$ samples. The *m*-th over-sampled OFDM symbol is:

$$x'_m(n) = \sum_{k=-N/2}^{\frac{N}{2}-1} d_{k,m} e^{j\frac{2\pi k(n-m\ )}{L}} \tag{4.4}$$

which can be rewritten as:

$$x'_m(n) = \sum_{k=-N/2}^{\frac{N}{2}-1} d_{k,m} e^{j\frac{2\pi kn}{L}}, n = mL, mL+1, \dots, mL + (L-1) \tag{4.5}$$

Secondly, the sequence of impulses, *s(n)*, must be spaced at *M* sample intervals, which is given by:

$$s(n) = \sum_{\tau=-\infty}^{\infty} \partial(n - \tau M) \tag{4.6}$$

$s(n)$ can also be expressed as a Fourier series as:

$$s'(n) = \frac{1}{M} \sum_{\beta=-\infty}^{\infty} e^{j2\pi\beta\frac{n}{M}} \tag{4.7}$$

where 1/*M* is the normalized fundamental frequency of the Fourier series. The up-sampled signal is therefore:

$$x''_m(n) = s'(n)x'_m(n) = s'(n)\sum_{k=-\frac{N}{2}}^{\frac{N}{2}-1} d_{k,m}e^{j\frac{2\pi kn}{L}}$$

$$= \frac{1}{M}\sum_{\beta=-\infty}^{\infty}\sum_{k=-\frac{N}{2}}^{\frac{N}{2}-1} d_{k,m}e^{j\frac{2\pi}{L}}e^{j2\pi\ \frac{n}{M}}$$

$$= \frac{1}{M}\sum_{\beta=-\infty}^{\infty}\sum_{k=-\frac{N}{2}}^{\frac{N}{2}-1} d_{k,m}e^{j2\pi n(\frac{k}{L}+\frac{\beta}{M})}$$

(4.8)

From Eq. (4.8), it can be seen that the up-sampled signal consists of multiple images where the β-th image is centred at a frequency of $\frac{\beta}{M}$ with β being an integer number. As an image has a bandwidth of *N/L* and the centre frequency spacing between two neighbour images is $\frac{1}{M} = \frac{N}{L}$, the images are thus contiguous with no spectral gaps. Digital filters can therefore be used to select any image located at a desired spectral region.

As shown in Fig. 4.1, after performing the *M*× up-sampling, digital filtering is then applied to the up-sampled signal. Assuming an ideal shaping filter, the *b*-th shaping filter selects the *b*-th image with its corresponding subcarriers referred to as d_{pos}, and its copy referred to as d_{neg}. Defining $d_{k,m,b}$ as the *k*-th subcarrier of the up-sampled *m*-th OFDM symbol after applying the *b*-th shaping filter, we have:

$$\sum_{k=-N}^{k=N-1} d_{k,m,b} = \{d_{neg}\}, \{d_{pos}\}, k \in [-N, N-1], m \in [1, \infty), b \in [0, B-1] \quad (4.9)$$

where *B* is the maximum number of shaping filters that can be uniformly distributed within the available spectral region, thus $B = \frac{M}{2}$. The first half of the subcarriers ($k \in (-N, -1)$)

are located in the negative frequency bins, which is an exact copy of the subcarriers ($k \in (1, N-1)$) in the positive bins:

$$d_{neg} = d_{-N,m,b}, \dots d_{k,m,b}, \dots d_{-1,m,b} = d_{pos} \tag{4.10}$$

The subcarriers in the positive bins include the data-bearing subcarriers and their conjugates, which are:

$$\begin{aligned} d_{pos} &= 0, d_{1,m,b}, \dots d_{k,m,b}, \dots, d_{N-1,m,b} \\ &= 0\,, d_{1,m,b}\,, \dots\,, d_{\left(\frac{N}{2}\right)-1,m,b}\,, 0, d^*_{\left(\frac{N}{2}\right)-1,m,b}\,, \dots, d^*_{1,m,b} \end{aligned} \tag{4.11}$$

Based on the above discussion, to locate the digitally filtered signal in a desired spectral region, from Eq. (4.8) the filtered signal can be written as:

$$\begin{aligned} x_{m,b}(n) &= \frac{1}{M}\left(\sum_{k=0}^{N-1} d_{pos} e^{j2\pi n\left(\frac{k}{L}+\frac{b}{M}\right)} + \sum_{k=-N}^{-1} d_{neg} e^{j2\pi n\left(\frac{k}{L}+\frac{-b}{M}\right)}\right) \\ &= \frac{1}{M}\sum_{k=-N}^{N-1} d_{k,m,b} e^{j2\pi n\left(\frac{k}{L}+\frac{\frac{k}{|k|}b}{M}\right)} \\ &= \frac{1}{M}\sum_{k=-N}^{N-1} d_{k,m,b} e^{j2\pi n\left(\frac{k+bN\frac{k}{|k|}}{L}\right)} \end{aligned} \tag{4.12}$$

As seen in Fig. 4.1, the digitally filtered data sequence $x_{m,b}(n)$ is then fed to a DAC to generate an analogue electrical signal. The generated electrical signal is combined with an optimum DC bias current to drive an optical intensity modulator. After that, different optical signals from various ONUs are passively combined in an optical coupler located at the remote node to generate an aggregated upstream optical signal that propagates to the OLT.

To obtain a simple analytical solution capable of offering an overall view of the proposed hybrid OFDM-DFMA technique, linear transmission systems are assumed in this subsection,

and numerical simulations are performed in subsection 4.3 to examine the feasibility of the proposed technique in practical non-linear PON transmission systems. As a direct result of the linear system assumption, the passively coupled signal from *B* ONUs can be expressed as:

$$y(n) = \sum_{b=0}^{B-1} x_{m,b}(n)$$

$$= \sum_{b=0}^{B-1} \left(\frac{1}{M} \sum_{k=-N}^{N-1} d_{k,m,b} e^{j2\pi n \left(\frac{k+bN\frac{k}{|k|}}{L} \right)} \right)$$

$$= \frac{1}{M} \left(\sum_{b=0}^{B-1} \sum_{k=-N}^{N-1} d_{k,m,b} e^{j\frac{2\pi\left(k+bN\frac{k}{|k|}\right)n}{L}} \right)$$

(4.13)

Let $\rho = k + bN\frac{k}{|k|}, k \in [-N, N-1], b \in [0, B-1], \rho \in [-BN, BN-1]$, so the above combined signal becomes:

$$y(n) = \frac{1}{M} \sum_{\rho=-BN}^{BN-1} d_{m,\rho} e^{j\frac{2\pi\rho n}{L}}, d_{m,\rho} = d_{k,m,b} \quad (4.14)$$

Eq. (4.14) indicates that the combined signal can be considered to be produced by the *L*-point IFFT operation with *L*= 2*BN*. As such, in the OLT, the *L*-point FFT can be applied to $y(n)$ to recover the sequence $d_{k,m,b}$, which can be expressed as:

$$d_{k,m,b} = \sum_{\rho=0}^{2BN-1} r(n) e^{-j\frac{2\pi\rho n}{L}}, k \in [-N, N-1] \quad (4.15)$$

where $r(n)$ is the received signal after the ADC in the OLT, as seen in Fig. 4.1, and $r(n)$ is given by:

$$r(n) = Cy(n) \quad (4.16)$$

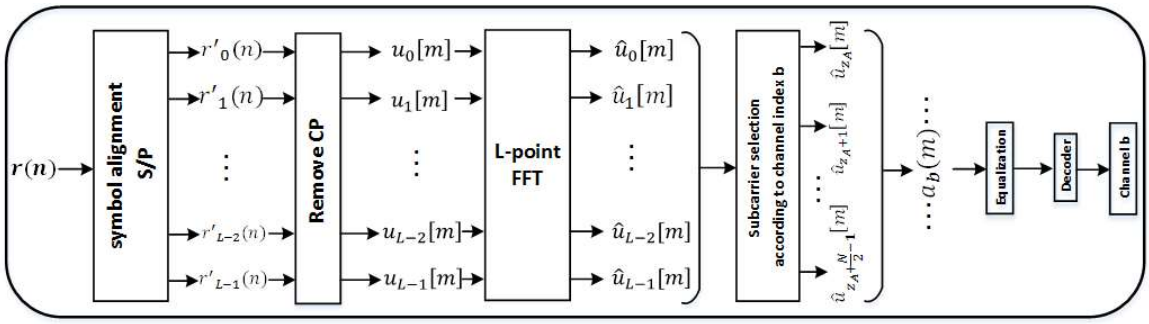

Fig. 4.2 Signal recovery block diagram of the hybrid OFDM-DMFA PONs.

where C is the scale factor accounting for the signal power variation in the linear system. Here it is also worth noting that the DC component is not included in the analysis, as such a component is removed completely and immediately after O-E conversion.

The signal emerging from the ADC passes through a deserialiser to provide parallel signal samples corresponding in length to one symbol period, but arbitrarily located and so not aligned to the symbol boundaries. A symbol alignment block is employed to achieve symbol alignment and compensate for any possible symbol offset. This can be undertaken using synchronisation techniques similar to OFDMA-PONs [14, 21]. As shown in Fig. 4.2, after the symbol alignment and S/P conversion of the received signal $r(n)$, the sample sequence $\{r'_z(n)\}$ is obtained. The CP can then be removed as it has no useful data, thus the remaining L time-domain samples are obtained for each symbol, which is expressed as $u_0[m], u_1[m] \ldots u_{L-1}[m]$ in Fig. 4.2. After performing the L-point FFT operation, the output sample sequence $\hat{u}_0[m], \hat{u}_1[m], \ldots, \hat{u}_z[m], \ldots, \hat{u}_{L-1}[m], z \in [0, L-1]$ is obtained, which is exactly the reverse replica of Eq. (4.15).

In the sequence of $\{\hat{u}_z[m]\}, z \in [0, L-1]$, the first half of the sequence ($z \in [0, \frac{L}{2} - 1]$) corresponds to the positive frequency bin d_{pos}, and the lowest frequency starts from $z = 0$. Whilst the second half ($z \in [\frac{L}{2}, L-1]$)) corresponds to the negative frequency bin d_{neg}, which is the copy of d_{pos}. Theoretically speaking, the subcarriers located in either d_{pos}or d_{neg} can be selected to recover the targeted signal in the b-th ONU channel $a_b(m)$. To obtain the best results from $\{\hat{u}_z[m]\}$, Eq.(4.17) is utilized, which presents the rules of the subcarrier selection, and the corresponding subcarrier index z is given in Eq.(4.18):

$$a_b(m) = \left[\begin{array}{c} \overbrace{\hat{u}_z[m], \hat{u}_{z+1}[m] \dots, \hat{u}_{z+\frac{N}{2}-1}[m]}^{the\ first\ and\ \frac{N}{2}-1\ data-bearin\ \ subcarriers} \\ \underbrace{\hat{u}_{z+N-1}[m], \hat{u}_{z+N-2}[m], \dots, \hat{u}_{z+\frac{N}{2}}[m]}_{\frac{N}{2}\ conjugate\ subcarriers} \end{array} \right], \quad b = 0,1, \dots, B-1 \tag{4.17}$$

$$z = \begin{cases} 0, & b = 0 \\ \frac{L}{2} + (B-b-1) \cdot N, & b \geq 1 \end{cases} \tag{4.18}$$

where b is the channel index for the b-th ONU channel and B is the total number of ONU channels. Thus the recovered signal from the b-th channel is identified, which is then followed by further equalization and decoding operations. The equalization process is the standard OFDM equalization as reported in [14,18]. For simplicity without losing any generality, the ideal shaping filters are applied in the above described mathematical derivations, though other non-ideal shaping filters mentioned below are also applicable, and their distortions can be recovered by the following equalization process. Filter parameters optimizations are discussed in subsection 4.3.

From the above analysis, it can be seen that without implementing numerous parallel MFs, the OLT simultaneously recovers the signals from different ONUs utilizing a single L-point FFT operation. Here it is also worth emphasizing the following two aspects: 1) Any orthogonal digital filter construction approaches such as the Hilbert-pair approach [18] and the Gaussian approach [22] are applicable for the hybrid OFDM-DFMA PONs. When the Hilbert-pair approach is adopted, from the transceiver complexity point of view, the same type (either quadrature-phase or in-phase) of the digital filters at different RF central frequencies are preferable, which, however, halves the maximum achievable signal transmission capacity for a fixed DAC/ADC sampling speed. Such a technical problem can be solved when use is made of the Gaussian approach [22]. 2) The digital filtering and the FFT operation are controlled and managed using DSP controllers embedded in the ONUs and the OLT, respectively, as shown in Fig. 4.1. To establish a reconfigurable and elastic connection, according to transmission system frequency response characteristics and network traffic status, the centralized SDN controller works together with the embedded

DSP controllers to dynamically set optimum digital filter coefficients and map each individual channel with its corresponding subcarriers of the *L*-point FFT operation.

4.3 Hybrid OFDM-DFMA PON Verification and Optimum Filter Design

To evaluate the validity of the theoretical model derived in subsection 4.2, and to explore the performance characteristics of the proposed hybrid OFDM-DFMA PON, numerical simulations of the upstream performances of 25 km SSMF IMDD hybrid OFDM-DFMA PON (abbreviated as 'hybrid' case) are undertaken in this subsection. Signal generation and detection are simulated using MATLAB and the optical fibre transmission is simulated using VPI Transmission maker. To highlight the upstream hybrid OFDM-DFMA PON performance, comparisons are also made to the DFMA PON with corresponding MFs in the OLT (abbreviated as 'DFMA' case). It is worth mentioning that the channel interference cancellation technique presented in chapter 3 is not considered in the hybrid OFDM-DFMA PON systems proposed in this chapter.

To simulate OFDM signal generation and detection, the approach reported in [23] is adapted. Throughout the chapter, each ONU is assigned a whole OFDM channel, with each channel consisting of fifteen, 16-QAM modulated, data-bearing subcarriers (*N*=32). In each ONU, an ideal optical intensity modulator is utilised, which produces an optical field signal $S_o(n)$, having a waveform governed by $S_o(n) = \sqrt[2]{y'(n)}$, here $y'(n) > 0$ is the electrical driving current of the signal with an optimum DC bias current being added. Apart from simplicity, the utilisation of the ideal optical intensity modulator can also completely eliminate the optical beat interference (OBI) effect [24]. For practical upstream IMDD PON systems, the OBI effect is negligible when the optical wavelength spacing between adjacent ONUs is larger than the threshold experimentally identified in [24].

For simplicity, here two ONUs are considered in the adopted multipoint-to-point upstream PONs. The construction of the digital filters in the ONUs is undertaken using the Hilbert-pair approach described in subsection 2.2.1.5 [18]. Each Hilbert-pair includes both in-phase and quadrature-phase filter components to support two spectrally-overlapped orthogonal channels. In this chapter, for both ONU1 and ONU2, only the in-phase filters are utilised at different RF central frequencies governed by Eq. (4.19):

Table 4.1 List of Parameters

PARAMETER	VALUE	PARAMET	VALUE
DAC/ADC sample rate	12.5 GS/s	DAC/ADC resolution	8 bits
Clipping ratio	13 dB	Cyclic Prefix	25%
Modulation formats	16 QAM	Total number of IFFT points of each channel	32
Transmitted optical power	0 dBm	Received optical power	-2 dBm (if unstated)
SSMF length	25 km	Up sampling factor M	4
SF/MF filter length range	2/8/16/32	Hybrid OFDM-DFMA FFT size	128

$$f_b = (2b + 1)\frac{f_s}{2M}, b = 0,1, \dots, B-1 \quad (4.19)$$

where f_s is the DAC/ADC sampling speed. The central frequencies are chosen to uniformly distribute the filter frequency responses within the available spectral region determined by the DAC/ADC sampling speeds. To accommodate the two ONUs in the entire spectral region, the up-sampling factor *M* is taken to be 4, $f_1 = f_s/8$, $f_2 = 3 \times f_s/8$, and all other simulation parameters are listed in Table 4.1, and the corresponding SSMF and PIN parameters are the same as in Table 3.1. For each case considered, identical parameters are applied to both the hybrid OFDM-DFMA PON and the DFMA PON. For each ONU, the achievable signal bit rate R_b can be calculated using Eq. (3.14). By utilising the parameters listed in Table 4.1, a signal bit rate of 4.7 Gb/s can be easily calculated for each ONU.

From Table 4.1, it can be seen that the IFFT size for generating the OFDM signal by each ONU is *N*=32, and the up-sampling factor *M* is 4, thus in the OLT of the hybrid OFDM-DFMA PON, there are *L*=128 samples per symbol applied to the FFT operation after the S/P conversion. From Eq. (4.17) and Eq. (4.18) it can also be seen that the samples of subcarrier index 1-16 (the first and 15th data-bearing subcarriers) from ONU 1 are located in the sequence $\hat{u}_0, \hat{u}_1 .., \hat{u}_{15}$, and the sequence $\hat{u}_{64}, \hat{u}_{65} .., \hat{u}_{79}$ is selected to construct the data-bearing subcarriers for ONU2. Thus, after equalization and decoding, the two signals from

both ONUs are recovered.

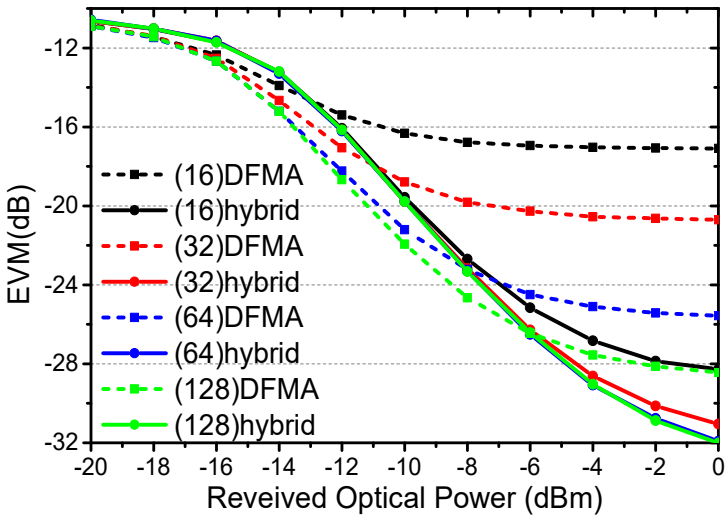

Fig.4.3 EVM of ONU 1 versus received optical power with different digital filter tap-counts for both the hybrid OFDM case and DFMA case.

Under the above numerical simulation conditions, the ONU1 EVM versus ROP performances of both the hybrid OFDM-DFMA and DFMA PONs are presented in Fig. 4.3 for different digital filter tap counts. The FEC limit of 1.0×10^{-3} is considered, which corresponds to -17 dB (or 14%) of EVM [25]. Fig. 4.3 shows that the proposed hybrid OFDM-DFMA PON can reach EVMs of -17 dB when ROPs are higher than -12 dBm. This indicates that the proposed technique works well for both linear and non-linear IMDD PON systems, thus the feasibility of the proposed hybrid OFDM-DFMA technique is confirmed. Moreover, when varying digital filter tap counts between 16, 32, 64 and 128, the proposed hybrid OFDM-DFMA PON performances are very robust to the variations in filter tap count. On the contrary, the DFMA PON performances significantly depend on filter tap count, especially over the noise floor region. This is because the finite tap count-induced non-flat frequency response of the digital filter leads to signal distortions: the filter frequency response ripple variation range and associated signal distortions increase with decreasing the number of taps. The DFMA PONs suffer stronger imperfect filter impairments as both the SFs and MFs are implemented in the ONUs and OLTs respectively, whilst the hybrid OFDM-DFMA PONs are free from the OLT-embedded MFs, thus introducing less signal distortions. This results in the hybrid OFDM-DFMA EVM curves almost perfectly overlapping for different tap counts, as shown in Fig. 4.3.

Such a feature reveals that in comparison with the DFMA PON, the proposed hybrid OFDM-DFMA PON is less sensitive to imperfect digital filter-induced signal distortions. For achieving the same transmission performance, the proposed technique not only permits lower digital filter complexity but also significantly enhances the PON robustness and flexibility. Such a statement is further signified by the performance for the 16 tap count case, where the noise floor in the hybrid OFDM-DFMA PON is significantly lower than the DFMA PON with the filter taps as large as 64. In addition, for a specific filter tap count and over relatively low ROPs, the DFMA PON performance is slightly better than the hybrid OFDM-DFMA PON, the ROP corresponding to such performance cross-point between two PON technologies increases with increasing filter count, as shown in Fig. 4.3. This is because the DFMA-associated MFs can reduce the system noise effect. In Fig.4.3, only ONU1 performance is presented, because ONU2 employs the identical digital filter parameters, except that ONU2 operates at a higher RF frequency. Our numerical simulations show that for the same simulation conditions, the performance of ONU2 is very similar to ONU1. This suggests that the hybrid OFDM-DFMA PON performance is independent of ONU spectral allocation.

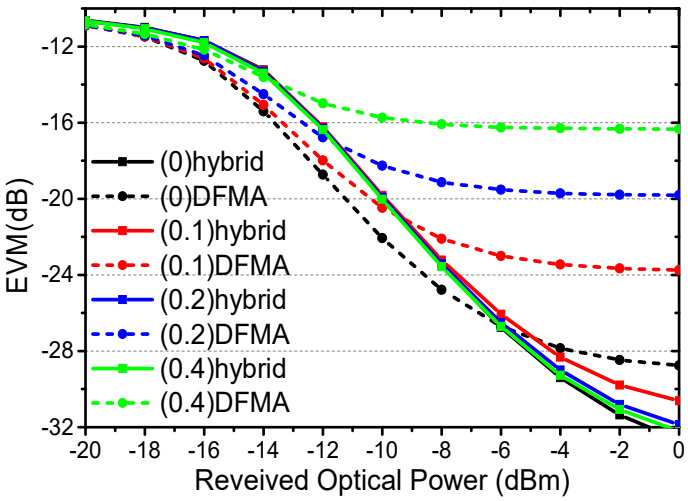

Fig.4.4 EVM of ONU 1 versus received optical power with different excess of bandwidth parameters (alpha value) for hybrid OFDM case and DFMA case.

Fig. 4. 4 presents the ONU1 EVM versus ROP for different levels of ACI. Here the different ACI levels are introduced by varying the filter's alpha parameter [18], which controls the excess of bandwidth with respect to the minimum bandwidth determined by the symbol period. Generally speaking, for a given filter tap count, a larger alpha value produces lower in-band frequency response ripples, but gives rise to larger filter response side lobes, thus

leading to greater ACI. When numerically simulating Fig. 4.4, the alpha parameter values are taken to be 0, 0.1, 0.2 and 0.4, and the tap counts are fixed at 128 to minimise the finite tap count-induced signal distortions. All other simulation parameters are kept the same as those adopted in Fig. 4.3.

It can be seen in Fig. 4.4 that the proposed hybrid OFDM-DFMA PON performances are almost independent of ACI level. In sharp contrast, the performance of the DFMA PON varies considerably with ACI level, in particular over the noise floor region. The physical mechanism underlying such observed behaviour is the system nonlinearity-induced imperfect orthogonality between the SFs and MFs, which means that the DFMA-embedded MFs cannot fully reject the leaked signal power from its adjacent channels, and due to the filter's excess of bandwidth some adjacent channel power aliases into the wanted signal after down-sampling. However, for the hybrid OFDM-DFMA PON, the system nonlinearity gives each SF the same effect, thus the power leakage from the adjacent channels is largely rejected by the single FFT operation and its following data recovery process. As such the hybrid OFDM-DFMA PON mainly suffers from out-of-band channel leakage due to the finite out-of-band attenuation of the SFs. These behaviours clearly demonstrate that the proposed technique is highly tolerant to ACI. The existence of the performance cross-points between the hybrid OFDM-DFMA PON and the DFMA PON is very similar to that observed in Fig. 4.3.

To further explore the proposed technique's robustness against the ACI effect, the overlaid and equalised combined constellations and subcarrier EVM distributions for both ONUs are plotted in Fig. 4.5 (a) and (b) for the DFMA PON and the hybrid OFDM-DFMA PON, respectively. Here the ROPs are fixed at -10 dBm, and the tap count and the alpha parameter value are taken to be 128 and 0.2 respectively. These parameters give rise to the FEC limit of EVM at -17 dB or 14% [25] for the DFMA PON, as shown in Fig. 4.4. As a direct result of the large alpha parameter value-induced enhancement in the ACI effect, and given the fact that lower frequency subcarriers are located at the edges of the frequency band, the first two subcarriers of both ONU channels are almost destroyed in the DFMA PON, as seen in Fig. 4.5 (a). However, in the hybrid OFDM-DFMA PON, shown in Fig. 4.5 (b), these two low frequency subcarriers are hardly affected by the ACI effect, leading to almost flat EVM distributions across all the subcarriers. In comparison with the DFMA PON, the superior ACI rejection capability associated with the hybrid OFDM-DFMA PON is further evidenced

by its corresponding clear constellations, illustrated in Fig. 4.5 (a) and Fig. 4.5 (b).

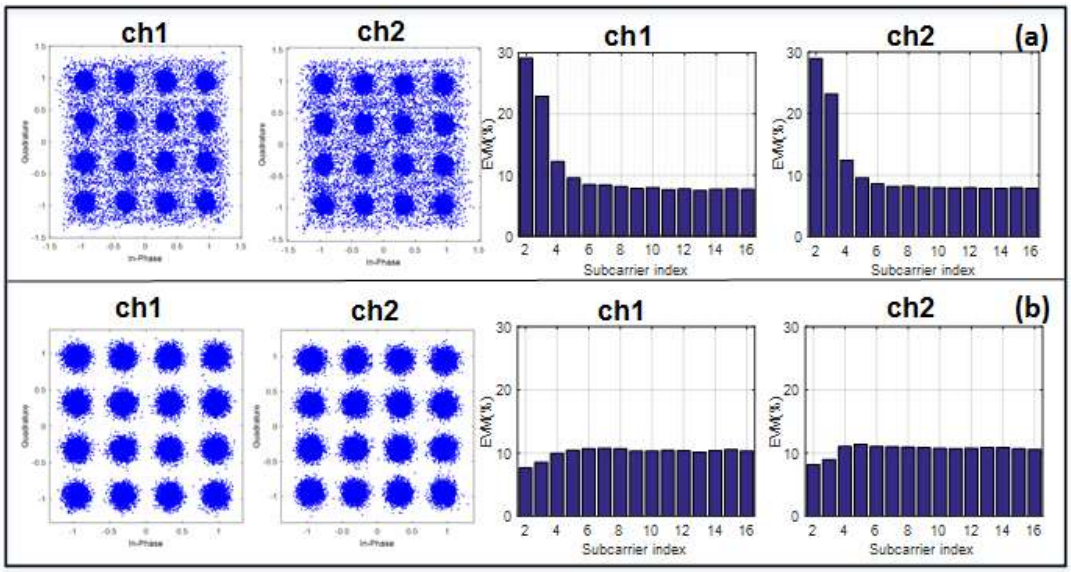

Fig. 4.5 Constellations and EVM distribution among all subcarriers, (a) DFMA case, (b) hybrid OFDM case. (Note: subcarrier index=1 corresponds to the unused DC frequency)

In summary, the excellent performance of the hybrid OFDM-DFMA PONs not only validates the proposed technique for use in the application scenarios of interest of the thesis, but also demonstrates the hybrid OFDM-DFMA PON's unique advantages over the DFMA PONs in terms of upstream transmission performance improvement, digital filter complexity reduction and increased tolerance to signal distortions and ACI caused by the finite tap count-induced digital filter imperfection and system nonlinearity.

4.4 Hybrid OFDM-DFMA-induced DSP Complexity Reductions

This subsection evaluates in detail the claimed advantage of the proposed hybrid OFDM-DFMA PONs in terms of DSP complexity reduction compared with the DFMA PONs.

As discussed in subsection 4.2, for the upstream operation, various independent signals from different ONUs are simultaneously de-multiplexed and subsequently recovered with a single FFT in a pipelined approach. The non-necessity of employing parallel signal processing functions in the OLT greatly reduces the overall OLT hardware and software complexity.

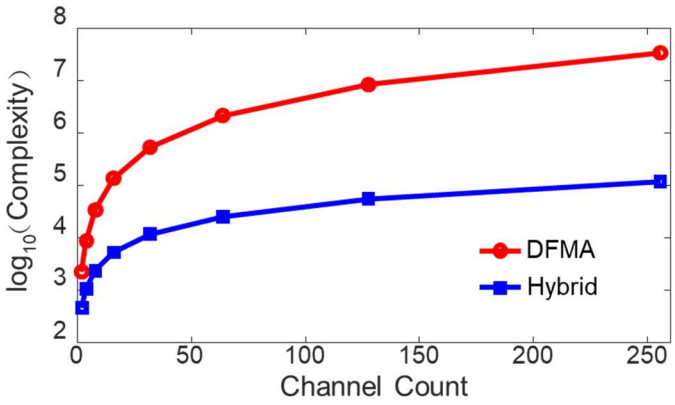

Fig. 4.6 DSP complexity comparison between the hybrid OFDM-DFMA PONs and the DFMA PONs as a function of channel count.

For example, from the DSP complexity reduction point of view, for simplicity, if the DSP complexity is measured by the minimum required multiplier elements only (the number of taps), to support maximum B ONU channels in the hybrid OFDM-DFMA PONs, the up-sampling factor M satisfies $M=2\times B$, and the multiplier count required by the L-point FFT is $L/2(\log_2 L)$ with $L=M\times N$ proportional to the channel count B. On the other hand, for the DFMA PONs supporting B ONU channels, the required corresponding MF multiplier count T is proportional to channel count, satisfying $T=L\times M'$ [18], where $M'=B$, and L is the digital filter length, thus the total MF DSP complexity of the B ONU channels increases to $B\times T\times N$ [26]. In addition, after the matching filtering processes, each channel also requires a separate OFDM signal demodulation process, which additionally increases the DSP complexity by $B\times N/2(\log_2 N)$. Based on the above analyses, the overall DSP complexities $\mathcal{C}$ of the hybrid case and the DFMA case can be expressed as:

$$\begin{cases} \mathcal{C}_{\text{hybrid}} = \frac{L}{2}(\log_2 L) = BN(\log_2 2BN) \\ \mathcal{C}_{\text{DFMA}} = B \times T \times N + B \times \frac{N}{2}(\log_2 N) = B^2 NL + \frac{BN}{2}(\log_2 N) \end{cases} \tag{4.20}$$

By making use of Eq. (4.20), the calculated OLT DSP complexity as a function of channel count is plotted in Fig. 4.6, in which the IFFT size N for each OFDM signal is 32 and the digital filter length is fixed at 16. It is clear from Fig. 4.6 that for channel counts of ≥ 32, the overall OLT DSP complexity can be reduced by a factor of more than 100 when adopting the hybrid OFDM-DFMA technique.

In addition to the OLT DSP complexity reduction, subsection 4.3 also indicates that considerable DSP complexity reductions can also be achieved in ONUs as a direct result of

the relaxation of the ONU-embedded SF DSP complexity requirements for achieving an acceptable BER performance.

4.5 Hybrid OFDM-DFMA PON Upstream Performance Characteristics

4.5.1 Differential ONU Launch Power Dynamic Range

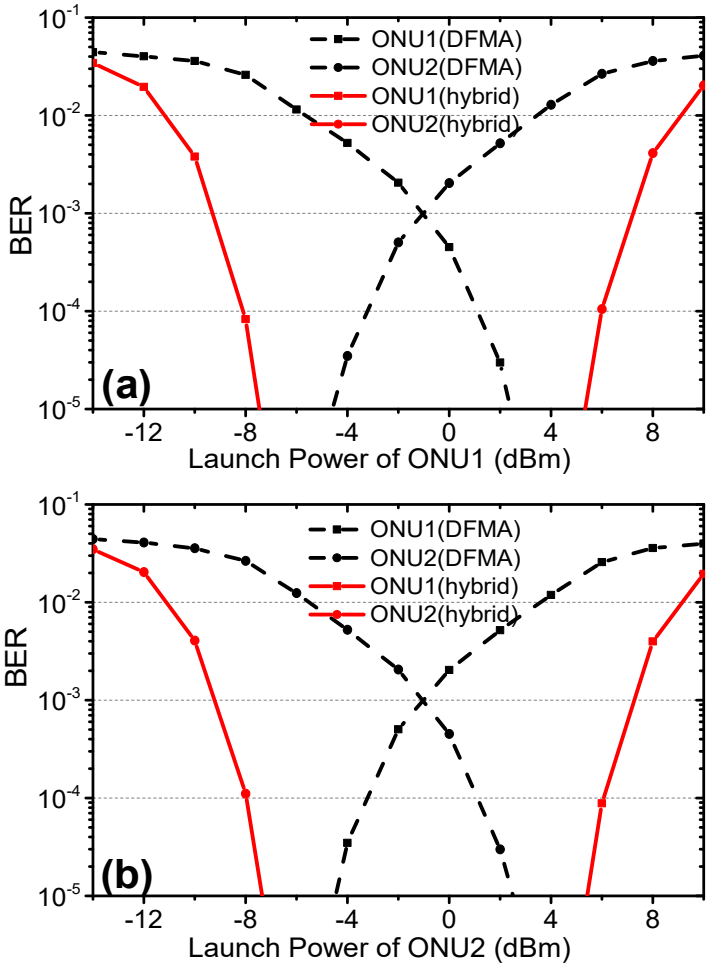

Fig.4.7 BER performance versus ONU optical launch power. (a) power-varying ONU1, (b) power-varying ONU2. The black curves refer to the DFMA PON, the red curves refer to the hybrid OFDM-DFMA PON.

The hybrid OFDM-DFMA performance robustness to differential ONU launch power is examined in Fig. 4.7, where the BER performance of a power-varying ONU is plotted as a function of its optical launch power, whilst the other fixed-power ONU's launch power is kept constant at -1 dBm. For simplicity but without losing generality, here just two ONUs are considered and the ROP in the OLT is fixed at -2 dBm. The digital filters have 32 taps,

and the alpha parameters are set at 0 to allow fair comparison with the previous performances presented in Fig. 4.3. All other parameters are identical to those listed in Table 4.1.

As expected, an increase in optical launch power from one ONU improves its own BER performance, but simultaneously degrades the BER performance of the other ONU, as shown in Fig. 4.7 (a) and (b). This mainly results from the opposite changes in effective OSNR experienced by these ONUs. In this context, the differential ONU launch power dynamic range is defined as the same in subsection 3.4.1. At an ROP of -2 dBm, the differential launch power dynamic range of the DMFA PON is virtually 0 dB, however for the hybrid OFDM-DFMA PON, the differential launch power dynamic range of both ONU1 and ONU2 significantly increases to 16 dB. Such a huge improvement mainly results from the excellent tolerance of hybrid OFDM-DFMA to the low filter tap count-based imperfect filter-induced signal distortions. The hybrid OFDM-DFMA-enhanced differential ONU dynamic range also brings improved PON performance robustness.

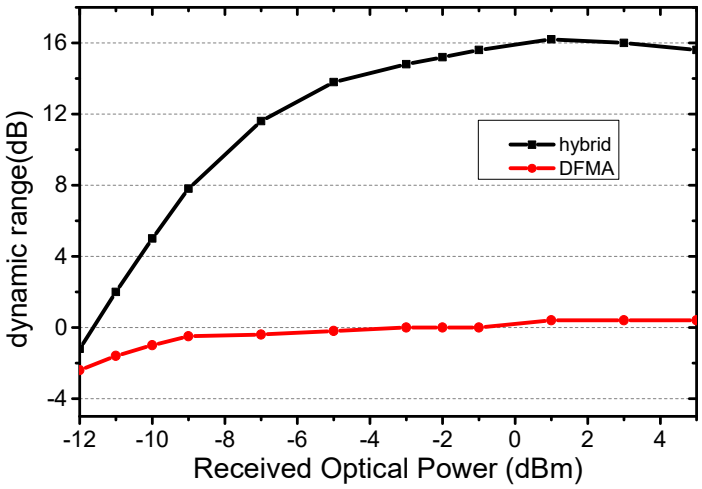

Fig.4.8 Optical launch power dynamic range of ONU1 as a function of received optical power.

The ROP-dependent differential launch power dynamic range characteristics are explored in Fig. 4.8, where ONU1 is power-varying with all other parameters kept identical to those adopted in Fig. 4.7. It is shown in Fig. 4.8 that for the DFMA PON, the differential launch power dynamic range is always around 0 dB, whilst for the hybrid OFDM-DFMA PON, the dynamic range increases almost linearly from 0 dB to 16 dB when ROPs increasing from -12 dBm to 1 dBm, beyond which the differential launch power dynamic range plateaued at around 16 dB. The flattening of the differential launch power dynamic range to a maximum

value is mainly attributed to nonlinearities and noise associated with the transmission channel. As expected from Fig. 4.7, the same ROP-dependent differential launch power dynamic range characteristics also hold when ONU2 power varies. In addition, at an ROP of around -11.5 dBm, the hybrid OFDM-DFMA dynamic range is 0 dB, indicating that both channels reach the FEC limit at the same time, which is in agreement with that in Fig. 4.3, where the corresponding EVM is -17 dB for the 32-tap case. Meanwhile for the DFMA PON, the corresponding dynamic range value is negative when ROPs are lower than -1 dBm, this means both of the two channels fail to operate below the FEC limit.

4.5.2 ONU Count-Dependent Performance

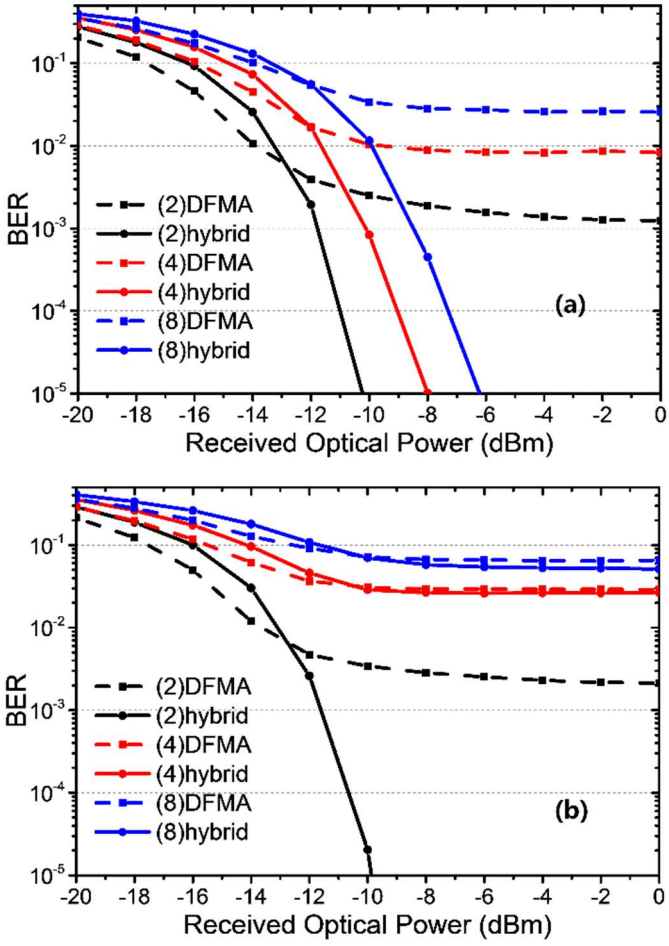

Fig.4.9 BER versus received optical power in multiple ONU cases when filter tap count is 32, (a) channel 1; (b) channel 2.

Having demonstrated the effectiveness of the hybrid OFDM-DFMA PON in improving differential launch power dynamic range for the two ONU case, this subsection further extends the application scenario to multi-ONU hybrid OFDM-DFMA PONs.

The ONU count-dependent hybrid OFDM-DFMA PON performance is examined in Fig. 4.9, where for each case considered, equal ONU launch powers and a constant total optical launch power of 0 dBm are always used at the remote node, and the up-sampling factors are twice the total number of ONUs simultaneously accommodated, i.e., $M=2B$. Here the tap count is fixed at 32 and the alpha parameter is set at 0.1 to provide a practically achievable trade-off between side lobes and in-band frequency response ripples. Each ONU is located at a dedicated RF central frequency governed by Eq. (4.19). Other adopted simulation parameters are identical to those utilised in previous subsections.

The BER performances of ONU1 and ONU2 as a function of ROP are plotted in Fig. 4.9 (a) and Fig. 4.9 (b) respectively, where the total number of ONUs varies from 2 to 8. It can be seen in Fig. 4.9 (a) that in the DFMA PON, both ONU1 and ONU2 fail to reach the FEC limit of 1.0×10^{-3} over the entire ROP variation range. However, in the hybrid OFDM-DFMA PON incorporating 2/4/8 ONUs, ONU1 reaches the FEC limit at -12/-10/-8dBm respectively. Furthermore, for each case considered, the hybrid OFDM-DFMA PON has a significantly lower noise floor than the corresponding DFMA PON. This manifests from the fact that ONU1 suffers smaller interference from other ONUs. Here it is also worth mentioning that when the number of ONUs is doubled, as observed in Fig. 4.9 (a), the effective signal power from each ONU is decreased by 1.5 dB (half of 3 dB in the electrical domain) rather than the value of 2 dB. The 0.5 dB difference is mainly contributed by the multiple access interference (MAI) effect [27].

It is observed in Fig. 4.9 (b) that ONU2 in the hybrid OFDM-DFMA PONs incorporating 4 and 8 ONUs fail to reach the adopted FEC limit and tend to have similar performances compared to the corresponding DFMA PONs. This is because the crosstalk effects from other ONUs are extremely large for the adopted digital filter parameters. The fixed filter tap count of 32 gives rise to a filter length of 4 (2) for the 4-ONU (8-ONU) case. As the filter length corresponds to the number of non-zero samples that a SF processes at any time, for multiple ONU cases, such short filter lengths thus result in the extremely strong crosstalk effect experienced by ONU2. It has been shown [18] that for multiple ONU cases, spectral location-independent ONU performance is still obtainable when filter lengths (filter length = (tap count)/M) are >8 and the alpha parameter values are <0.05.

4.6 Conclusions

A novel hybrid OFDM-DFMA PON has been proposed and investigated, for the first time, where multiple independent OFDM channels are multiplexed using ONU-embedded dynamically reconfigurable and adaptive digital filters, and simultaneously recovered in the OLT by a single FFT operation. An analytical theoretical hybrid OFDM-DFMA PON model has been developed to give an in-depth understanding of the proposed technique, and extensive numerical simulations of upstream hybrid OFDM-DFMA transmission performances have been investigated in representative 25km SSMF IMDD PON systems. It has been shown that the proposed technique greatly relaxes filter DSP complexity and improves PON performance flexibility and robustness because of its insensitivity to filter-induced signal distortions and system nonlinearity. Moreover, the numerical results have also demonstrated that the hybrid OFDM-DFMA PON can increase the differential ONU launch power dynamic range by 16 dB compared to the DFMA PONs.

References

[1] I. Tomkos, F. Effenberger, and J.-K. K. Rhee, "Introduction to the Special Issue on Optical Networking for 5G Mobile and Wireless Communications," *J. Opt. Commun. Netw.*, vol. 8, no. 12, pp. FGM1–FGM4, 2016.

[2] J. S. Wey and J. Zhang, "Passive Optical Networks for 5G Evolution," in *Broadband Access Communication Technologies XII*, vol. 10559, pp. 22, 2018.

[3] L. López, Á. Caraguay, and M. Monge, et al., "Key Technologies in the Context of Future Networks: Operational and Management Requirements," *Futur. Internet*, vol. 9, no. 1, pp. 1–15, 2016.

[4] J. Kani, M. Yoshino, and K. Asaka et al., "Flexible Access System Architecture (FASA) to Support Diverse Requirements and Agile Service Creation," *J. Light. Technol*., vol. 36, no. 8, pp. 1510–1515, 2018.

[5] A. Otaka, J. Terada, and J. Kani, et al., "Solutions for Future Mobile Fronthaul and Access-network Convergence," *J. Light. Technol*. vol. 35, no. 3, pp. 527-534, 2017.

[6] X. Liu and F. Effenberger, "Emerging Optical Access Network Technologies for 5G Wireless," *J. Opt. Commun. Netw*., vol. 8, no. 12, pp. B70-B79, 2016.

[7] H. Abbas and M. Gregory. "The Next Generation of Passive Optical Networks: A Review," *J. Netw. and Comput. Appl.*, vol. 67, pp. 53-74, 2016.

[8] H. F. Arrano and C. A. Azurdia-Meza, "OFDM: Today and in the Future of Next Generation Wireless Communications," *IEEE Central America and Panama Student Conference*, 2016.

[9] R. Nath Mitra and D. P. Agrawal, "5G Mobile Technology: A Survey," *ICT Express*, vol. 1, pp. 132–137, 2015.

[10] K. Kanonakis, I. Tomkos, and H. Krimmel, et al., "An OFDMA-based Optical Access Network Architecture Exhibiting Ultra-high Capacity and Wireline-wireless Convergence," *IEEE Commun. Mag*., vol. 50, no. 8, pp. 71–78, 2012.

[11] N. Cvijetic, "OFDM for Next-Generation Optical Access Networks," *J. Light. Technol.*, vol. 30, no. 4, pp. 384–398, 2012.

[12] S.Y. Jung, C.H. Kim, and S.M. Jung, et al., "Optical Pulse Division Multiplexing-based OBI Reduction for Single Wavelength Uplink Multiple Access in IM/DD OFDMA-PON," *Opt. Express*, vol. 24, no. 25, pp. 29198–29208, 2016.

[13] C. Zhang, W. Zhang, and C. Chen, et al., "Physical-enhanced Secure Strategy for OFDMA-PON using Chaos and Deoxyribonucleic Acid Encoding," *J. Light. Technol*., vol. 36, no. 9, pp. 1706–1712, 2018.

[14] R. Giddings, "Real-time Digital Signal Processing for Optical OFDM-based Future Optical Access Networks," *J. Light. Technol*. vol. 32, no. 4, pp. 553–570, 2014.

[15] X. Zhang, C. Zhang, and C. Chen, et al., "Non-optical Carrier SSB-OFDM PONs with the Improved Receiver Sensitivity and Potential Transmission Nonlinearity Tolerance," *IEEE Photon. J*., vol. 9, no. 1, pp. 1–10, 2017.

[16] W. Zhang, C. Zhang, and C. Chen, et al., "Experimental Demonstration of Security-enhanced OFDMA-PON using Chaotic Constellation Transformation and Pilot-aided Secure Key Agreement", *J. Light. Technol*., vol. 35, no. 9, pp. 1524-1530, 2017.

[17] T. Wu, C. Zhang, and C. Chen, et al., "Security Enhancement for OFDM-PON using Brownian Motion and Chaos in Cell", *Opt. Express*, vol. 26, no. 18, pp.22857-22865, 2018.

[18] M. Bolea, R. P. Giddings, and M. Bouich, et al., "Digital Filter Multiple Access PONs with DSP-enabled Software Reconfigurability", *J. Opt. Commun. Netw*, vol. 7, no. 4, pp. 215-222, 2015.

[19] X. Duan, R. P. Giddings, and S. Mansoor, et al., "Experimental Demonstration of Upstream Transmission in Digital Filter Multiple Access PONs with Real-time Reconfigurable Optical Network Units," *J. Opt. Commun. Netw*., vol. 9, no. 1, pp. 45-52, 2017.

[20] C. Zhang, Y. Yan, and T. Wu, et al., "Phase Masking and Time-Frequency Chaotic Encryption for DFMA-PON", *IEEE Photon. J*., vol.10, no. 4, pp. 1-9, 2018.

[21] X. Q. Jin, R. P. Giddings, E. Hugues-Salas, and J. M. Tang, "Real-time Experimental Demonstration of Optical OFDM Symbol Synchronization in Directly Modulated DFB Laser-based 25km SMF IMDD Systems," *Opt. Express*, vol. 18, no. 20, pp. 21100-21110, 2010.

[22] B. Farhang-Boroujeny, "OFDM versus Filter Bank Multicarrier", *IEEE Signal Process. Mag*., pp.92-112, 2011.

[23] Y. Dong, E. Al-Rawachy, and R. P. Giddings, et al., "Multiple Channel Interference Cancellation of Digital Filter Multiple Access PONs," *J. Light. Technol*., vol. 35, no. 1, pp. 34-44, 2016.

[24] X. Q. Jin and J. M. Tang, "Experimental Investigations of Wavelength Spacing and Colorlessness of RSOA-based ONUs in Real-time Optical OFDMA PONs", *J. Light. Technol*., vol. 30, no. 16, pp. 2603-2609, 2012.

[25] R. A. Shafik, M. S. Rahman and A. R. Islam, "On the Extended Relationships among EVM, BER and SNR as Performance Metrics," in *Proc. International Conference on Electrical and Computer Engineering*, Dhaka, pp. 408-411, 2006.

[26] E. Al-Rawachy, R. P. Giddings, and J. Tang, "Experimental Demonstration of a Real-Time Digital Filter Multiple Access PON with Low Complexity DSP-Based Interference Cancellation," *J. Light. Technol.*, vol. 37, no. 17, pp. 1–1, 2019.

[27] X. Q. Jin, J. Groenewald, and E. Hugues-Salas, et al., "Upstream Power Budgets of IMDD Optical OFDMA PONs incorporating RSOA Intensity Modulator-based Colorless ONUs," *J. Light. Technol.*, vol. 31, no. 12, pp. 1914–1920, 2013.

5. Hybrid DFT-Spread OFDM-Digital Filter Multiple Access PONs for Converged 5G Networks

Contents

5.1 Introduction

To achieve the targeted 5G performances specifications including significantly increased signal transmission capacities, massive machine-type communications as well as ultra-reliable low-latency real-time services [1, 2], a wide diversity of unprecedented technical challenges across all layers must be addressed, among which non-incremental solutions should be developed to seamlessly converge, in a cost-effective manner, the separately implemented and operated legacy optical and wireless networks [3]. To deliver such an objective, PONs are widely considered as one of the most promising solutions [4]. To enable the PON-based converged 5G networks to offer on-demand heterogeneous services in a multiple virtual operator-shared environment, SDN is vital to transfer the present inflexible and vendor-locked network infrastructure into an agile and flexible platform [5, 6]. Furthermore, it is also greatly advantageous if the abovementioned flexible networks have good backward compatibility to existing OFDM-based 4G networks [7].

To address the abovementioned challenges, recently novel hybrid OFDM-DFMA PONs [8] capable of providing excellent transparency to OFDM-based 4G networks have been proposed, where DSP-based software-reconfigurable digital filtering is applied to individual OFDM signals produced by each ONU, while in the corresponding OLT, a single FFT operation and its following data recovery processes are implemented in a pipelined approach, regardless of the ONU count accommodated by the network. Compared to the conventional OFDM PONs, such a network not only extends the highly desirable SDN network control functions to the physical layer, but also considerably enhances the upstream performance robustness to practical transceiver/system impairments. In addition, compared to the DFMA PONs, the hybrid OFDM-DFMA PONs also greatly relax the stringent requirements on the high DSP complexity of SFs in the ONUs, and more importantly, they completely eliminate the matching filtering operations in the OLT, thus resulting in greatly reduced OLT DSP complexity and considerably enhanced flexibility [8].

It is well known that OFDM's inherent multi-subcarrier modulation feature can cause the time-domain waveforms associated with various subcarriers to be added up coherently after the IFFT operation. This gives an OFDM signal a high PAPR [9]. A high PAPR not only requires large dynamic operation ranges of electrical/optical devices but also produces high quantization noise for fixed quantization bits. The quantization noise effect is particularly

strong when current market-available high-speed DACs/ADCs are implemented, as their performances are bit resolution-limited. In addition, when transmitting over fibre systems, a high PAPR signals may also impose enhanced system performance sensitivity to fibre nonlinearities. Therefore, from the cost-effective transceiver design point of view, it is greatly beneficial if the generated OFDM signals have relatively low PAPRs.

To reduce the PAPR of an OFDM signal, apart from the widely adopted simple clipping technique, several other techniques have also been reported including selective mapping (SLM) and partial transmit sequences (PTS) [10, 11], both of which, however, suffer from high computational complexity. Apart from that, the SLM-induced PAPR reduction strongly depends upon the total number of employed IDFT blocks, whilst the PTS requires a large bandwidth overhead. Given the fact that the DFT can spread the spectrum of the subcarriers and subsequently decrease the probability of independently modulated subcarrier's waveforms being added up coherently by the IFFT operation, the PAPRs of the produced signals can thus be reduced considerably [12, 13]. In the LTE mobile standards, DFT-spread OFDM is adopted due to its effectiveness in reducing the PAPRs and relatively low DSP complexity [12-14].

To effectively address the PAPR challenge associated with the hybrid OFDM-DFMA PON and further enhance its compatibility to existing 4G network, it is great beneficial if the DFT-spread technique is utilized in the hybrid OFDM-DFMA PON. In this chapter, hybrid DFT-spread OFDM-DFMA PONs are proposed and numerically explored for the first time. The proposed PONs are shown to maintain all the features of the hybrid OFDM-DFMA PONs and further improve system transmission performance flexibility. We show that for upstream 13.125 Gb/s signals transmitted over 25 km SSMF PON systems based on IMDD, the proposed technique saves one quantization resolution bit and increases the system power budget by 3 dB, compared to the previously published hybrid OFDM-DFMA PONs [8].

This chapter is organized as following: in subsection 5.2, a detailed theoretical model of the proposed hybrid DFT-spread OFDM-DFMA PONs is developed, which considerably extends the previously reported hybrid OFDM-DFMA PON model [8]. From the physical PON operation point of view, the hybrid DFT-spread OFDM-DFMA PON model confirms the feasibility of utilizing DFT-spread OFDM in hybrid OFDM-DFMA PONs. Subsection 5.3 presents numerically simulated upstream transmission performances of the proposed PONs and their corresponding optimum transceiver designs. It is shown that, apart from the

aforementioned ≥3 dB increase in upstream system power budget and ≥1 bit reduction in minimum required DAC/ADC quantization bits, the proposed PON also gives rise to a ≥2 dB reduction in upstream signal PAPR. Moreover, in this subsection, detailed explorations of the impact of DAC/ADC quantization bit and clipping ratio on the upstream transmission performance are also undertaken for optimum transceiver designs. The results presented in this chapter indicate that the proposed PONs not only enhances the upstream transmission performance but also reduces the hardware/DSP complexity. Finally, the chapter is summarized in subsection 5.4.

5.2 Principle of Hybrid DFT-Spread OFDM-DFMA PONs

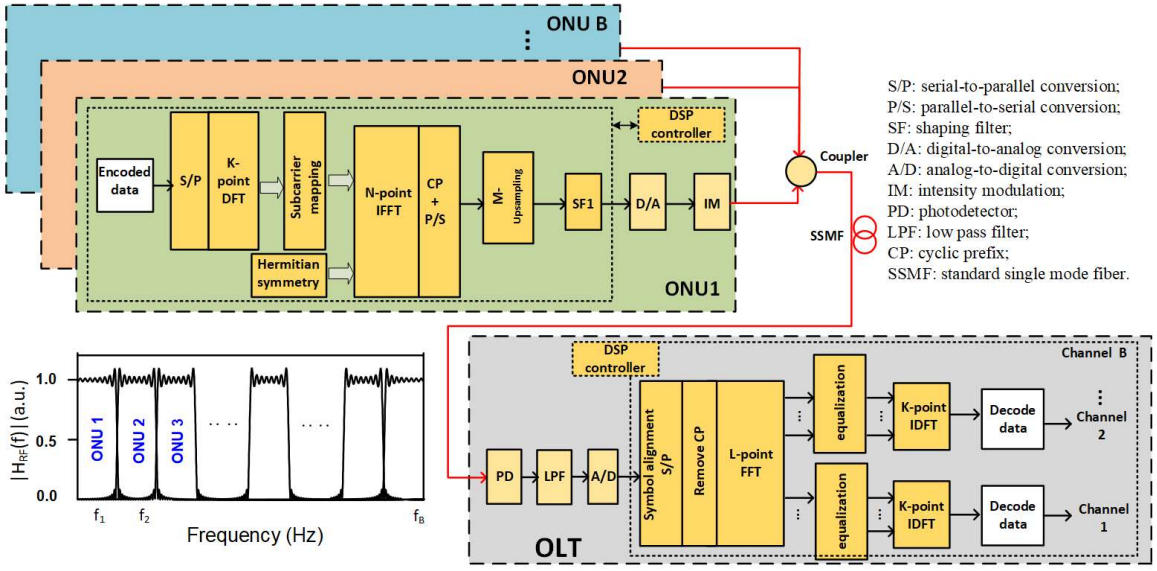

Fig. 5.1 Proposed hybrid DFT-spread OFDM-DFMA IMDD PONs simultaneously accommodating B ONUs.

Fig. 5.1 depicts the diagram of the proposed hybrid DFT-spread OFDM-DFMA IMDD PONs. Here special attention is focused on the more challenging multipoint-to-point upstream transmission only. As illustrated in Fig. 5.1, the upstream optical signals from *B* ONUs, labelled as 1st, 2nd … *B*-th ONU, are passively combined for upstream transmission. At each ONU arbitrarily encoded samples are converted from serial to parallel, and a *K*-point DFT operation is then applied to produce *K* spectrum spread samples. The obtained *K*-point DFT-spread signal $a(k')$ is expressed as:

$$a(k') = \sum_{k''=-\frac{K}{2}}^{\frac{K}{2}-1} d(k'')e^{-j\frac{2\pi k'k''}{K}}, k' = 0,1,\dots,K-1 \quad (5.1)$$

where $d(k'')$ is the time-domain sample sequence.

In the subsequent IFFT operation, the first subcarrier is set at zero, and the *K* spectrum spread samples are mapped onto the *K* respective subcarriers, while all the remaining unused subcarriers are set to be zeros to produce $\frac{N}{2}$ subcarriers in total, here $K \leq \frac{N}{2} - 1$, the parallel sample sequence $c(k)$ can be expressed as:

$$c(k) = \begin{cases} a(k'), for\ K\ subcarriers \\ 0,\ for\ other\ subcarriers \end{cases}, k = 0,1, \dots, \frac{N}{2} - 1 \tag{5.2}$$

After that, the Hermitian symmetry is applied to generate a real-valued DFT-spread OFDM signal after the *N*-point IFFT operation. The *m*-th OFDM symbol generated by the *N*-point IFFT of the set of *N* subcarriers can be written as:

$$x_m(n) = \sum_{k=-\frac{N}{2}}^{\frac{N}{2}-1} c_m(k) e^{j\frac{2\pi k(n-mN)}{L}},$$

$$n = 0, \dots, L-1; m = 0,1,2 \dots \tag{5.3}$$

where $c_m(k)$is the *m*-th data block of $c(k)$ after enforcing Hermitian symmetry, *L* is the symbol length in samples. For conventional OFDM without any up-sampling, we have *L*=*N*. As these subcarriers are localized mapping [12], for a given *N*, a large *K* gives rise to an enhanced PAPR reduction. Following the IFFT operation, the DFT-spread OFDM signal is up-sampled by a factor of *M*, thus an up-sampled OFDM symbol contains $L = MN$ samples, which then passes through a digital orthogonal SF to locate the signal at a desired spectral region. Using an ideal shaping filter that has a rectangle-shaped frequency response, the filtered signal in the *b*-th channel can be expressed as [8]:

$$x_{m,b}(n) = \frac{1}{M} \sum_{n=-N}^{N-1} c'_{m,b}(k) e^{j2\pi n\left(\frac{k+bN\frac{k}{|k|}}{L}\right)}$$

$$c'_{m,b}(k) = \{c_{m,b}(k)_{neg}, c_{m,b}(k)_{pos}\} \tag{5.4}$$

where $c_{m,b}(k)$ represents the *m*-th data block of $c(k)$ in the *b*-th channel, $c_{m,b}(k)_{pos}$ ($c_{m,b}(k)_{neg}$) refers to the subcarriers located at positive (negative) bin, which satisfies [8]:

$$c_{m,b}(k)_{neg} = c_{m,b}(k)_{pos} = c_{m,b}(k) \tag{5.5}$$

Finally, the digitally filtered signal samples $x_{m,b}(n)$ are fed to a DAC to generate an analogue electrical signal $x_b(t)$. After that, optical intensity modulation can be performed, as seen in Fig. 5.1. The coupled optical field from a total number of *B* ONUs can be expressed as:

$$S_{opt}(t) = \sum_{b=0}^{B-1}\left[\sigma_b(t)e^{j\beta_b(t)} \cdot \sqrt{1+\zeta_b * x_b(t)}\right]e^{j2\pi f_{opt}t} \tag{5.6}$$

where f_{opt} is the optical carrier frequency and ζ_b is the optical intensity modulation index of the *b*-th channel , $\sigma_b(t)$ and $\beta_b(t)$ take into account the optical intensity modulation impacts on the amplitude and phase of the *b*-th optical signal.

To simplify the theoretical analyses for the proposed hybrid DFT-spread OFDM-DFMA PONs, similar to the treatments reported in [8], linear transmission systems are assumed in this subsection only and numerical simulations are performed in subsection 5.3 to examine the feasibility of the proposed technique in practical non-linear PON transmission systems. Under these assumptions, in the OLT, after optical-electrical conversion and an ADC, the received signals emitted from a total number of *B* ONUs can be expressed as:

$$y(n) = \sum_{b=0}^{B-1} x_{m,b}(n) = \frac{1}{M}\left(\sum_{b=0}^{B-1}\sum_{k=-N}^{N-1} c'_{m,b}(k)e^{j\frac{2\pi\left(k+bN\frac{k}{|k|}\right)n}{L}}\right) \tag{5.7}$$

Let $\rho = k + bN\frac{k}{|k|}$, the following expressions can then be satisfied:

$$\begin{cases} k \in [-N, N-1] \\ b \in [0, B-1] \\ \rho \in [-BN, BN-1] \end{cases} \tag{5.8}$$

Thus the received signal $y(n)$ can be rewritten as:

$$y(n) = \frac{1}{M}\sum_{\rho=-BN}^{BN-1} c'_m(\rho)e^{j\frac{2\pi\rho n}{L}}$$

$$c'_m(\rho) = c'_{m,b}(k) \tag{5.9}$$

Eq. (5.9) indicates that the received signal can be processed by the L-point IFFT operation with $L= 2BN$. As such, in the OLT, the L-point FFT can be applied to $y(n)$ to recover the data sequence $c'_{m,b}(k)$ without implementing the digital filtering process required by conventional DFMA systems. The elimination of the OLT-embedded digital filtering process significantly reduces the OLT DSP complexity [8]. After the FFT operation, the obtained data sequence can be expressed as:

$$c'_m(\rho) = \sum_{n=-B}^{BN-1} \; y(n)e^{-j\frac{2\pi\rho n}{L}} \tag{5.10}$$

In the OLT, as shown in Fig. 5.1, after the photodetector, LPF and ADC, the obtained digital samples are firstly converted into parallel samples corresponding in length to one symbol period by a deserialiser. Similar to conventional OFDMA PONs [15], a symbol alignment block is employed to achieve symbol alignment and compensate for any possible symbol offset. The CP can then be removed, thus the remaining L time-domain samples are obtained for each symbol. After the following L-point FFT operation, the FFT-output sample sequence $\{c'_m(\rho)\} = \{c'_m(0), c'_m(1), \dots, c'_m(L-1)\}$ is obtained [8]. To identify the corresponding spectrum spread subcarriers $\{a_b\}$ from $\{c'_m(\rho)\}$ for a targeted ONU b, Eq. (5.11) is utilized, which presents the rules of the spread-subcarrier selection, and the corresponding spread-subcarrier index z is given in Eq.(5.12):

$$\{a_b\} = \left[\begin{array}{c} \overbrace{c'_m(z), c'_m(z+1) \dots, c'_m(z+\frac{N}{2}-1)}^{the\ first\ and\ \frac{N}{2}-1\ data-bearin\ \ subcarriers} \\ \underbrace{c'_m(z+N-1), c'_m(z+N-2), \dots, , c'_m\left(z+\frac{N}{2}\right)}_{\frac{N}{2}\ conjugate\ subcarriers} \end{array}\right], b = 0,1, \dots, B-1 \tag{5.11}$$

$$z = \begin{cases} 0, & b = 0 \\ \frac{L}{2} + (B-b-1)\cdot N, & b \geq 1 \end{cases} \tag{5.12}$$

After having identified the spectrum spread subcarriers from the b-th ONU, standard OFDM equalization [15] can be utilized for signal recovery, followed by the K-point IDFT in Eq. (5.13):

$$d(k'') = \sum_{k'=-\frac{K}{2}}^{\frac{K}{2}-1} a(k') e^{j\frac{2\pi k' k''}{K}} \tag{5.13}$$

where $a(k')$ is the parallel samples selected from $\{a_b\}$ through the corresponding K subcarrier positions, and the IDFT-operation generated data $d(k'')$ is ready for the further decoding operations to recovery the transmitted information.

From the above-described digital signal processing procedures in both the ONU and the OLT, it is easy to understand the following aspects: 1) the hybrid DFT-spread OFDM-DFMA PONs retain the advantages of previously-reported hybrid OFDM-DFMA PONs, such as reduced OLT DSP complexity; 2) as will be demonstrated in subsection 5.3, for practical implementation in 5G networks, the proposed hybrid DFT-spread OFDM-DFMA PONs further improve transmission system performance and reduce overall network installation expenditures, and 3) the downlink operation of the proposed hybrid DFT-spread OFDM-DFMA PONs is identical to those associated with DFMA PONs and OFDMA PONs when the corresponding digital filtering processes in both the OLT and ONUs are switched on and off respectively. This statement also holds true for the hybrid OFDM-DFMA PON downlink operation. Clearly, such a PON operation feature further enhances the network flexibility and adaptability to practical hardware impairments and/or dynamic network traffic status. As detailed downlink operation characteristics of DFMA PONs and OFDMA PONs have already been reported in [9] and [15] respectively, only the more challenging upstream operation of the proposed PONs is thus explored in the chapter.

5.3 Hybrid DFT-Spread OFDM-DFMA PONs Performance

In this subsection, numerical simulations of the upstream performances of 25 km SSMF IMDD hybrid DFT-spread OFDM-DFMA PONs (abbreviated as ‘DFT-hybrid’ case) are undertaken, and performance comparisons are made with the previously reported hybrid OFDM-DFMA PONs (abbreviated as ‘hybrid’ case) to highlight the unique advantages associated with the proposed technique. The approach reported in chapter 4 is adopted for OFDM signal generation/detection and the digital filter construction in the ONUs, and optical fibre transmission is simulated using VPI Transmission Maker. Given the fact that, according to our numerical results, the ONU-count dependent upstream performance of the proposed hybrid DFT-spread OFDM-DFMA PONs is very similar to the previously

Table 5.1 List of Parameters

PARAMETER	VALUE	PARAMETER	VALUE
DAC/ADC sample rate	12.5 GS/s	DAC/ADC resolution	7 bits
Clipping ratio	11 dB	Cyclic Prefix per channel	25%
Modulation formats	64 QAM	Total number of IFFT points of each channel	32
Transmitted optical power	0 dBm	Received optical power	-8 dBm
SSMF length	25 km	Up sampling factor M	4
SF filter length/ alpha factor	64/0	Hybrid OFDM-DFMA FFT size	128

published hybrid OFDM-DFMA PONs [8], for simplicity but without losing generality, two ONUs are considered throughout this chapter. Each ONU employs an ideal optical intensity modulator for E-O conversion as reported in [8], thus the parameters of σ_b and β_b included in Eq. (5.6) are taken to be 1 and 0 respectively, and the intensity modulation index is set to 0.99. In addition, as ideal intensity modulation does not introduce the optical beat interference effect, no optical frequency offset and polarization mismatch between ONU carriers are considered, as these effects are not significant over typical operation conditions for the application scenarios of interest of this chapter [16]. In implementing the digital filtering process in the considered ONUs, only in-phase filters [8] are utilised at different RF central frequencies governed by Eq. (4.19). The locations of the in-phase filters assigned to individual ONUs are illustrated at the bottom left of Fig. 5.1. To enable the considered two ONUs to occupy the entire spectral region, an up-sampling factor *M* is taken to be 4, thus the involved digital filter central frequencies satisfy: $f_1 = f_s/8$ and $f_2 = 3 \times f_s/8$. Generally speaking, the minimum *M* factor for supporting a total *B* ONUs should be 2*B* [9]. In generating the required real-valued OFDM signals, a 32-point IFFT (*N*=32) is used, thus the maximum usable data-bearing subcarriers in each ONU is 15. To reduce the channel interferences between the two ONUs channels and maximise their signal transmission capacity, ONU1(ONU2) has fourteen 64-QAM encoded data-bearing subcarriers, i.e., from subcarrier index 2 to 15(3 to 16), thus the DFT block size is *K*=14. For both the hybrid and

DFT-hybrid cases, their PAPR developing trends are almost independent of signal modulation format, as seen in Fig. 5.2(a). In this figure, their complementary cumulative distribution function (CCDF) curves for various modulation formats varying from 16-QAM to 256-QAM are presented for channel 1, channel 2's PAPR curves are not plotted in the figure as they are similar to channel 1. As such, for all numerical simulations, the signal modulation format of 64-QAM is adopted in exploring the upstream performances of the proposed PONs. All other parameters are listed in Table 5.1 and the SSMF and PIN parameters are the same as listed in Table 3.1, and the total aggregated signal transmission capacity of 13.125 Gb/s can be calculated from Eq. (3.14) for both the hybrid case and the DFT-hybrid case. After up-sampling, the signal bandwidth of each ONU is f_s/M. At the

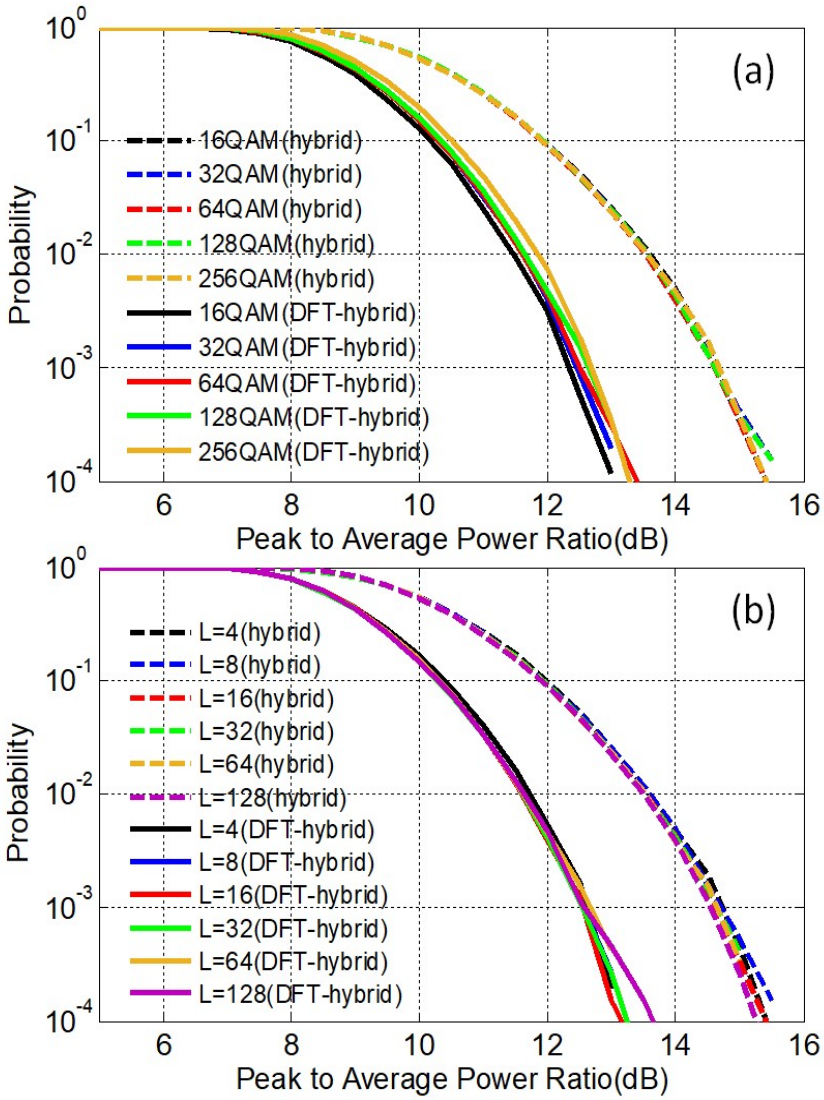

Fig. 5.2 CCDF curves of channel 1: (a) for different QAM modulation formats and fixed filter lengths of 64; (b) for different filter lengths from 4 to 128 and adopted signal modulation formats of 64-QAM.

OLT side, to avoid the aliasing effect, an ideal electrical filter with a bandwidth of 6.25 GHz is utilized to remove unwanted high frequency out-of-band noise before the ADC.

The PAPR performances of the hybrid OFDM-DFMA PONs with and without DFT-spread are respectively explored utilizing the parameters described above, and their CCDF curves are plotted in Fig. 5.2. It shows that at the adopted 11 dB clipping ratio region, DFT-spread gives rise to a PAPR reduction as large as ≥ 2 dB. In addition, as expected, such DFT-spread induced PAPR reductions are independent of both signal modulation format and digital filter length, as shown in Fig. 5.2 (a) and Fig. 5.2 (b) respectively. As a direct result of the digital filter length-independent PAPR reductions, the DFT-hybrid case also demonstrates almost identical upstream transmission performances over a large digital filter length variation range, similar to those reported in [8]. Since the performances of the typical hybrid OFDM-DFMA PONs are mainly limited by digital filter-induced signal distortions [8], to highlight the effectiveness of the DFT-spread technique by effectively minimizing the digital filter impairments, in this chapter a fixed digital filter length of 64 is adopted, as listed in Table 5.1.

The abovementioned considerable PAPR reduction not only improves the fibre transmission performance, but also increases the performance robustness to quantization noise caused by the bit resolution-limited DAC/ADC, as well as relaxing the stringent requirements on linear dynamic operation ranges of transceiver-embedded optical/electrical devices. This statement is confirmed in Fig. 5.3 (a), where BERs versus DAC/ADC quantization bits are illustrated utilizing the parameters in Table 5.1. It is clear that the DFT-hybrid case can reach BERs below the FEC limit of 1.0×10^{-3} when the resolution bits are as small as 6, while for the hybrid case, the minimum DAC/ADC resolution bits required for achieving the similar performance are increased to 7. Therefore, the performance tolerance to the quantization noise is improved by the DFT-spread technique. Such improvement is highly preferable for cost-sensitive application scenarios where low-cost DAC/ADCs with relatively low resolution bits and power consumptions can be applied. In addition, for a specific DAC/ADC resolution of 7 bits, the improved transmission performance by the DFT-spread technique is presented in Fig. 5.3 (b). It can be seen that the DFT-hybrid case can improve the system power budget by 3 dB compared to the hybrid case. Such improvement is mainly due to the

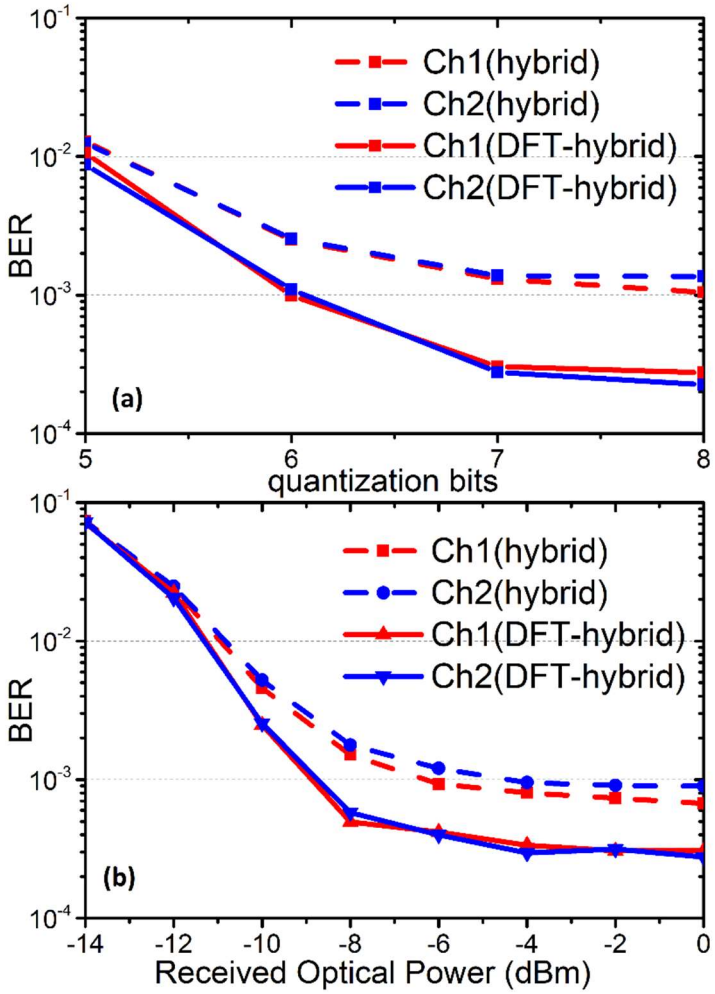

Fig. 5.3 (a) BER versus quantization bits; (b) BER versus received optical power when resolution bits are 7.

fact that the quantization noise is considerably decreased for the DFT-spread OFDM signals. In addition, this power budget improvement further enhances the network capability of accommodating higher traffic load and/or increasing the network coverage.

To extensively explore the dynamics between bit resolution and clipping ratio for the optimum design of transceivers incorporated in the hybrid DFT-spread OFDM-DFMA PONs, Fig. 5.4 is presented where the obtained BER contours are plotted against clipping ratio and quantization bit. It can be seen that for quantization bits ranging from 7 to 8, to maintain the BERs < 1.0×10^{-3}, clipping ratios should always be ≥11 dB for the hybrid case, while for the DFT-hybrid case, such a clipping ratio value is decreased to 10 dB over the same quantization bit variation region. The results in Fig. 5.3 and Fig. 5.4 also imply that: 1) the similar transmission performance of the considered ONUs with/without incorporating the DFT-spread technique indicates that the performance improvements induced by the

DFT-spread technique is independent of channel frequency locations, which are valuable for practical multi-channel applications; 2) the DFT-spread technique allows the transceivers to adopt even smaller clipping ratios to further reduce PAPRs, but without compromising the BER performances; 3) the DFT-hybrid case can save at least one quantization bit in comparison with the hybrid case; 4) the hybrid DFT-spread OFDM-DFMA PONs are promising for implementation in cost-sensitive 5G networks; and 5) The proposed PON can reduce the transceiver DSP complexity because of the reduction in minimum required DAC/ADC bit resolution. This enables the decrease in data processing-induced latency at physical layer (the effect of the additional *K*-point DFT and IDFTs on latency is negligible). As a direct result, the proposed PON is expected to reduce the overall latency between the OLT and ONUs in comparison with the hybrid OFDM-DFMA PONs under the same network operation conditions.

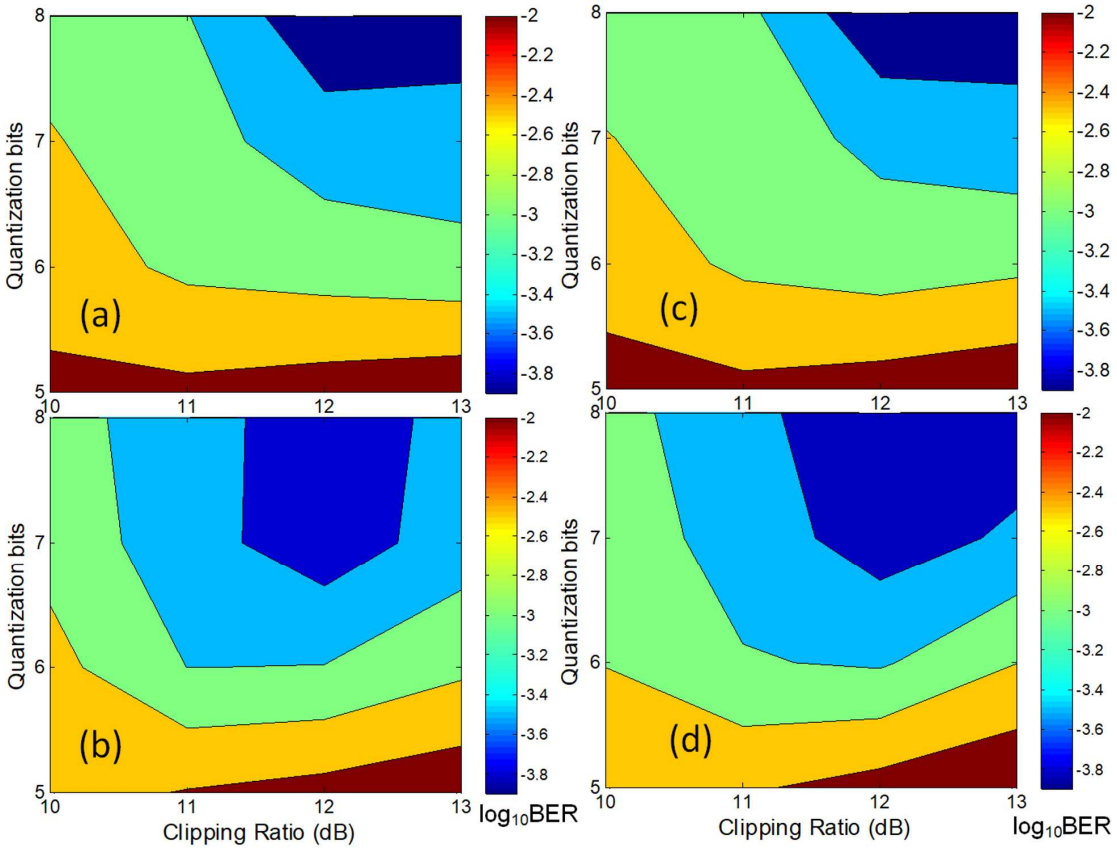

Fig. 5.4 BER contour versus quantization bit resolution and clipping ratio, (a) channel 1 in hybrid case; (b) channel 1 in DFT-hybrid case; (c) channel 2 in hybrid case; (d) channel 2 in DFT-hybrid case.

5.4 Conclusions

The novel hybrid DFT-spread OFDM-DFMA PONs have been proposed and numerically investigated for the first time, and performance comparisons have been made for representative 25km SSMF IMDD hybrid OFDM-DFMA PONs with and without incorporating the DFT-spread technique. The proposed network maintains all the salient features associated with the hybrid OFDM-DFMA PONs, in particular, they additionally reduce the upstream signal PAPRs by more than 2 dB. As a direct result, in comparison with the hybrid OFDM-DFMA PONs, the proposed PONs increase the upstream system power budget by more than 3 dB and reduce the minimum required DAC/ADC quantization bits by at least 1 bit.

References

[1] ITU-R Recommendation, "IMT Vision – Framework and Overall Objectives of the Future Development of IMT for 2020 and Beyond," [Online]. Available: https://www.itu.int/dms_pubrec/itu-r/rec/m/R-REC-M.2083-0-201509-I!!PDF-E.pdf.

[2] Cisco, "Cisco Visual Networking Index: Forecast and Trends, 2017–2022," [Online], Available: https://www.cisco.com/c/en/us/solutions/collateral/serviceprovider/visual-networking-index-vni/white-paper-c11-741490.html.

[3] A. Otaka, J. Terada, and J. Kani, et al., "Solutions for Future Mobile Fronthaul and Access-Network Convergence," *J. Light. Technol*., vol. 35, no. 3, pp. 527–534, 2017.

[4] X. Liu and F. Effenberger, "Emerging Optical Access Network Technologies for 5G Wireless [Invited]," *J. Opt. Commun. Netw*., vol. 8, no. 12, pp. B70-B79, 2016.

[5] G. Talli, F. Slyne, and S. Porto, et al., "SDN Enabled Dynamically Reconfigurable High Capacity Optical Access Architecture for Converged Services," *J. Lightwave Technol*., vol. 35, no. 3, pp. 550-560, 2017.

[6] N. Cvijetic, "Optical Network Evolution for 5G Mobile Applications and SDN-based Control," in *Proc. 16th Int. Telecommunications Network Strategy and Planning Symp. (Networks)*, pp. 1–5, 2014.

[7] H. F. Arrano and C. A. Azurdia-Meza, "OFDM: Today and in the Future of Next Generation Wireless Communications," *IEEE Central America and Panama Student Conference*, pp. 1–6. 2016.

[8] Y. Dong, R. Giddings, and J. Tang, "Hybrid OFDM-Digital Filter Multiple Access PONs," *J. Lightwave Technol*., vol. 36, no. 23, pp. 5640-5649, 2018.

[9] M. Bolea, R. P. Giddings, and M. Bouich, et al., "Digital Filter Multiple Access PONs with DSP-enabled Software Reconfigurability", *IEEE J. Opt. Commun. Netw*, vol. 7, no. 4, pp. 215-222, 2015.

[10] Y. Rahmatallah and S. Mohan, "Peak-To-Average Power Ratio Reduction in OFDM Systems: A Survey and Taxonomy," *IEEE Commun. Surv. Tutorials*, vol. 15, no. 4, pp. 1567-1592, Fourth Quarter 2013.

[11] T. Jiang and Y. Wu, "An Overview: Peak-to-Average Power Ratio Reduction Techniques for OFDM Signals," *IEEE Trans. on Broadcast.*, vol. 54, no. 2, pp. 257-268, 2008.

[12] H. G. Myung, J. Lim and D. J. Goodman, "Single Carrier FDMA for Uplink Wireless Transmission," *IEEE Veh. Technol. Mag.*, vol. 1, no. 3, pp. 30-38, 2006.

[13] S. A. Aburakhia, E. F. Badran, and D. A. Mohamed, "Distribution of the PAPR for Real-valued OFDM Signals," in *Proc. Int. Conf. Inf. Technol*., pp. 1-8, 2009.

[14] B. E. Priyanto, H. Codina, S. Rene, T. B. Sorensen, and P. Mogensen, "Initial Performance Evaluation of DFT-spread OFDM based SC-FDMA for UTRA LTE Uplink," in *Proc. IEEE Veh. Tech. Conf.*, Dublin, Ireland, pp. 3175–3179, 2007.

[15] R. Giddings, "Real-time Digital Signal Processing for Optical OFDM-based Future Optical Access Networks," *J. Lightwave Technol*., vol. 32, no. 4, pp. 553–570, 2014.

[16] X. Q. Jin and J. M. Tang, "Experimental Investigations of Wavelength Spacing and Colorlessness of RSOA-based ONUs in Real-time Optical OFDMA PONs," *J. Lightwave Technol*., vol.30, no.16, pp.2603-2609, 2012.

6. DSP-Enabled Flexible ROADMs Without Optical Filters and O-E-O Conversions

Contents

6.1 Introduction

In the previous chapters, various new cost-effective PONs have been proposed and investigated for seamlessly integrating traditional optical access networks, metropolitan optical networks and mobile front-haul/back-haul networks [1, 2]. From practical application point of view, it is greatly advantageous if the converged network has separate the dropped signal from the destroyed and unrecoverable not only strong adaptability to highly dynamic traffic with arbitrary bandwidth granularity, but also desirable performance capability of simultaneously accommodating a wide diversity of key network operation features including, for example, various signal modulation formats, different signal detection schemes, flexible WDM grids, diversified network topologies and various multiple access techniques. In addition, it is also preferable to equip the converged networks with a diversity of SDN functionalities [3, 4] to dynamically provide fast on-demand connections/services at wavelength, sub-wavelength and sub-band levels. As one of the most important networking devices offering fast connectivity between an expanded number of individual optical networks, ROADMs [5, 6] with advanced architectures and flexible functionalities are expected to play a vital role in ensuring the achievement of all the aforementioned networking features required by converged networks, whilst still allowing a technical strategy of significantly reducing both the CapEx and the OpEx.

Recently, a number of new ROADM architectures have been reported with advanced functionalities in terms of colourlessness, directionlessness, contentionlessness and WDM-gridlessness [7-14]. However, all those complicated ROADMs are not capable of fully offering, in a cost-effective manner, the above-mentioned networking functions required by the fixed-mobile converged networks, because of their hard-wired switching element-induced operation limitations on ROADMs' upgradability, adaptability and flexibility [15]. On the other hand, given the fact that the converged networks are very cost-sensitive and dynamic, O-E-O-free, SDN-controllable ROADM configurations are also highly desirable.

To overcome this drawback and further enhance the ROADM practicability, utilizing Hilbert-pair-based digital filtering, intensity modulation, and passive optical coupling, DSP-enabled flexible ROADMs are reported [16, 17], which are free from optical filters and O-E-O conversions and offer excellent flexibility, colourlessness, gridlessness, contentionlessness, adaptability, and transparency to physical-layer network characteristics.

Making use of Hilbert-pair-based digital filtering, for each specific wavelength, the proposed ROADM incorporates an intensity modulator driven by an SDN-controllable drop RF signal to perform the drop operation. Whilst the add operation is performed by passive optical coupling in an optical coupler (OC). Extensive numerical simulations are undertaken to evaluate the add/drop operation characteristics of the proposed ROADMs in IMDD-based optical network nodes. It is shown that the proposed ROADMs can dynamically and flexibly perform add/drop operations at wavelength, subwavelength, and spectrally overlapped orthogonal sub-band levels. The drop operation introduces optical power penalty of 3 dB, whilst the optical power penalty associated with the add operation can be 3.5 dB. In addition, the ROADM performance robustness against variations in digital filter lengths and transmission system characteristics/impairments is explored.

The main advantages of the ROADMs presented include: a) optical-domain colourless and contentionless add/drop operations at wavelength, sub-wavelength and orthogonal sub-band levels; b) DSP-enabled ROADM operation tunability, adaptability and scalability; c) inherent transparency to physical-layer network characteristics including signal modulation formats, signal detection schemes, multiple access techniques and network topologies; d) high spectral efficiency; e) flexible granularity at wavelength, sub-wavelength and sub-band levels; f) applicability in IMDD optical network nodes, and g) potentially low-cost, high energy consumption efficiency and small footprint.

6.2 Proposed ROADM Architectures and Operating Principles

Fig. 6.1 (a) shows the schematic diagram of the proposed ROADM architecture fully supporting the SDN solution, and the involved drop and add function elements are also illustrated in Fig. 6.1 (b) and Fig. 6.1 (c), respectively. The input and output optical signals of each wavelength consist of multiple sub-wavelength bands at different RFs. Each individual sub-wavelength band can have either two digital filtering-enabled spectral-overlapped orthogonal sub-bands (an in-phase sub-band "*I*" and a quadrature-phase sub-band "*Q*") or a single sub-band (*I* or *Q*) [18, 19]. For a specific optical carrier frequency, f_o, the optical signal containing *n* sub-wavelength bands can be expressed as:

$$s(t) = \sum_{i=1}^{n} \sum_{w=\{I,Q\}} y_i^w(t) e^{j2\pi f_o t} \tag{6.1}$$

where $y_i^w(t), (w = I \text{ or } Q)$ is the sub-band signal that is up-sampled and subsequently

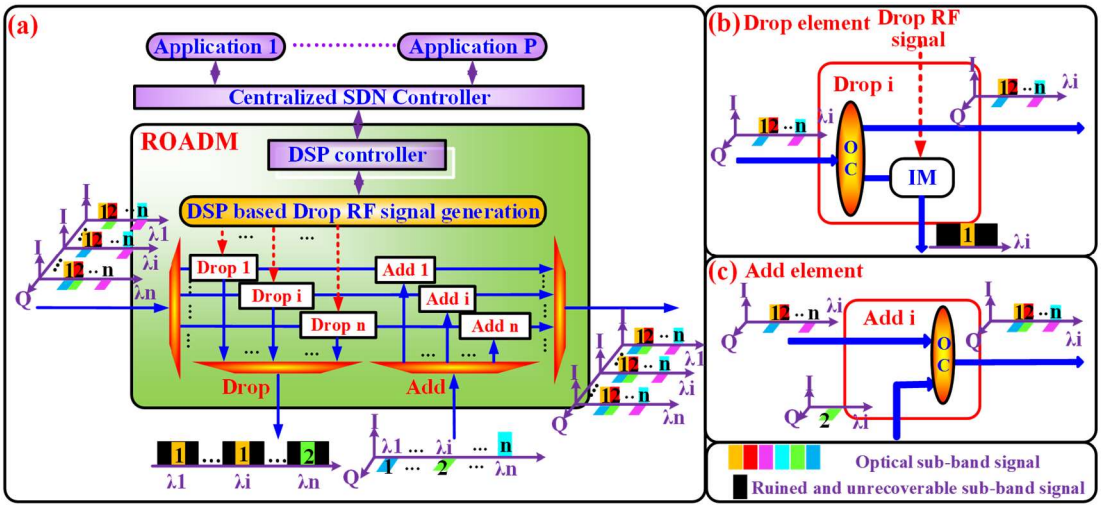

Fig. 6.1. (a) Schematic diagram of the proposed ROADM architecture supporting the SDN solution; (b) drop function element; (c) add function element. IM: intensity modulator; OC: optical coupler.

filtered by the corresponding *I* or *Q* component of the *i*-th orthogonal digital filters in the terminal equipment transceivers (TETs). These digital filters' central frequencies are located at f_{ci} (*i*=1,2,3,4 ….*n*).

As shown in Fig. 6.1 (a) and Fig. 6.1 (b), in each drop function element, the input signal of a specific wavelength is firstly split into two portions: the first portion is directly delivered to the add function element, whilst the second portion passes through a drop RF signal driven-IM to drop a targeted sub-band. The SDN-controllable drop RF signal for the *w*-th sub-band of the *i*-th sub-wavelength can be expressed as:

$$RF_i^w(t) = \begin{cases} Re\left\{\frac{1+ke^{j2\pi f_{ci}t}}{1+k}\right\} & ,\mathrm{w} = \mathrm{I} \\ Re\left\{\frac{1+ke^{j\left(2\pi f_{ci}t+\frac{\pi}{2}\right)}}{1+k}\right\} & ,\mathrm{w} = \mathrm{Q} \end{cases} \tag{6.2}$$

where *k* (0<*k*<1) is introduced to ensure that the drop RF signal amplitude varies within a dynamic range from 0 to 1. At the IM output, the dropped sub-band with a reversed spectrum is shifted to the baseband spectral region, while all other sub-bands of the same wavelength are destroyed and unrecoverable. As detailed in subsection 6.3.2, after the direct detection of the dropped optical signal in a TET, a simple baseband digital filter suitable for performing all the drop operations can be utilized to separate the dropped signal from and

simultaneously destroyed all other sub-bands destroyed and unrecoverable sub-bands. A relatively large *k* in Eq. (6.2) increases the optical signal power of the dropped sub-band [17].

As indicated in Eq. (6.2), by simultaneously using *I* and *Q* drop RF signals in two parallel drop function elements, the drop operation can also be conducted at sub-wavelength level. Moreover, to perform the drop operation at entire wavelength level, *k*=0 can be taken to enable the IM to simply act as an optical passway. On the other hand, in the add function element, similar to the procedure reported in [19], the add operation at a specific wavelength can be performed by passive optical coupling in an OC, as illustrated in Fig. 6.1 (c). Such an operation can be expressed as:

$$|s_{out}(\mathrm{t})|^2 = |s_{in}(t)|^2 + |s_{add}(t)|^2 \tag{6.3}$$

where $S_{in}(t)$ and $S_{out}(t)$ are the input and output optical signals of the add function element, and $S_{add}(t)$ is the optical sub-band/sub-wavelength signal to be added. To achieve the contention-free add operation, $S_{add}(t)$ has to be located in a free location within the digital filtering space. This can be easily realised by selecting a free digital filter type (*I* and/or *Q*) for a given central RF frequency and/or shifting the central RF frequency of a digital filter having a specific type in the digital domain prior to performing the E-O conversion in the corresponding TET [19]. Moreover, the desired directionless operation is also achievable if conventional broadcasting and selecting techniques are incorporated in the proposed ROADMs.

As shown in Fig. 6.1 (a), the ROADM operations described above are fully controlled by a ROADM-embedded DSP controller, which automatically produces a dynamic parameter set through periodically communicating with the centralised SDN controller via extended OpenFlow [21, 22]. The dynamic parameter set may include digital filter characteristics employed by the targeted sub-bands/sub-wavelengths, drop RF signal characteristics when the drop operation is required, and free filters in the digital filtering space when the add operation is required. As the parameter set can be dynamically generated and finely adjusted using DSP algorithms according to the prevailing tasks, traffic status and network characteristics, the operations of the proposed ROADMs are thus flexible, scalable, adaptive and physical-layer network characteristic-transparent.

6.3 ROADM Performances

In this chapter, for each sub-wavelength, use is made of Hilbert-pair-based digital filtering [18,19] to generate two spectral-overlapped orthogonal sub-band signals encoded using any modulation formats. For simplicity without loss of generality, OFDM is considered throughout this chapter. In a TET, an OFDM signal, $s_{i-signal}(t)$, is firstly up-sampled to generate $s_{i-upsampled}(t)$, and then digitally filtered using a Hilbert-pair-based filter $h_i^w(t)$ as described in subsection 2.2.1.5. After digital filtering, the sub-band signal can be written as:

$$y_i^w(t) = s_{i-upsampled} \otimes h_i^w(t) \tag{6.4}$$

To support *N* independent sub-wavelengths for a specific wavelength, f_{ci} is governed by [19]:

$$f_{ci} = (2i-1)\frac{f_{DAC/ADC}}{4N} \quad i = 1,2,3,\cdots,N \tag{6.5}$$

where $f_{DAC/ADC}$ is the sampling speed of the DAC/ADC, i represents the *i*-th sub-wavelength.

Each electrical OFDM sub-band is generated using adaptively power- and bit-loaded 15 data-bearing subcarriers with various signal modulation formats ranging from DBPSK, DQPSK, 16-QAM to 256-QAM. A cyclic prefix is taken to be 1/8. The DAC/ADC operates at 15 GS/s at 7-bit. The electrical OFDM signal clipping level is fixed at 14 dB. The digital filter length of *L*=32 and the excess of bandwidth of α =0 are also considered. Here the choice of α=0 is to reduce the overlapping regions between the frequency responses of the same type filters (*I* or *Q*), thus resulting in a reduced add operation penalty. To considerably simplify numerical simulations without loss of generality, throughout the chapter, the signal up-sampling factor, *M*, is fixed at 8, and the digital filter's central frequencies satisfying Eq. (6.5) with *i* = 2, 3 and 4 are adopted, for a given optical wavelength and after intensity modulation, this results in three sub-wavelengths, each of which has two orthogonal OFDM sub-bands (*I* and *Q*). For the considered transmission system consisting of six data-conveying sub-bands and two empty basebands for performing the drop operation, the minimum up-sampling factor is *M*=8 [19]. The selection of such a factor in the chapter not only maximizes the aggregated signal transmission capacity but also improves the spectral

Table 6.1 Bit rate of each sub-band

Sub-band	Signal Bit Rate (Gb/s)
I/Q, *i*=2	2.9
I/Q, *i*=3	2.9
I/Q, *i*=4	2.9
Total	17.4

efficiency when the DAC/ADC sampling speeds are fixed. For such a transmission system, a further increase in up-sampling factor lowers the maximum achievable aggregated transmission capacity, but it reduces the channel cross-talk effect, which subsequently results in a decreased add operation penalty. To highlight the impact of the add/drop operation on the signal quality, ideal intensity modulators are considered. As an example of illustrating the ROADM performance characteristics, a representative 1550 nm optical carrier is used

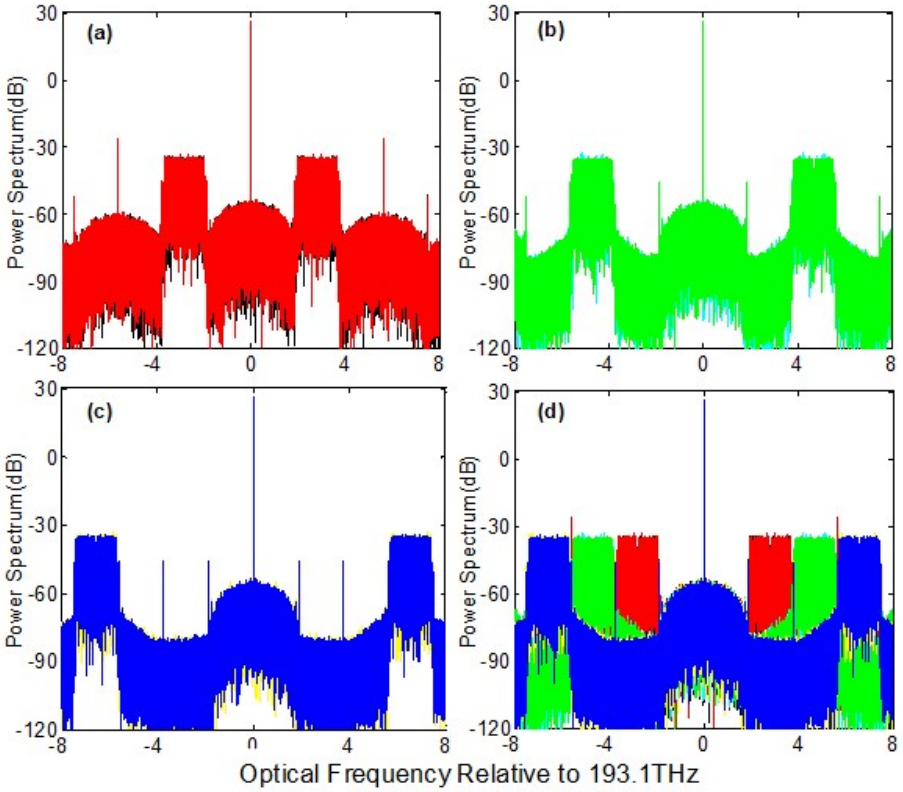

Fig. 6.2. In-phase "I" and quadrature-phase "Q" spectra of OFDM sub-bands. (a) overlapped I and Q sub-band spectra before the add operation for i=2. (b) overlapped I and Q sub-band spectra before the add operation for i=3. (c) overlapped I and Q sub-band spectra before the add operation for i=4. (d) combined six OFDM sub-band spectra after the add operation.

here to convey sub-wavelength/sub-band signals. Unless explicitly stated, the total transmitted optical power is fixed at -2 dBm. To directly detect an optical signal in a TET, an APD is employed with a quantum efficiency of 0.8 and a power sensitivity of -26 dBm. Based on the above-mentioned parameters, the maximum achievable signal bit rates of these six OFDM sub-bands contained in these three sub-wavelengths are summarised in Table 6.1.

6.3.1 Add Operation Performance

Before performing the add operation at a specific wavelength, each individual optical carrier of the same wavelength is assumed to contain only one of these six OFDM sub-bands, and each individual sub-band is allocated at a free location of the digital filtering space assigned to the wavelength, as illustrated in Fig. 6.2 (a)-(c). Having performed the add operation, the signal spectra of the passively combined six sub-bands are shown in Fig. 6.2 (d). After the square-law detection of the combined optical signals in a TET, making use of the DSP procedure presented in [19], the BER performances of these six OFDM sub-bands are calculated individually, which are plotted as a function of received sub-band optical power in Fig. 6.3. To identify the ROADM add operation impairments, for each sub-band, Fig. 6.3 shows two BER curves corresponding to the cases of before and after the add operation.

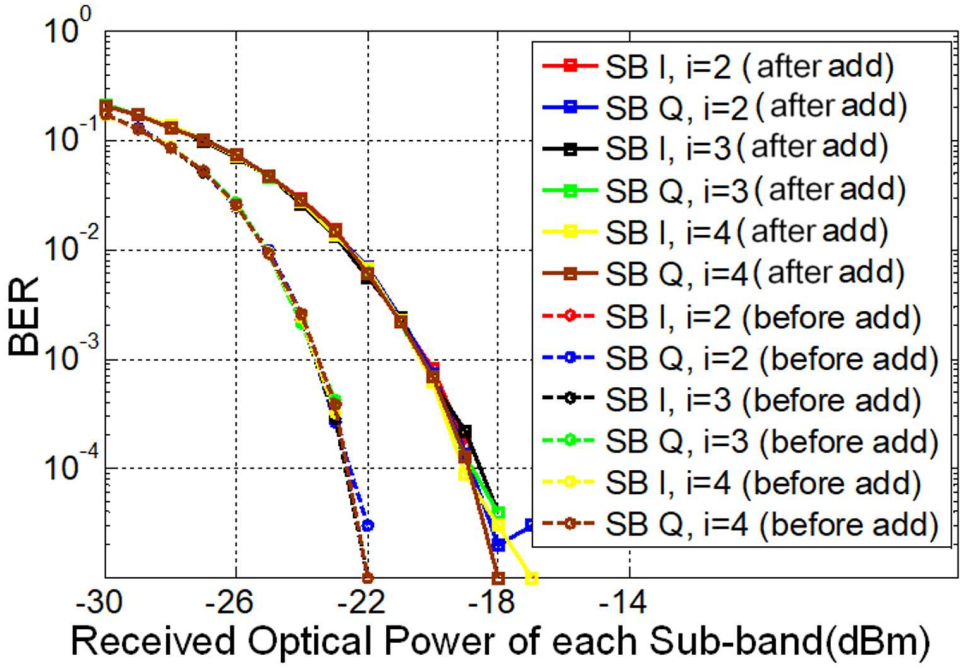

Fig. 6.3. BER versus received optical power of each OFDM sub-band before and after performing the add operation. SB: sub-band.

As expected from theoretical [19] and experimental [20] results, it can be seen in Fig.6.3 that the add operation gives rise to very similar BER performances for all these six OFDM sub-bands. This indicates that the add operation is independent of the sub-band's location in the digital filtering space. In addition, the add operation brings about a 3.5 dB power sensitivity degradation. The major physical mechanisms underpinning the observed add operation penalty are: a) the reduction in effective OSNR after the add operation, as the total optical signal power launched into the APD is fixed; b) the add operation-enlarged cross-talk effect occurring because of the overlaps among the frequency responses of the same types of digital filters located in neighbour sub-wavelengths. From the above analysis, it can be understood that the add operation penalty can be reduced, to some extent, when the digital filter associated with the added signal is orthogonal with respect to other digital filters associated with the signals located at its neighbour sub-wavelengths.

6.3.2 Drop Operation Performance

In numerically simulating the drop operation performance of the proposed ROADM, an input optical signal of a representative wavelength is assumed to consist of six individual OFDM sub-bands distributed at three RF frequencies satisfying Eq. (6.5) with i=2,3,4. For each filter type (I or Q), three different drop RF signals are utilised, which have different RF frequencies and optimum k parameters of k=0.99. As already stated in subsection 6.2, the drop operations undertaken in six parallel IMs produce six dropped optical signals at the same wavelengths, as shown in Fig. 6.4 (a)-(f). In performing the drop operation for each sub-band, the drop operation shifts the targeted sub-band to the baseband spectral region, and simultaneously destroyed all other sub-bands contained in the same wavelength, thus causing those destroyed sub-bands unrecoverable.

After the direct detection of the dropped optical signal in a TET, a simple baseband digital filter having a form $h(t) = p(-t)$, can be employed in the digital domain to separate the dropped signal from all the destroyed and unrecoverable sub-bands. This implies that, in the TET end, a universal baseband digital filter is capable of recovering all dropped sub-bands, regardless of their locations in the digital filtering space prior to the drop operation. In addition, the feature of automatically locating the dropped sub-band at the baseband spectral region can also relax significantly the requirement on high-speed ADCs in the TET end. These abovementioned two ROADM features are valuable for cost-sensitive application

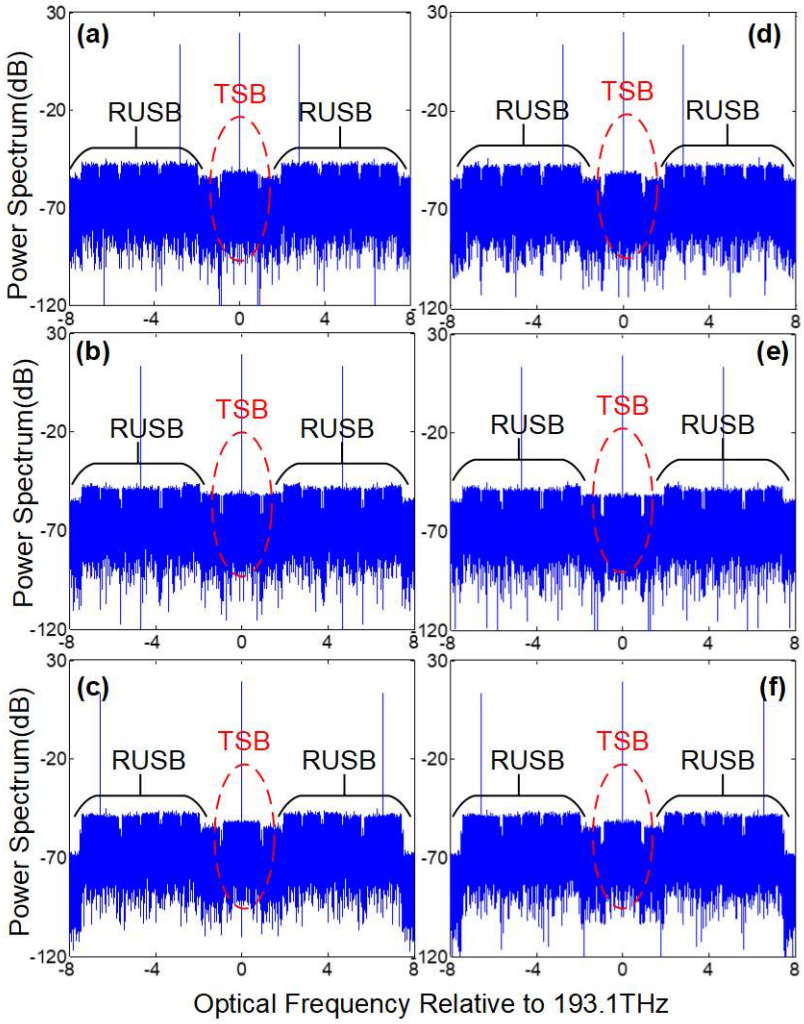

Fig. 6.4. Sub-band signal spectra after the drop operation. (a) Dropped sub-band, I, for i=2. (b) Dropped sub-band, I, for i=3. (c) Dropped sub-band, I, for i=4. (d) Dropped sub-band, Q, for i=2. (e) Dropped sub-band, Q, for i=3. (f) Dropped sub-band, Q, for i=4. TSB: targeted sub-band, which is shifted to the baseband spectral region after the drop operation. RUSB: ruined and unrecoverable sub-bands of the same wavelength after the drop operation.

scenarios such as ONUs, since these features simplify significantly the TET architecture, reduce the digital filter DSP complexity, and subsequently lower the TET cost and power consumption.

The drop operation performance of the proposed ROADM is examined in Fig. 6.5, where the BER performances of each OFDM sub-band before and after performing the drop operation are plotted against received sub-band optical power, here the BER performance of

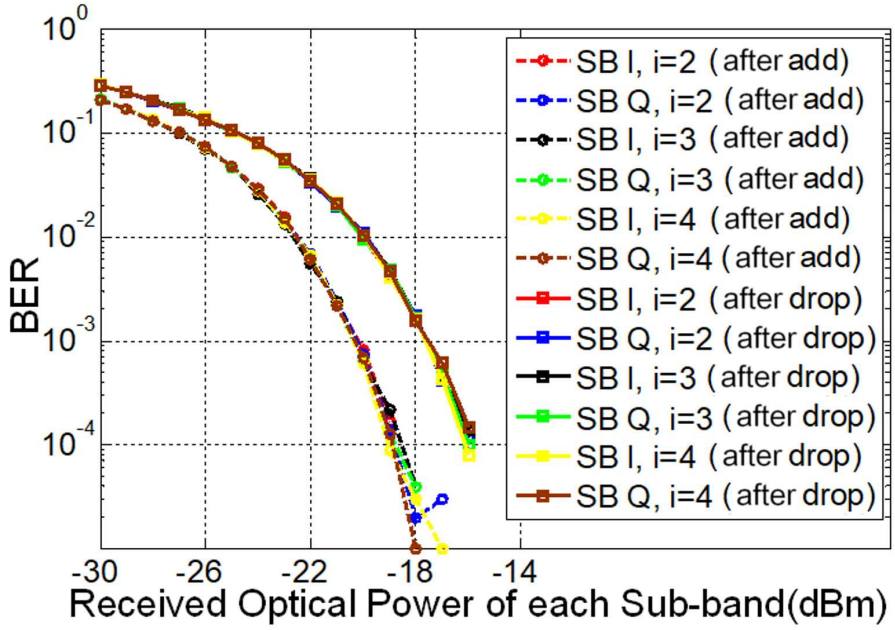

Fig. 6.5. BER versus received optical power of each OFDM sub-band before and after the drop operation. SB: sub-band.

after add operation is similar to that of before drop operation for each corresponding sub-bands. In Fig. 6.5, for different sub-bands before and after the drop operation, very similar BER developing trends are observed, indicating, once again, the sub-band digital filtering space location-independent ROADM operation. It is also note that the drop operation give rise to around 3 dB power penalty at the FEC limit, as seen in Fig. 6.5, which is due to the ROADM drop operation-induced nonlinearities.

6.3.3 Robustness to Digital Filter Length Variations

From the analysis undertaken in subsections 6.3.1 and 6.3.2, it is easy to understand that digital filters are critical in determining the ROADM operation characteristics. The main objectives of this subsection are therefore to explore the trade-offs between the ROADM performance and digital filter design, based on which optimum filter design criteria are identified to effectively reduce the digital filter DSP complexity and simultaneously improve the ROADM performance.

To explore the impact of digital filter length on the ROADM add operation performance, different digital filter lengths varying from 8, 16, 32, 64 to 128 are adopted in digitally generating and recovering each individual sub-band. The same ROADM operation conditions adopted in computing Fig. 6.3 are still considered here, i.e., before the add

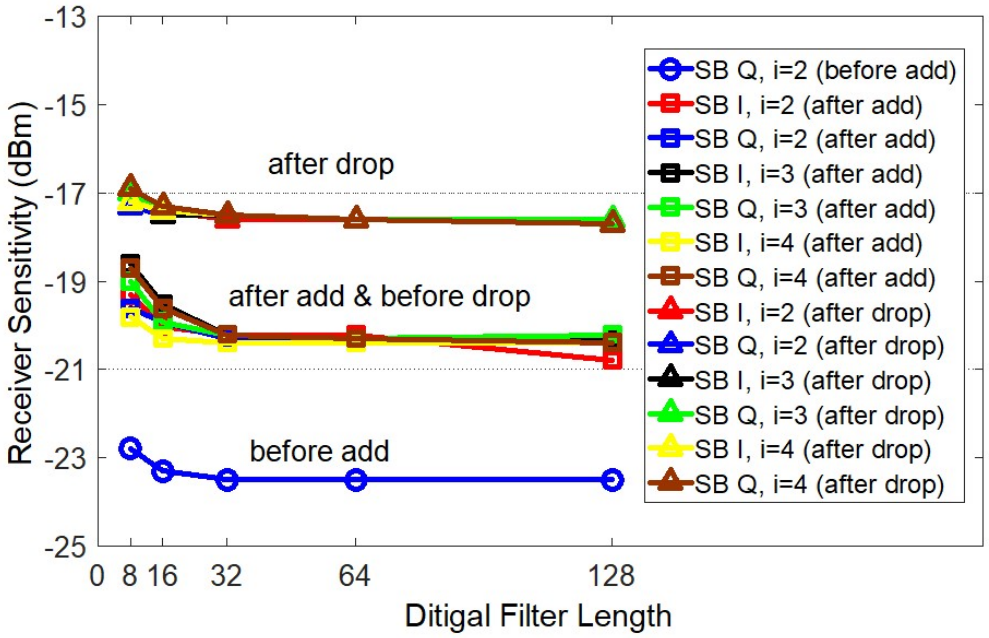

Fig. 6.6. Digital filter length-dependent receiver sensitivity of each OFDM sub-band before/after the add/drop operation.

operation, each individual optical carrier contains only one OFDM sub-band allocated at a free location in the digital filtering space. Before directly detecting the combined six OFDM sub-band signal, its optical power is adjusted to -11.2 dBm, which is equivalent to an optical power of -19 dBm for each individual OFDM sub-band before the add operation. After the add operation, Fig. 6.6 shows the digital filter length-dependent receiver sensitivity of all the involved six OFDM sub-bands. It can be seen in Fig. 6.6 that, a long filter length improves the add operation performance for all the sub-bands, however for the digital filter lengths of $L \geq 32$, such performance improvement becomes small. Here only the curve of sub-band Q in the 2nd sub-wavelength (i = 2) before the add operation is plotted in Fig. 6.6, as all the curves of other sub-bands before the add operation are similar.

Furthermore, making use of numerical simulation conditions similar to those adopted in producing Fig. 6.4, the filter length-dependent drop operation performances are also explored in Fig. 6.6, where the receiver sensitivity of each dropped OFDM sub-band is plotted against digital filter length. In obtaining Fig. 6.6, the k parameters for all the drop RF signals are set at k=0.99, and the total optical power of the optical signal after the drop operation is set to be -12.2 dBm, which corresponds to an optical power of -20 dBm for each individual OFDM sub-band before the drop operation. The results show that similar to the add operation performance, the adoption of a relatively long digital filter length enhances

the drop operation performance for all involved sub-bands, and such performance improvement becomes smaller when the digital filter lengths $L \geq 32$.

Generally speaking, a long filter length flattens the digital filter frequency response at its top region [19], as a direct result, the long filter length-induced ROADM operation improvements occur in Fig. 6.6. Considering the fact that an increase in digital filter length requires a large number of DSP logical blocks, thus enlarging the digital filter DSP complexity and power consumption, the results shown in Fig. 6.6 indicate that an optimum filter length of L=32 should be chosen for practical implementation.

6.3.4 Robustness to Transmission System Characteristics/Impairments

Given the fact that the ROADM add operation is very similar to the passive optical coupling-based combination of various optical upstream signals in the remote node of a PON network, and that the upstream signal transmission performances have been reported in [19], thus special attention in this subsection is mainly focused on the ROADM drop performance robustness to fibre chromatic dispersion.

Using digital filter lengths of L=64, the receiver sensitivity variations against different fibre transmission distance for OFDM signals are shown in Fig. 6.7, in obtaining which only the chromatic dispersion effect with a parameter of 16 ps/(km·nm) is considered. After the fibre transmission, each of the OFDM sub-bands is dropped using a parameter k of 0.99. It can be

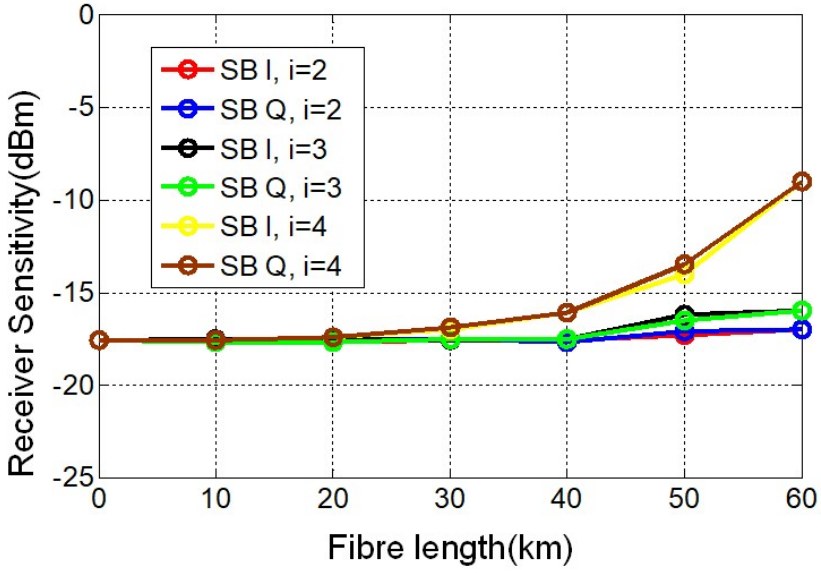

Fig. 6.7 ROADM drop performance robustness to fibre chromatic dispersion.

seen in Fig. 6.7 that for higher frequency sub-bands, the receiver sensitivity is higher than those for lower frequency sub-bands, this is because the cumulated chromatic dispersion effect induces the channel fading effect, as described in chapter 2. For transmission distances less than 40 km, the ROADM drop operation is robust to chromatic dispersion-induced channel impairments.

6.4 Conclusions

Making use of Hilbert-pair-based digital filtering, SDN-controllable drop RF signal-driven intensity modulation and passive optical coupling, optical filter- and O-E-O conversion-free ROADMs with excellent flexibility, colourlessness, contentionlessness, gridlessness, adaptability and transparency to physical-layer network characteristics have been proposed and examined, which offer DSP-enabled dynamic add/drop operations at wavelength, sub-wavelength and orthogonal sub-band levels. To evaluate the operation characteristics of the proposed ROADMs in IMDD-based optical network nodes, detailed numerical simulations have been undertaken, which show: i) the add/drop operation is digital filtering space location-independent; ii) the drop operation introduces around 3 dB power penalties, and iii) power penalties induced by the add operation can be 3.5 dB. Furthermore, the impacts of key digital filter parameters on the add/drop performance have also been explored, based on which optimum ROADM design criteria have been identified for not only effectively reducing the digital filter DSP complexity but also simultaneously improving the ROADM performance. iv) the ROADM drop performance robustness to fibre chromatic dispersion is also explored, which shows for a distance less than 40 km, the ROADM drop operation is robust to CD-induced transmission impairments.

References

[1] J. S. Wey and J. Zhang, "Passive Optical Networks for 5G Transport: Technology and Standards," *J. Light. Technol*., vol. 37, no. 12, pp. 2830-2837, 2018.

[2] D. H. Hailu, B. G. Gebrehaweria, and S. H. Kebede, et al., "Mobile Fronthaul Transport Options in C-RAN and Emerging Research Directions : A Comprehensive Study," *Opt. Switch. Netw*., vol. 30, pp. 40–52, 2018.

[3] L. Valcarenghi, K. Kondepu, and A. Sgambelluri, et al., "Experimenting the Integration of Green Optical Access and Metro Networks Based on SDN," *Int. Conf. on Transparent Optical Networks*, 2015.

[4] M. Ruffini, F. Slyne, and C. Bluemm, et al., "Software Defined Networking for Next Generation Converged Metro-access Networks," *Opt. Fiber Technol*., vol. 26, pp. 31–41, 2015.

[5] B. Schrenk, A. Poppe, and M. Stierle, et al., "Fully-passive Optical Switch Introducing Dynamicity and Flexibility to Metro-access," *IEEE Photonics Technol. Lett*., vol. 27, pp. 486–489, 2015.

[6] S. Gringeri, B. Basch, and V. Shukla, et al., "Flexible Architectures for Optical Transport Nodes and Networks," *IEEE Commun. Mag*.,vol.48, no.7, pp. 40–50, 2010.

[7] T. Watanabe, K. Suzuki, and T. Goh, et al., "Compact PLC-based Transponder Aggregator for Colorless and Directionless ROADM," in *Proc. Opt. Fiber Commun. Conf. Nat. Fiber Optic Eng. Conf.*, 2011.

[8] Z. Shen, H. Hasegawa, and K. Sato, et al., "A Novel Semi-flexible Grid Optical Path Network that Utilizes Aligned Frequency Slot Arrangement," in *Proc. Eur. Conf. Opt. Commun.*, 2013.

[9] W. J. Jiang, A. Lebedev, and Y. M. Lin, et al., "Degree-expandable Colorless, Directionless, and Contentionless ROADM without Drop-side EDFAs," in *Proc. Opt. Fiber Commun. Conf. Nat. Fiber Optic Eng. Conf.*, 2015.

[10] W. I. Way, "Optimum Architecture for M×N Multicast Switch-based Colorless, Directionless, Contentionless, and Flexible-grid ROADM," in *Proc. Opt. Fiber Commun. Conf. Nat. Fiber Optic Eng. Conf.* 2012.

[11] X. Yu, M. Tornatore, and M. Xia, et al., "Brown-field Migration from Fixed Grid to Flexible Frid in Optical Networks," in *Proc. Opt. Fiber Commun. Conf. Nat. Fiber Optic Eng. Conf.*, 2015.

[12] S. Thiagarajan and S. Asselin, "Nodal Contention in Colorless, Directionless ROADMs using Traffic Growth Models," in *Proc. Opt. Fiber Commun. Conf. Nat. Fiber Optic Eng. Conf.*, 2012.

[13] M. D. Feuer, S. L. Woodward, and P. Palacharla, et al., "Intra-node Contention in Dynamic Photonic Networks," *J. Lightwave Technol*., vol. 29, pp. 529–535, 2011.

[14] W. I. Way, P. N. Ji, and A. N. Patel, "Wavelength Contention-free via Optical Bypass within a Colorless and Directionless ROADM [Invited]," *J. Opt. Commun. Netw*., vol. 5, pp. A220–A229, 2013.

[15] A. Muhammad, G. Zervas, and G. Saridis, et al., "Flexible and Synthetic SDM Networks with Multicore Fibres Implemented by Programmable ROADMs," in *Proc. Eur. Conf. Opt. Commun.*, 2014.

[16] W. Jin, X. Duan, and Y. Dong, et al., "DSP-Enabled Flexible ROADMs Without Optical Filters and O-E-O Conversions," *J. Light. Technol*., vol. 33, no. 19, pp. 4124–4131, 2015.

[17] W. Jin, C. Zhang, and X. Duan, et al., "Improved Performance Robustness of DSP-Enabled Flexible ROADMs Free from Optical Filters and O-E-O Conversions," *J. Opt. Commun. Netw*., vol. 8, no. 8, pp. 521–529, 2016.

[18] M. Bolea, R. P. Giddings, and J. M. Tang, "Digital Orthogonal Filter-enabled Optical OFDM Channel Multiplexing for Software-reconfigurable Elastic PONs," *J. Lightw. Technol*., vol. 32, no 6, pp. 1200–1206, 2014.

[19] M. Bolea, R. P. Giddings, and M. Bouich, et al., "Digital Filter Multiple Access PONs with DSP-enabled Software Reconfigurability," *J. Opt. Commun. Netw*., vol. 7, no. 4, pp. 215–222, 2015.

[20] X. Duan, R. P. Giddings, and M. Bolea, et al., "Real-time Experimental Demonstrations of Software Reconfigurable Optical OFDM Transceivers utilizing DSP-based Digital Orthogonal Filters for SDN PONs," *Opt. Express*., vol. 22, no. 16, pp. 19674–19685, 2014.

[21] N. Cvijetic, "Software-defined Optical Access Networks for Multiple Broad-band Access Solutions," in *Proc. OptoElectronics Commun. Conf., Int. Conf. Photon. Switching*, 2013.

[22] N. Cvijetic, A.Tanaka, and P. N. Ji, et al., "First OpenFlow-based Software-defined λ-Flow Architecture for Flex-grid OFDMA Mobile Backhaul over Passive Optical Networks with Filterless Direct Detection ONUs," in *Proc. Opt. Fiber Commun. Conf. Nat. Fiber Optic Eng. Conf.* 2013.

7. Conclusions and Future Work

Contents

7.1 Conclusions

To satisfy the ever-increasing data traffic growth and greatly diversified emerging network applications and services, 5G has been proposed with three representative usage scenarios including eMBB, uRLLC and mMTC. To meet these usage scenario-associated stringent requirements on data rate, configurability, end-to-end latency and connection density, a wide range of technique challenges across all the 5G network layers have to be addressed, among which the seamless convergence of independently developed and operated optical access/metro networks and mobile fronthaul/backhaul networks is greatly desirable. To cost-effectively achieve such an objective, PONs have been considered as one of the most promising technical strategies. To enable PON-based converged 5G networks to offer various on-demand services to end-users, it is advantageous if the PONs can provide sufficiently high flexibility, elasticity, reconfigurability, and adaptability to arbitrary signal bandwidth, as well as transparency to signal modulation format and signal bit rate. In addition, the implementation of SDN solutions operating from the high layers down to the physical layer is also preferable in the future PONs. On the other hands, to offer the dynamic connectivity between an expanded number of individual network nodes, advanced ROADMs are expected to play a vital role. The new ROADMs should not only operate at wavelength, sub-wavelength and sub-band levels, but also transparently accommodate various signal modulation formats, different signal detection schemes, flexible WDM-grids, diversified network topologies, and various multiple access techniques. To address all the aforementioned challenges, in this thesis, four advanced techniques targeting the future converged 5G networks have been proposed and explored, including: i) multiple channel interference cancellation of DFMA PONs; ii) hybrid OFDM-DFMA PONs; iii) hybrid DFT-spread OFDM-DFMA PONs; iv) DSP-based optical filter- and O-E-O conversion-free ROADMs.

It is well known that the previously published DFMA PONs can provide sufficient flexibility and reconfigurability for the converged 5G networks. However, in the low-cost IMDD-based DFMA PONs, the degradation of digital filtering-based channel orthogonality introduces significant cross-channel interferences for multiple channel application scenarios. In chapter 3, the DCIC technique has been proposed and investigated to effectively reduce the cross-channel interference in both downstream and upstream IMDD DFMA PONs. A comprehensive DCIC theoretical model has been developed, and through extensive

numerical fitting with experimental measurements, the developed theoretical model has been rigorously verified and a set of accurate transceiver/system parameters has also been identified. Detailed numerical simulations have shown that the proposed DCIC technique increases the aggregated upstream signal transmission capacity by a factor of >2 and extends the differential ONU launch power dynamic range by >14 dB. The aforementioned performance improvements are ONU-count independent and just require one DSP iteration stage. Other salient DCIC advantages include low DSP complexity, negligible latency and excellent transparency to signal modulation format, signal bit rate and initial operation conditions.

To further improve the PON performance and simultaneously reduce its hardware/software complexity and installation/operation expenditure, the hybrid OFDM-DFMA PON has been proposed and investigated in chapter 4. In the proposed new PONs, multiple independent OFDM channels are multiplexed using ONU-embedded dynamically reconfigurable and adaptive digital filters, and simultaneously recovered in the OLT by a single FFT operation. The proposed PONs have all the desired advantages of the DFMA PONs including: i) DSP-enabled dynamic network reconfigurability, flexibility and elasticity, ii) inherent transparency to signal modulation format, signal bit rate, existing PON access techniques and network topologies, iii) capability of SDN-based network abstraction and virtualization across all the layers including the physical layer. In chapter 4, an analytical theoretical hybrid OFDM-DFMA PON model has been developed to give an in-depth understanding of the proposed technique, and extensive simulations of upstream hybrid OFDM-DFMA transmission performances have been numerically explored in representative 25km SSMF IMDD PON systems. It has been shown that apart from the advantages listed above, the proposed PON offers additional new salient features including greatly relaxing digital filter DSP complexity and further improving PON performance flexibility and robustness because of its insensitivity to digital filter-induced signal distortions and system nonlinearity. Moreover, the numerical results have also demonstrated that the hybrid OFDM-DFMA PON can increase the differential ONU launch power dynamic range by 16 dB compared to the previously reported DFMA PONs.

To overcome the OFDM-induced high signal PAPRs, the hybrid DFT-spread OFDM-DFMA PONs have been explored in chapter 5. The performance comparisons have been made for the representative 25km SSMF IMDD hybrid OFDM-DFMA PONs with and

without incorporating DFT-spreading. As expected, the proposed network architecture maintains all the salient features associated with the hybrid OFDM-DFMA PONs, more importantly, they additionally reduce the upstream signal PAPRs by ≥2 dB. As a direct result, in comparison with the hybrid OFDM-DFMA PONs, the proposed PONs have been shown to increase the upstream system power budget by ≥3 dB and reduce the minimum required DAC/ADC quantization bits by at least 1 bit.

To cost-effectively provide dynamic and flexible network connectivity with reduced latency, in chapter 6, the DSP-based optical filter- and O-E-O conversion-free ROADMs with excellent flexibility, adaptability and transparency to physical-layer network characteristics have been investigated, which offer DSP-enabled dynamic add/drop operations at wavelength, sub-wavelength and orthogonal sub-band levels. To evaluate the add/drop operation characteristics of the proposed ROADMs, detailed numerical simulations have been undertaken in IMDD-based network nodes, and the results have shown that: i) the add/drop operation is digital filtering space location-independent; ii) the drop operation introduces around 3 dB power penalties, iii) power penalties induced by the add operation can be 3.5 dB, and iv) for distances less than 40 km, the ROADM drop operation is robust to chromatic dispersion-induced transmission impairments.

In summary, this PhD dissertation research has proposed and extensively explored a number of key elements required for forming, in a cost-effective manner, the converged 5G networks capable of satisfying the major 5G network requirements. These elements range from novel transparent network architectures with excellent forward and backward compatibility, to versatile low-cost networking devices capable of performing on-line RF channel manipulations in the optical domain, and to a range of advanced DSP approaches for further improving the network performance, robustness, functionalities and cost-effectiveness. The converged fixed-mobile 5G networks incorporating the dissertation research-developed technologies are envisaged to offer sufficient flexibility, dynamic reconfigurability and low end-to-end latency. In addition, such converged networks are also capable of supporting not only various data rates at arbitrary bandwidth granularity but also excellent transparency to various network design characteristics namely signal modulation format, signal bit rate and network topology. As such, the dissertation research work has paved a solid path leading to practical implementation of the converged 5G networks.

7.2 Future Work

Although extensive research for the future converged 5G networks have been conducted successfully, in this thesis, a number of technical challenges, however, still need to be solved in order to further confirm the feasibility of practically implementing these techniques in the converged 5G networks. Three major technical challenges are listed below, each of which can be regarded as a future research topic:

1) Spectral efficiency improvement of the hybrid OFDM-DFMA PONs

The hybrid OFDM-DFMA PON presented in chapter 4 utilises a double sideband (DSB) to transmit each individual ONU signal in both the lower sideband (LSB) and the upper sideband (USB), and each ONU is only located at a RF central frequency with a single in-phase filter, this leads to a halved spectral efficiency and transmission capacity compared to the DFMA PONs [1]. Therefore, it is highly desirable if the spectral efficiency of the hybrid OFDM-DFMA PONs can be improved. Technically speaking, two approaches may be adopted: one is to use single sideband (SSB) (either the LSB or the USB) for each ONU channel; and the other one is to introduce an extra DSP operation in the receiver to allow the simultaneous utilisation of both in-phase digital filters and quadrature-phase filters to carry data independently. For the first approach, to produce SSB signals, the Hilbert transform can be used in each ONU in the digital domain [2], whist for the second approach, extra DSP algorithms in the OLT receiver need to be developed for recovering the signals at each orthogonal sub-bands. For IMDD PON systems suffering the negligible channel fading effect, it is expected that these two approaches will double the signal transmission capacity and spectral efficiency compared to the DSB case presented in chapter 4. On the other hand, for long IMDD PON systems suffering the strong channel fading effect, the improvement factor is envisaged to be <2. As such, for each approach, detailed explorations of the trade-off between its performance and hardware/software complexity should be conducted to identify optimum transceiver/network designs for targeted application scenarios.

2) Experimental demonstration of the hybrid OFDM-DFMA PONs

Chapter 4 has conducted the proof-of concept investigations of the hybrid OFDM-DFMA PON. To further evaluate its feasibility for practical implementation in the converged 5G networks, conducting experimental investigations of the proposed PON is vital. In the initial

experimental investigation stage, off-line experimental demonstrations of the hybrid OFDM-DFMA PON consisting of two ONUs should be undertaken first to: a) identify optimum transceiver/system parameters such as the digital filter parameters in the ONUs; and b) explore its maximum achievable downstream/upstream performance and corresponding robustness to practical channel impairments such as chromatic dispersion. In particular, for the upstream operation, various fibre distances and signal processing procedures between different ONUs may introduce a time delay, which could cause symbol timing offset (STO) in the OLT receiver [3]. As the STO effect plays an important role in determining the achievable upstream performance, it is thus necessary to investigate and develop DSP algorithms capable of automatically estimating the STO and subsequently compensating for the STO effect. The effectiveness of using DFT-spread and DCIC in further improving the PON performances should also be studied in the considered PONs. Of course, the exploration of ONU-count dependent performance is of another important task for the feasibility study. After the off-line experimental investigation stage, real-time experimental demonstrations of the PON should be carried out by using FPGA-based real-time DSP platforms available in Bangor. During this stage, special attention will be focused on real-time implementations of relevant DSP algorithms in terms of their performances, complexity, latency and power consumption.

3) Demonstrations of converged 5G networks incorporating the proposed PONs and ROADMs

The overall objective of this future work is to incorporate all major technical solutions achieved in the previous tasks to establish and rigorously verify a cutting-edge converged 5G network with SDN-enabled network control for specific use cases. More specifically, in this stage, the following technical aspects will be pursued:

- Utilise the procedure of establishing the converged 5G network as a unique opportunity to comprehensively evaluate and further optimise each individual technical solution at different levels;
- Extensively evaluate the established converged 5G network in a comprehensive carrier-like lab environment. If necessary, field trials may also be undertaken in existing networks carrying live end-users' traffic to test the compatibility of the developed DSP solutions with other commercial networks;

- Explore innovative technical solutions addressing various 5G ecosystems. Along with the field trials, these activities are valuable for accelerating the process of transferring academic research to practical applications.

References

[1] M. Bolea, R. P. Giddings, and M. Bouich, et al., "Digital Filter Multiple Access PONs with DSP-enabled Software Reconfigurability," *J. Opt. Commun. Netw*., vol. 7, no. 4, pp. 215-222, 2015.

[2] Y. Zeng, Z. Dong, and Y. Chen, et al., "A Novel CAP-WDM-PON Employing Multi-Band DFT-Spread DMT Signals Based on Optical Hilbert-Transformed SSB Modulation," *IEEE Access*, vol. 7, pp. 29397-29404, 2019.

[3] P. Dat, A. Kanno, and N. Yamamoto, et al., "Seamless Convergence of Fiber and Wireless Systems for 5G and Beyond Networks," *J. Light. Technol*., vol. 37, no. 2, pp. 592-605, 2019.

[4] E. Al-Rawachy, R. P. Giddings, and J. M. Tang, "Real-time Experimental Demonstration of DSP-enabled Soft-ROADMs with Multi-level Flexible Add/drop Functions for Cloud Access Networks," *Opt. Express*., vol. 27, no. 1, pp. 16–33, 2019.

Appendix

Publications

1. Y. Dong, W. Jin, R. P. Giddings, et al. “Hybrid DFT-spread OFDM-Digital Filter Multiple Access PONs for Converged 5G Networks” *Journal of Optical Communications and Networking*, vol. 11, no. 7, pp. 347, 2019.

2. Y. Dong, W. Jin, and J. M. Tang, “DFT-spread Hybrid OFDM-DFMA PONs Incorporating Directly Modulated DFB Laser-based ONUs,” in *Conference on Lasers and Electro-Optics/Europe and the European Quantum Electronics Conference (CLEO/Europe-EQEC)* 2019.

3. Y. Dong, R. P. Giddings, and J. M. Tang, "Hybrid OFDM-Digital Filter Multiple Access PONs," *Journal of Lightwave Technology*, vol. 36, no. 23, pp. 5640-5649, 2018.

4. Y. Dong, E. Al-Rawachy, R. P. Giddings, W. Jin, D. Nesset and J. M. Tang, "Multiple Channel Interference Cancellation of Digital Filter Multiple Access PONs," *Journal of Lightwave Technology*, vol. 35, no. 1, pp. 34-44, 2017.

5. X. Gong, L. Guo, Y. Dong, M. Deng, R P. Giddings, and J. M. Tang, "SPM-Improved Transmission Performance of Software-Reconfigurable IMDD PONs Based on Digital Orthogonal Filtering," *Journal of Lightwave Technology*, vol. 35, no. 20, pp. 4488-4496, 2017.

6. W. Jin, C. F. Zhang, X. L. Zhang, X. Duan, Y. X. Dong, P. Giddings, K. Qiu, J. M. Tang, "OSNR Penalty-free Add/drop Performance of DSP-enabled ROADMs in Coherent Systems," *Journal of Optical Communications and Networking*, vol. 9, no. 9, pp. 730-738, 2017.

7. W. Jin, C. Zhang, X. Duan, M. Kadhum, Y. Dong, R P. Giddings, N. Jiang, K. Qiu and J. M. Tang, "Improved Performance Robustness of DSP-enabled Flexible ROADMs Free From Optical Filters and O-E-O Conversions," *Journal of Optical Communications and Networking*, vol. 8, no. 8, pp. 521-529, 2016.

8. W. Jin, X. Duan, Y. Dong, B. Cao, R P. Giddings, C. Zhang and J. M. Tang, "DSP-Enabled Flexible ROADMs Without Optical Filters and O-E-O Conversions," *Journal of Lightwave Technology*, vol. 33, no. 19, pp. 4124-4131, 2015.

9. M. L. Deng, B. Y. Cao, R. P. Giddings, Y. X. Dong, N. Jiang, D. Nesset, K. Qiu, J. M. Tang, "Intra-Cavity Chromatic Dispersion Impacts on 10-Gb/s Optical OFDM Transmissions Over 25-km Dual-RSOA-Based Self-Seeded PON Systems," *IEEE Photonics Journal*, vol. 7, no. 1, pp. 1-12, 2015.

10. M. L. Deng, B.Y. Cao, R.P. Giddings, Y. Dong, N. Jiang, D. Nesset, K. Qiu, J.M. Tang, "Intra-cavity Dispersion-induced Performance Degradations of Dual-RSOA-based Self-Seeded PON systems," in *Optical Fiber Communications Conference and Exhibition (OFC)* 2015.